DEVELOPMENT AND CHARACTERIZATION OF A NOVEL THREE-DIMENSIONAL HUMAN TISSUE-ENGINEERED LUNG MODEL TO STUDY IMMUNE RESPONSE TO RESPIRATORY SYNCYTIAL VIRUS IN VULNERABLE POPULATIONS

By

TAYLOR DO

Bachelor of Science in Biosystems Engineering
Oklahoma State University
Stillwater, OK
2016

Master of Science in Biosystems Engineering
Oklahoma State University
Stillwater, OK
2018

Submitted to the Faculty of the
Graduate College of the
Oklahoma State University
in partial fulfillment of
the requirements for
the Degree of
DOCTOR OF PHILOSOPHY
May, 2023

DEVELOPMENT AND CHARACTERIZATION OF A NOVEL THREE-DIMENSIONAL HUMAN TISSUE-ENGINEERED LUNG MODEL TO STUDY IMMUNE RESPONSE TO RESPIRATORY SYNCYTIAL VIRUS IN VULNERABLE POPULATIONS

Dissertation Approved:

Dr. Heather Fahlenkamp

Dissertation Adviser

Dr. Josh Ramsey

Dr. Yu Feng

Dr. Tom Oomens

ACKNOWLEDGEMENTS

If you are taking the time to read this dissertation, please read this part first. None of this would have been possible without any of the following people involved, and I would really like for their acknowledgment to be known to those who are willing to take the time to read about my research. First, I would like to thank my research advisor, Dr. Fahlenkamp, for sticking with me these past four years. I appreciate your patience in teaching me how to work with difficult cell cultures, and more importantly, for teaching me how to examine everything critically and to never take anything at face value. I would also like to thank our collaborators at the Oklahoma Medical Research Foundation, specifically Dr. Susan Kovats and Dr. Mandi Roe. You all are doing amazing research, and there are so many techniques I was able to acquire only because you all worked with us on this project. Next, I would like to thank my wonderful family. I was so blessed to have a supportive family during this process. My mom and dad, who encouraged me to finish what I started, especially on the worst days when I felt there was no way for me to continue forward with my degree. My sister, who went through this process herself just a few years ago, so she knew exactly the wisdom to pass down to me to get me through the hard times. Most importantly, the love of my life, my husband, who was willing to marry me during this crazy time in my life and helped me let go of the little things so I could focus on the important things in life.

If you are involved in science, then you know that a lot of times, things don't work out, and it can be frustrating after spending so much time working on experimental planning and implementation. When this happened to me, I was able to draw peace and hope from my Lord and Savior, Jesus Christ. If you acknowledge that there is a brokenness in you, as there is in all of us, He can fix you. If you realize that nothing in this world can make you whole, there is hope that can be found in Jesus. "Peace I leave you, My peace I give you; not as the world gives, do I give to you. Do not let your hearts be troubled, nor fearful." (John 14:27, NASB). If you have not yet, I implore you to repent of your sins and believe in Jesus Christ as your savior. No degree I earn or scientific finding I discover will ever amount to a fraction of the importance of knowing my Savior and that my soul can eternally rest in Him. Only through the God of the Bible will salvation be found, for He stated "I am the way, the truth, and the life. No one comes to the Father except through me." (John 14:6, NIV). He loves you and wants you to come to Him. He made you in His image, lived the perfect life without sin, and took your place in the death you deserved, then rose from the grave to defeat death. No other God does that. "For God so loved the world, that He gave His only Son, so that everyone who believes in Him will not perish, but have eternal life." (John 3:16, NASB). This is not only the Good News of the Gospel, but the best news you will ever receive.

Name: TAYLOR DO

Date of Degree: MAY, 2023

Title of Study: DEVELOPMENT AND CHARACTERIZATION OF A NOVEL THREE-DIMENSIONAL HUMAN TISSUE-ENGINEERED LUNG MODEL TO STUDY IMMUNE RESPONSE TO RESPIRATORY SYNCYTIAL VIRUS IN VULNERABLE POPULATIONS

Major Field: CHEMICAL ENGINEERING

Abstract: Lower respiratory illnesses are one of the leading causes of mortality in the United States. Viral lung infections, such as respiratory syncytial virus (RSV), often lead to chronic complications in immunocompromised populations. One of the first steps in reducing or eliminating complications caused by lower respiratory infections is accurately modeling the response of human tissue and cells. This work focused on developing and characterizing a three-dimensional human tissue-engineered lung model (3D-HTLM) using primary human cells to examine the immune response of vulnerable populations to RSV. To achieve this, a collagen hydrogel scaffold was constructed on a PET membrane in a hanging cell culture insert. Human small airway epithelial cells (SAECs), human pulmonary endothelial cells (HPMECs), human pulmonary fibroblasts (HPFs) and myeloid cells were then seeded on the scaffold to create a complete model. Each cell type was characterized within the model using flow cytometry, immunofluorescence, hematoxylin and eosin (H&E) stain, and trans-epithelial electrical resistance (TEER). Myeloid cells successfully migrated into the collagen hydrogel matrix, mimicking *in vivo* conditions. Models were digested to harvest and characterize cells. Myeloid cells recovered from the models upregulated tissue resident markers, CD169, CD206, and CD163, indicating differentiation into lung macrophages. Models were then challenged with TLR-4 agonist lipopolysaccharide (LPS) to validate the immunocompetency of the 3D-HTLM. Cells within the model demonstrated a response to LPS challenge by upregulating ICAM and interleukin (IL)-10, as well as donor-dependent tumor necrosis factor (TNF)-α. The 3D-HTLM was infected with varying multiplicities of infection (MOI) of RSV to determine an appropriate concentration to illicit an immune response. Models with adult myeloid cells demonstrated an immune response to RSV with MOI 10 by significantly upregulating IL-10 and CCL2. Myeloid cells from elderly (65+) and neonatal donor samples were utilized in the 3D-HTLM to determine expression levels of costimulatory markers in response to RSV infection. There was no significant change in costimulatory marker levels between populations upon RSV infection. Future studies can focus on other aspects of immune response to RSV in vulnerable populations within the established 3D-HTLM, such as cytokine expression.

TABLE OF CONTENTS

Chapter Page

LIST OF TABLES

Table Page

LIST OF FIGURES

Figure Page

Figure Page

Figure Page

Figure Page

Figure Page

Figure Page

Figure Page

CHAPTER I

INTRODUCTION

1.1 Background and literature review

Lower respiratory infections remain one of the most prevalent causes of illness worldwide. Respiratory viruses, including the recent SARS-CoV-2, are constantly emerging, causing a need for more effective ways to study pathogens. Respiratory viruses that are commonly studied include, but are not limited to, influenza A virus (IAV), respiratory syncytial virus (RSV), parainfluenza, adenovirus, enterovirus, and coronavirus. SARS-CoV-2 has led to over 5.878 million deaths worldwide since its outbreak [6]. Viruses infect and replicate through cells which leads to an immune response. Severe immune responses can lead to complications by causing local inflammation to the infected area. While many that are infected show mild to moderate symptoms, respiratory viruses can cause more serious complications such as pneumonia, which can be fatal. By understanding the immune response of cells in the lower respiratory system, the severe complications and long-term effects of viruses can be halted and eliminated.

Lung models are necessary to better understand the immune response of cells in the lower respiratory system to viruses and other pathogens. Current lung models that are utilized to understand respiratory pathogens include animal models, *ex vivo* tissue explants, and *in vitro* models, which encompasses both two-dimensional (2D) and three-dimensional (3D) models. The most common animal models to study respiratory disease includes rodents such as mice, guinea pigs, and rats, non-human primates, and pigs. While rodent models are widely available and well-understood, there are documented differences between murine and human immune functionality. From a physiological standpoint, mice lack submucosal glands below the trachea [7-9], as well as respiratory bronchioles [10]. Furthermore, viral distribution and subsequent infection are inherently different due to anatomical dissimilarities, which causes interspecies variation in infectivity [11]. Pattern recognition receptors also vary between humans and mice, specifically the expression levels of toll-like receptors, which are responsible for recognizing pathogens and triggering an immune response [12]. To overcome challenges presented by murine models, studies have developed humanized mouse models where immunodeficient mice are implanted with human $CD34^+$ hematopoietic stem and progenitor cells (HSPCs) to develop a human immune system [13-15]. However, a lack of HSPC donors as well as incomplete human immune function and innate immune response to human donor tissues make widespread development and application of these models an issue [16].

Although highly comparable to human lungs, non-human primates are difficult to acquire and use in large-scale studies due to high costs, variability between subjects, and difficulty to maintain long-term for chronic conditions [17]. Apart from nonhuman primates, the porcine lung immune system is the most similar to that of humans and have shown

potential as a viable animal model [18]. Even so, pigs do not demonstrate the same susceptibility to certain diseases as humans [19]. Ferrets are commonly used to model RSV, but viral replication is only observed after immunosuppression [20]. Even with successful viral replication in ferrets, there are no clinical symptoms of infection. Though animal models are effective in certain pre-clinical studies, such as drug screening and vaccine development, variability between animal subjects and inherit differences with human lungs makes the option of utilizing *in vitro* models preferable for studying immune response mechanisms.

In juxtaposition to animal models, *in vitro* models typically utilize human cells to better mimic specific human responses to respiratory infections. Models that have been used to study viral infections include both two-dimensional (2D) and three-dimensional (3D) systems, with either a single cell culture or a co-culture of cell types. 2D monocultures utilizing human airway epithelial cells (HAECs) grown at an air-liquid interface to increase differentiation of the airway epithelium layer have been used to study viral diseases such as influenza A virus [21, 22], respiratory syncytial virus (RSV) [23], parainfluenza virus [24], and coronavirus [25]. While these models demonstrated successful infection and are effective in characterization of single cell type response, they lack cell-cell interaction and signaling with other lung cell types that are necessary to mimic an *in vivo* response.

Co-culture conditions have been explored to incorporate cellular "cross-talk" in viral pathogen studies. In the human lung, infections typically occur on the apical surface of the epithelial layer (Fig. 1). As a result, viruses such as influenza are capable of damaging the alveolar airspace which disrupts the gas exchange between the epithelial and endothelial cells [26]. To further support this, endothelial cells used in conjunction with epithelial cells have

been shown to increase barrier integrity of the epithelial layer [27, 28], suggesting a critical relationship between the two cellular layers and the consequential effects on the alveolar barrier. Other co-culture models take a close look at specific mechanisms that occur during RSV infection. One study examined the effect of extracellular matrix (ECM) production by combining primary fibroblasts with epithelial cells [29]. Another study utilized a co-culture model to analyze neutrophil-induced epithelial damage caused during RSV infection [30]. Ugonna et al. and the relationship between monocyte-derived dendritic cells (MoDC), macrophages, and epithelial cells [29-31]. These co-cultures allow further insight into *in vivo* conditions by looking at specific mechanisms between two types of cells but are not able to fully capture the 3D environment to mimic the pathophysiology and migration of viruses and immune cells during infection.

One of the most severe respiratory viruses for vulnerable populations, including children under the age of two and adults over the age of 65, is respiratory syncytial virus (RSV). Developing an accurate 3D tissue model to mimic the human lower respiratory system is paramount to understanding the immune response in both adults and neonates, which will ultimately lead to developing a treatment strategy for RSV. Additionally, an immunocompetent *in vitro* model can be used to study the immune response to other emerging and misunderstood viruses. The key components to a biomimetic *in vitro* model to study the response of RSV includes cells necessary to mimic small airways. Major cellular components involved in the small airway immune response include small airway epithelial cells, endothelial cells, pulmonary fibroblasts, and immune cells, such as alveolar macrophages. Some cells are readily available for culture, such as various types of epithelial cells, pulmonary microvascular endothelial cells, and pulmonary fibroblasts.

Epithelial cells are the site of RSV attachment and replication [30], endothelial cells aid in the recruitment and differentiation of added myeloid cells, and fibroblasts produce necessary extracellular matrix components. The model used in these studies will utilized small airway epithelial cells (SAECs), human pulmonary microvascular endothelial cells (HPMECs), and human pulmonary fibroblasts (HPFs) in a hanging cell culture insert. Myeloid cells will be introduced to study immune cell differentiation into tissue resident cells, as well as mimic *in vivo* immune response to viral agonists.

1.1.1 Small airway epithelial cells

Small airway epithelial cells are an integral part of any model attempting to mimic the human lung since the cells respond to viruses and are often the site of infection of many respiratory pathogens. Either primary cells or immortal cell lines can be selected when designing an *in vitro* lung model. Primary cells are isolated directly from a human donor and have a limited number of growth cycles, whereas cell lines will continue to expand and can be used indefinitely. However, cell lines only represent one type of cell, such as A549, a cell line for alveolar type II cells. In the human lung, alveolar type II cells are able to differentiate into alveolar type I cells, a mechanism that is lost in models containing only cell lines. For immunological studies, cell lines are not able to demonstrate differentiation or *in vivo* characteristics that primary cells exhibit in 3D models [32].

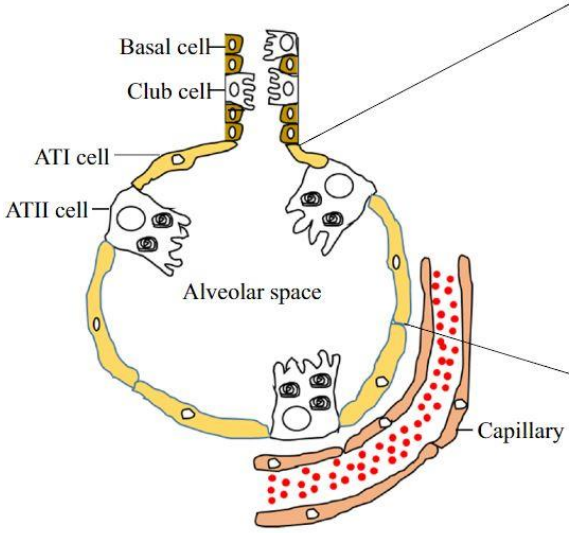

Figure 1. Schematic of small airway epithelial cells, including alveolar type I and II (ATI and ATII) *in vivo* contained in alveoli (adapted from Bhowmick et al. [3]).

The small airways of human lungs consist of mucociliary bronchiolar epithelium and an underlying microvascular endothelium [33]. The small airway epithelium contains ciliated, undifferentiated columnar, clara, and basal cells merged to alveolar epithelium with type I (ATI) and type II (ATII) pneumocytes. ATI cells are the major component of the thin air-blood barrier comprising approximately 95% of the alveolar surface area. The ATII cells cover approximately 4% of the alveolar surface but constitute 15% of all lung cells [34, 35]. These airway epithelial cells also provide a barrier function to maintain polarity and alveolar airspace by forming tight junctions [36]. Squamous ATI cells perform gas exchange, and cuboidal ATII cells are critical for immune response by producing surfactants and metabolizing drugs. Both epithelial cell types are known effector cells in inflammatory responses as the location of these epithelial cells increases the chances of ATII cells to encounter a pathogen [37].

Alveolar epithelial cells express pattern recognition receptors (PRRs), which recognize pathogen-associated molecular patterns (PAMPs) (Fig. 2). PRRs expressed by alveolar epithelial cells include toll-like receptors (TLRs)-2, 3, 4, and 9. Alveolar epithelial cells also produce cytokines and chemokines in response to pathogenic infections. Anti-inflammatory cytokines produced include interleukin (IL)-10 and transforming growth factor beta (TGFβ) [38, 39]. Pro-inflammatory cytokines include IL-1β, IL-6, IL-8, tumor necrosis factor (TNF), granulocyte-macrophage colony-stimulating factor (GM-CSF), macrophage inflammatory protein-1α (MIP-1α), and monocyte chemoattractant protein (MCP)-1 [40-42]. Moreover, human ATII cells also expresses MHC class II molecules on their surface and have been shown to present antigens to $CD4^+$ T cells [43, 44]. The resident stem cell population of the lung, known as basal cells, remains near the basement membrane and maintains the ability to replace goblet and club cells [45].

Cells other than alveolar epithelial cells also lend to the immune response to pathogenic invasion. Goblet cells secrete mucus, a key feature of the respiratory immune system as being the first line of defense by trapping bacteria and dust particles before they move further into the alveoli. Club cells express uteroglobin, a vital anti-inflammatory protein, as well as provide physical barrier functions to protect the alveolar airspace [46].

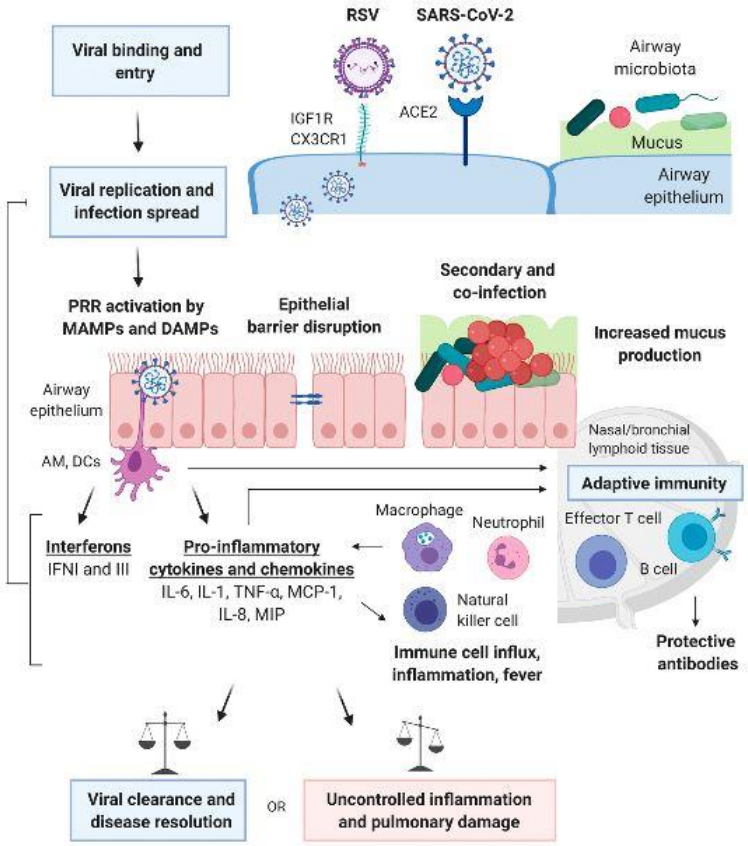

Figure 2. Response of alveolar epithelial cells to viral infection. Viruses such as SARS-CoV-2 and RSV bind and replicate via receptors on alveolar type II (ATII) cells. Microbe and damage associated molecular patterns (MAMPs and DAMPs, respectively) activate pathogen recognition receptors (PRRs) on alveolar macrophages (AMs) and dendritic cells (DCs), which release cytokines, chemokines, and interferons to illicit immune intervention, leading to either viral clearance or inflammation and damage. (Image courtesy of Spacova et al. [5])

1.1.2 Pulmonary microvascular endothelial cells

In addition to epithelial cells, endothelial cells play a vital role in the immune response to respiratory pathogens. Endothelial cells are understood to be the source of the destructive cytokine storm that leads to endothelial-epithelial barrier damage [47-49]. Some viruses utilize pulmonary endothelial cells as a replication site. For instance, microvascular endothelial cells

play an important role in both the infectivity and immune response of highly pathogenic influenza A virus (IAV) [50-54]. Endothelial cells isolated from small lung vessels infected with IAV have demonstrated successful propagation of two different strains of the virus. α-2,3-Sialic acid (SA) and α-2,6-SA receptors were found on the surface of endothelial cells, indicating the susceptibility of influenza virus infections of human pulmonary endothelial cells. Endothelial cells expressed interferon-β (IFN-β), IL-7, TNF, CCL2, and common inflammatory markers such as intercellular adhesion molecule-1 (ICAM-1) and vascular cell adhesion molecule-1 (VCAM-1) after infection with IAV H5N1 as compared to the H1N1 virus. Therefore influenza viruses can successfully infect and replicate through the endothelial cells, even though they may not be the initial target of the influenza virus [55]. Endothelial cells have also been shown to be activated upon infection with RSV by upregulating ICAM-1 [56, 57]. Furthermore, the study presented by Arnold et al. demonstrated increased adhesion of neutrophils to RSV-infected endothelial cells. This increased adhesion leads to migration of immune cells into the bronchoalveolar space, which is a critical immune response observed in the human lung. Human pulmonary microvascular endothelial cells (HPMECs) are responsible for much of the immune response required to recruit immune cells to the alveolar tissue. Therefore, to mimic this process *in vitro*, HPMECs should be included in the 3D lung models.

1.1.3 Fibroblasts

Human pulmonary fibroblasts are an indispensable component of the human lung tissue as they secrete extracellular matrix proteins such as collagen to provide a support structure for other cells to adhere. Fibroblasts have also been shown to aid in the growth and differentiation of epithelial cells in 3D cultures [58, 59], as well as establishing the extracellular matrix structure for a 3D lung organoid models [60, 61]. Furthermore, other studies have reported the

extracellular matrix (ECM) proteins produced by human lung fibroblasts in 3D *in vitro* models are crucial component for dendritic cell migration during viral infections [62]. The fibroblasts in the model described in Derakhshani et al. demonstrated a dense multilayer in H&E-stained imaging, illuminating their ability to develop a natural extracellular matrix to support and connect cells, increasing cell-cell interaction between layers. Fibroblasts are a vital component of 3D lung models due to their ability to contribute to the support system initially given by the scaffold structure of the model.

1.1.4 3D lung model scaffolds

The scaffold type used in a 3D model must have the appropriate chemical and physical properties to effectively simulate *in vivo* conditions. Depending on the location of the tissue, it might need to be particularly stiff, flexible, or porous to meet the demands of the body. Hydrogels are commonly used, which can include synthetic materials or proteins from the extracellular matrix (ECM). Materials may also be derived from living tissue, which more directly mimics the ECM. The materials must be biocompatible so that the cells can grow and differentiate naturally in the model. Given the correct conditions, resident cells added to an extracellular matrix will form multi-layered tissue structures. One of the most important components of a scaffold for a tissue model is maintaining moisture content to mimic conditions found in the human body while maintaining mechanical properties. To create a biomimetic environment for a lung model, the supporting scaffold must be conducive for gas exchange as well as maintain a strong barrier function to preserve the alveolar airspace. Porosity is another integral component necessary for mimicking recruitment and migration of immune cells into the lower respiratory system. The scaffold

should support high seeding efficiency and proliferation, as well as support viability of the cells.

Collagen is commonly used in scaffolds to make a soft, porous hydrogel. Collagen accounts for approximately 25% of dry mass in mammals, making it one of the most abundant proteins found in the body [63]. Due to its abundance, it is easily acquired and well-understood. In addition, collagen has weak antigenicity and high biocompatibility, making it an attractive option for the development of tissue models. ECM collagen is produced when fibroblasts are added to the system, which aid in organizing collagen into fibrils, lending to additional structural integrity. While it does have a weaker tensile strength when compared to other scaffold options, collagen has been found to provide enough structural integrity on its own to support 3D growth culture. Collagen combined with Dulbecco's modified eagle medium (DMEM) seeded with MRC-5 cell-line supported epithelial cell line 16HBE14o- infected with adenovirus (ADV) for at least 39 days, demonstrating the long-term structural integrity of pure collagen [59]. Cells grown in pure collagen or collagen cross-linked with additional polymers both demonstrate high viability and functionality. Bhowmick et al. demonstrated a continuous monolayer of differentiated airway epithelium [64], and Sundstrom et al. showed how pure collagen can also maintain viable cells for extended periods of time [59].

1.1.5 Immune cells

While respiratory epithelial cells are the first cells that encounter micro-organisms by their toll-like receptors, various components of the immune response in the lungs come from hematopoietic origin. These cells consist of neutrophils, monocytes, macrophages, mast cells,

dendritic cells, and lymphocytes [65]. Mast cells, dendritic cells, and macrophages are lung resident cells, while neutrophils, monocytes, and lymphocytes are recruited through cellular signaling during lung infection. It has recently been shown in a humanized mouse model that once recruited, monocytes can differentiate into resident macrophages [15]. Lung resident myeloid cells express multiple unique markers such as CD206, CD169, and CD163 [66-68]. There are two types of pulmonary macrophages: alveolar macrophages (AM) and interstitial macrophages (IM). Both types of macrophages are recruited into the lung parenchyma and release anti-inflammatory cytokines, which restrict inflammation and promote tissue repair [69]. Upon infection or experimentally induced loss of AM, blood Mo can flood into the lung and differentiate into AM [70]. Macrophages exposed to inflammatory stimuli begin secreting cytokines such as TNF and IL-1, -6, -8, and -12 [71]. Depletion of AM leads to increased susceptibility to viral infection, proteinosis, and decreased clearance of virus [70, 72]. The presence of macrophages helps understand the relationship between the endothelial-epithelial barrier [73]. Dendritic cells (DCs) aid in the recognition and processing of antigens. Therefore, DCs act as a part of the adaptive immune system. Since monocytes have the capability of migrating and differentiating into macrophage and dendritic cells, they play an important part in evaluating the immune response to viral aggregates in human lung models.

DCs are antigen-presenting cells crucial in the initiation of immune responses to viral infections. In humans, the DCs circulating in blood have been classified as myeloid DC (MDC) and plasmacytoid DC (PDC) [74]. MDC are of myeloid origin expressing CD13, whereas PDC are derived from lymphoid progenitors and express T- and B-cell molecules [75]. Dendritic cells and cells derived from peripheral blood mononuclear cells (PBMCs) are included in co-

cultures with epithelial cells to study immune responses to pathogens [64, 76]. A main focus of PBMCs to a co-culture in 3D tissue models is to examine the differentiation of mononuclear cells in response to specific viruses. PBMCs grown in co-culture with airway epithelial cells and cytokines, such as GM-CSF and IL-4, demonstrate the differentiation and maturation of monocytes into mature DCs. Migration of the DCs to the epithelial layer and DCs derived from monocytes demonstrate many *in vivo*-like qualities that can be used to study additional viral infections. In another study, PBMCs were grown in co-culture with epithelial cells to examine if IP-10 and IFN-α were upregulated after infecting the apical side of the epithelial cells with human rhinovirus [77]. The effect of PBMCs was quantified by the downregulation of IL-6, IP-10, and ENA-78 and upregulation of IL-28A, IFN-α, MCP-2, and MIP-1β. PBMCs are vital in modeling viral pathogenesis in lung models due to their ability to differentiate into resident macrophages as well as DCs. DCs have demonstrated viral replication and antigen recognition as a part of the immune response within the lung.

1.2 Project objectives and specific aims

The main objective of this study was to develop a 3D human tissue-engineered lung model (3D-HTLM) to study the immune response of vulnerable populations to RSV. To meet this objective, we demonstrated the differentiation of myeloid cells into resident immune cells within the 3D-HTLM and immunocompetence by challenging the cells with lipopolysaccharide (LPS). The 3D-HTLM was then utilized to observe the immune response of vulnerable individuals to RSV. We hypothesized that myeloid cells would successfully differentiate into resident immune cells when introduced to the 3D lung environment and demonstrate a response to LPS. Furthermore, we hypothesized that myeloid cells introduced from immunocompromised individuals would demonstrate a different response to RSV

infection when compared to a normal healthy adult. To meet the objective of this project, the following specific aims were completed:

1) **Developed resident immune cells within the 3D-HTLM from adult peripheral blood mononuclear cells.** Innate immune responses are directed within the microenvironment, so the development of resident macrophages and dendritic cells are key to understand the immune response to RSV.
2) **Characterized the response of immune cells within the 3D-HTLM to an LPS challenge.** LPS is a well-understood agonist of cells that binds to the TLR4 receptor of the cell, one of the primary receptors of many viruses such as RSV. By challenging with LPS, we established the immunocompetency of the model in order to validate moving forward and using the 3D-HTLM to study the response to RSV.
3) **Established the 3D-HTLM as a tool to study the response of immune cells from vulnerable populations within the 3D-HTLM to RSV.** Vulnerable populations, such as neonates and elderly, demonstrate increased complications to RSV infections when compared to the average population. This project sought to validate the 3D-HTLM to study the immune response of both neonates and elders to RSV infection.

The overall outcome of this project demonstrated the potential for the 3D-HTLM as a tool to study respiratory pathogen infections *in vitro*. By proving the differentiation of myeloid cells into tissue resident immune cells, the immune response can be studied without resorting to animal models, tissue explants, or other 2D *in vitro* models. Furthermore, in understanding the differing response to RSV between subpopulations, treatment options can be tested and explored.

1.3 Project significance

Respiratory disease is a leading cause of mortality worldwide, and with the recent COVID-19 pandemic, developing innovated methods of studying and treating both acute and chronic conditions has become paramount. While the 3D-HTLM will be used in this research to study RSV infection and immune response, once it is demonstrated that myeloid cells are able to differentiate into tissue resident immune cells, the 3D-HTLM can be used to study almost any respiratory pathogen response *in vitro*. This will help in studying the pathogenesis of less understood infections.

CHAPTER II

DETERMINING GROWTH CONDITIONS TO SUPPORT CELL CO-CULTURE IN A 3D HUMAN LUNG MODEL

2.1 Introduction

There are over 40 known types of cells in the human lung, many of which contribute to immune functionality [78]. Immune response to foreign invaders requires collaboration among many cell types within the lung in the form of cell-cell interactions. Most respiratory pathogens attack distal portions of the lung, so in order to study the immune response to such invaders, cell types from the small airways will be grown together *in vitro* in a three-dimensional human tissue-engineered lung model (3D-HTLM). However, primary cells isolated from donor lungs require a specific media type with nutrients catered to aid in healthy propagation and functionality.

The cells grown in the 3D-HTLM include small airway epithelial cells (SAECs), human pulmonary microvascular endothelial cells (HPMECs), and human pulmonary fibroblasts (HPFs). By characterizing individual primary cell types outside of the 3D-HTLM, we can predict how the cell should behave in the model.

However, each different cell type demonstrates optimized growth in specific media provided by the manufacturer. SAECs purchased from PromoCell (Heidelberg, Germany) grows ideally in Small Airway Epithelial Cell Culture Medium (SAECM). In addition to the basal media, a supplement cocktail designed for each cell type is used to "complete" the media. SAECM is completed with a supplement cocktail which includes 0.004 mL/mL bovine pituitary extract (BPE), 10 ng/mL recombinant human epidermal growth factor (EGF), 5 μg/mL recombinant human insulin, 0.5 μg/mL hydrocortisone, 0.5 μg/mL epinephrine, 6.7 ng/mL triiodo-L-thyronine, 10 μg/mL recombinant human transferrin, 0.1 ng/mL retinoic acid, and 2.5 mg/mL bovine serum albumin – fatty-acid free (BSA-FAF). The recommended media for HPMECs purchased from PromoCell is Endothelial Cell Growth Medium MV2 (ECGM-MV2), with a supplement cocktail that includes 0.05 mL/mL fetal calf serum (FCS), 5 ng/mL EGF, 10 ng/mL recombinant human basic fibroblast growth factor (bFGF), 20 ng/mL insulin-like growth factor (long R3 IGF), 0.5 ng/mL recombinant human vascular endothelial growth factor 165, 1 μg/mL ascorbic acid, and 0.2 μg/mL hydrocortisone. Since ECGM-MV2 contains a fibroblast growth factor, HPFs were cultured in the HPMEC-recommended medium.

While there is some nutrient overlap between the media supplements, such as EGF and hydrocortisone, there is discrepancy in the concentrations of the shared supplements. Importantly, most supplements are not shared between the two media types. Additionally, media and nutrient supplements are expensive to use and maintain and frequent media changes can disturb cellular growth. Therefore, this experiment also tested two separate media change frequencies to solidify the ideal time between each media change. Furthermore, an ideal media system to support growth of all three cell

types is necessary for functionality of the 3D-HTLM to study cellular response to respiratory pathogens.

2.2 Materials and methods

2.2.1 Cell culture

This experiment sought to isolate cell growth for the three cell types used to construct the 3D-HTLM. The construction of the 3D-HTLM consists of seeding HPFs and SAECs for one week, then adding HPMECs to the model on the seventh day of the growth cycle. Therefore, for the first seven days of the media test, SAECs and HPFs were grown in complete SAEC (CSAEC) media to reflect 3D-HTLM conditions. After the first seven days, HPFs and SAECs were then grown in the two experimental media types for an additional week. HPMECs were grown in the two experimental medias for ten days, which is the growth period of HPMECs in the 3D-HTLM. The experimental media and supplemental nutrient groups were basal small airway epithelial cell media supplemented with MV2 (basal media) and small airway epithelial cell media completed with the small airway epithelial cell supplements as well as MV2 supplements (complete media). Cells were grown in 48-well plates using the various growth media mentioned above. The bottom of each well was coated in a solution of fibronectin in Dulbecco's phosphate-buffered saline (DPBS) (25 μg/mL) for two hours to aid in cell growth and attachment. The fibronectin was coating solution was then removed before adding the respective cell culture and cells were added to each well with a seeding density of 10,000 cells/cm^2. Additionally, two separate media changing frequencies were also tested. One plate of each cell type had a media change once every 3 days, while the other plate had a media change once every 7 days.

2.2.2 Cell growth and viability

Images of cells were captured every 24 hours using light microscopy to monitor growth rates. Pictures were taken using a Nikon Eclipse TE2000-U microscope fixed with a Nikon Intensilight C-HGFI camera. Cells from representative images were then manually counted using Image J to determine approximate cell number for each media type, as well as observe cell morphology. At the end of the two-week growth period, viability was measured using CellTiter-Blue Cell Viability Assay (Promega, Madison, WI). The viability assay measures the metabolic functionality of the cells via a reduction of resazurin to resorufin (Fig. 4). Resorufin then emits fluorescence that was measured using a plate reader to quantify viability. The viability assay was utilized in this experiment by adding 20 μL directly to the media, then incubating for four hours. After four hours, 100 μL of the media-assay mixture was removed from the top of the cell layer and added to a 96-well plate. Fluorescence emissions were then measured using a Beckman Coulter DTX880 Multimode Detector plate reader and analyzed to determine cell viability.

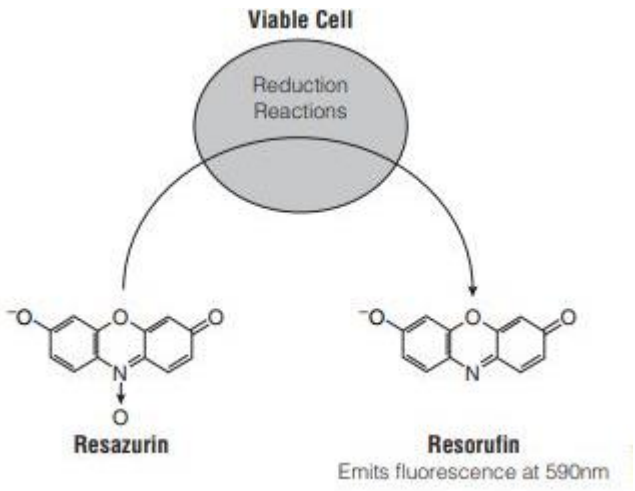

Figure 3. Reduction reaction of resazurin to resorufin used to quantify cell viability (from Promega CellTiter-Blue Technical Bulletin [1]).

2.2.3 Statistical analysis

All variables were tested in triplicate in three independent experiments. Statistical analysis was performed in GraphPad Prism v.9. One way ANOVA with multiple comparisons was used to determine significance between media types as well as media change frequency.

2.3 Results

2.3.1 Single media system to support growth of all cell types

The first objective was to determine a single media system that would support the growth and viability of all cell types to be grown in a 3D-HTLM. One of the initial indicators of promising cell growth is seeding efficiency, which demonstrates how well the cells attach to the surface to ensure propagation. To determine cell seeding efficiency, total number of cells was compared to the approximate number of cells attached to the growth surface after 24 hours (Fig. 4). It was expected that the positive control would

provide the best seeding efficiency since it is specifically designed for each cell type. However, there was no significant difference in seeding efficiency between experimental groups of the media systems.

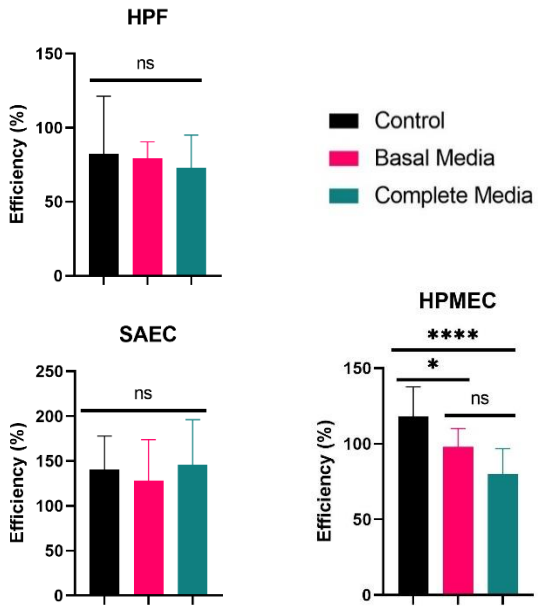

Figure 4. Seeding efficiency of each cell type in each media type. Both experimental media systems showed no significant change when compared to the control. While it was not significant, there was a decrease in seeding efficiency with complete media in HPMECs when compared to the basal media. n=3 * signifies $p<0.05$; ** signifies $p<0.01$; *** signifies $p<0.001$; **** signifies $p<0.0001$.

Cell counts show a representative view of cell growth from day to day to determine any sudden drop or increase in cell number. Representative images used for cell counting on Day 8 of growth can be seen in Fig. 6. Cell counts were determined by counting the cells within the captured image, which was measured using scale slides and ImageJ. The cells counted within the area was then multiplied by the 1.1 cm^2 area of the 48-well plate surface. Each cell type demonstrated steady growth over the two-week period in each media type (Fig. 5). As was expected, the positive control media yielded

the highest cell numbers for HPFs and HPMECs. However, SAECs resulted with overall higher cell counts in basal media when media was changed every three days. HPFs had the highest cell count of all cell types in each media system. Fibroblasts promote connectivity between cells by forming tight matrices as well as producing extracellular matrix-promoting proteins. Fibroblast is the most common spindle cell, meaning the cellular body is longer than it is wide. Therefore, more cells are able to fit in a given surface area, so HPFs are expected to yield the highest cell counts of all three cell types.

All three cell types grown in the basal media demonstrated morphology most similar to the control group. Dead cells appear as round and floating, while cells that are not healthy or dying become more granularized, where internal structures are more visible. HPFs, SAECs, and HPMECs all had less viable cells in complete media when compared to basal media, and SAECs appeared more granular in complete media as well. HPMECs grew in the signature "cobblestone" pattern associated with a healthy cell culture in all three media types. However, like the other two types of cells, more dead HPMECs were present in complete when compared with the other media systems.

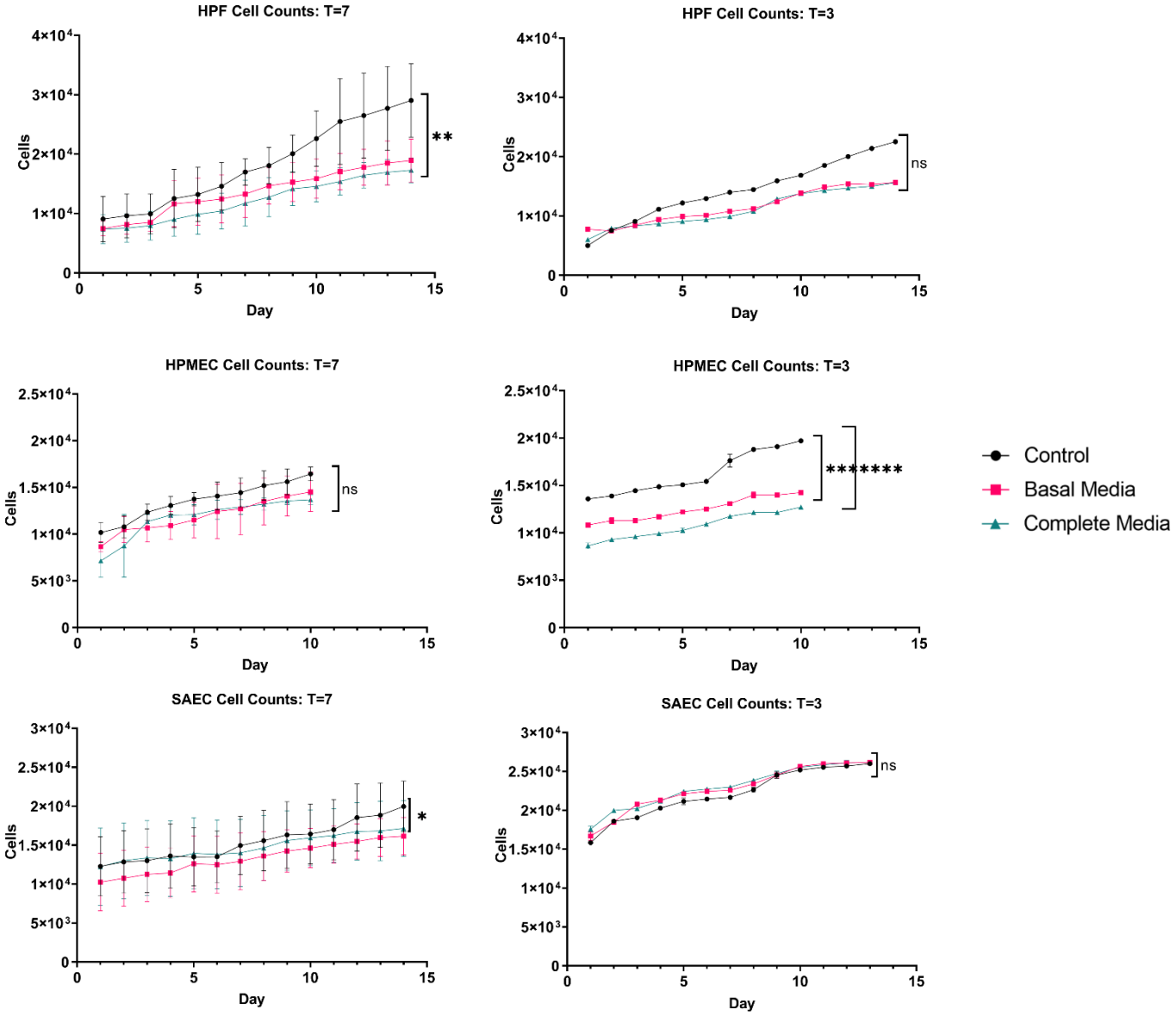

Figure 5. Cell counts of each cell with media changes every 7 days (T=7) and media changes every 3 days (T=3). Cells demonstrated increased in growth rates after media changes when media changes were performed for both media change frequencies. HPFs and SAECs had significantly lower cell counts in the complete and basal media, respectively, when media was changed every 7 days. However, only HPMECs experienced significantly lower cell counts in both experimental media types when compared to the control media when media was changed every 3 days. n=3 * signifies $p<0.05$; ** signifies $p<0.01$; *** signifies $p<0.001$; **** signifies $p<0.0001$.

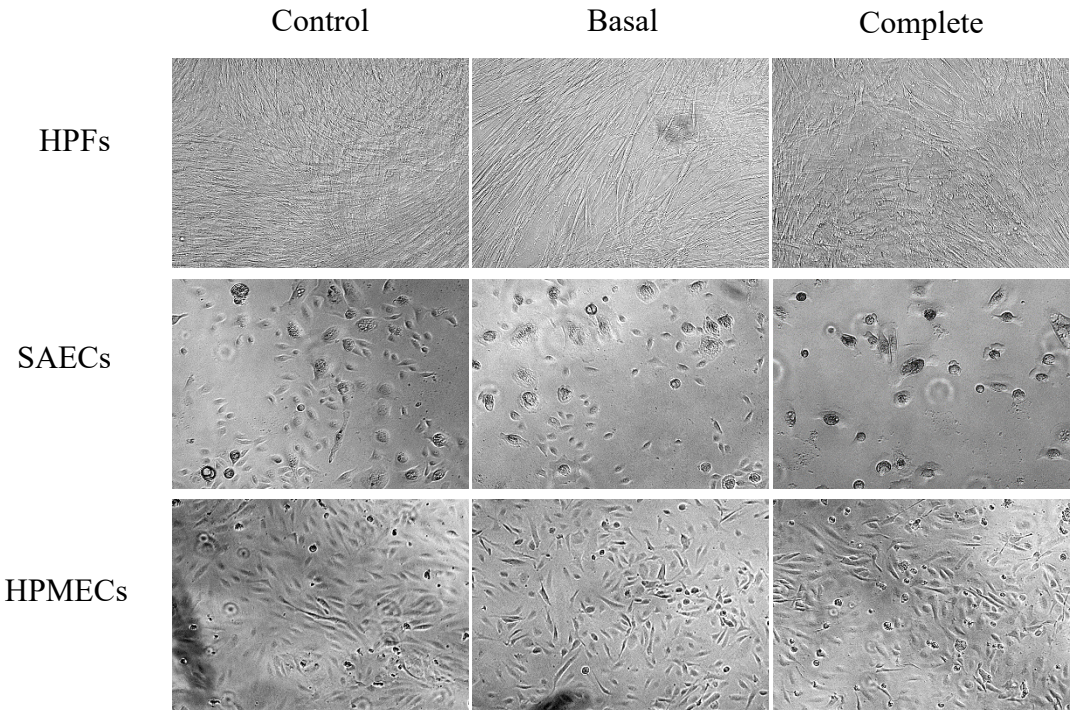

Figure 6. Representative images of each cell type in each media type taken on Day 8 of growth. Human pulmonary fibroblasts (HPFs) maintain spindle shape in each media system. However, HPFs grew in a more organized pattern in basal media, which is comparable to the control. Small airway epithelial cells (SAECs) were granular in all three media systems but had morphology most similar to the control in the basal media system. Human pulmonary microvascular endothelial cells (HPMECs) grew well in all three media systems, but also had fewer dead cells and morphology most similar to the control in the basal media system.

To further characterize the cells, the growth rate of each cell type was determined by first counting the cells using microscopy, then calculating the overall growth after the growth period (Fig. 7). The typical primary cell cultures have four major growth phases during their life cycles: lag phase, which occurs during initial cell attachment and adaptation to a new environment; log phase, where cells exponentially grow and are most viable; stationary phase, when cells are confluent in their environment and cell replication hits a plateau and decline or death phase. Cell growth rate was calculated

assuming cells were in the positive linear stage of the log phase, so the linear slopes of the cell counts were used to estimate the cell growth rate. As was expected and seen in the cell counts, the control media maintained the highest cell growth rate in each cell type. For HPFs, the control media perpetuated significantly higher growth rates in both media change frequencies. SAECs also had significantly higher growth rates in the control media when compared to both experimental media types during the 7-day media change frequency. However, there was no significant difference between any of the media systems when media was changed every 3 days. This could be due to the fact that epithelial cells do not enrich their own growth nutrients during proliferation, and a more frequent replenishment of nutrients from increased media changes impacts the replication of cells more than the exact type of nutrients. Additionally, SAECs demonstrated significantly higher growth rates in both experimental media systems (basal and complete) when media was changed every 3 days when compared to the respective media type with media changes every 7 days. However, HPFs had significantly lower growth rates for basal media when the media was changed every 3 days, and HPMECs also had lower growth rates with increased media change frequency. Unlike the SAECs, this could be due to the removal of supplemental nutrients released by the cells during the growth process or added stress from the media change.

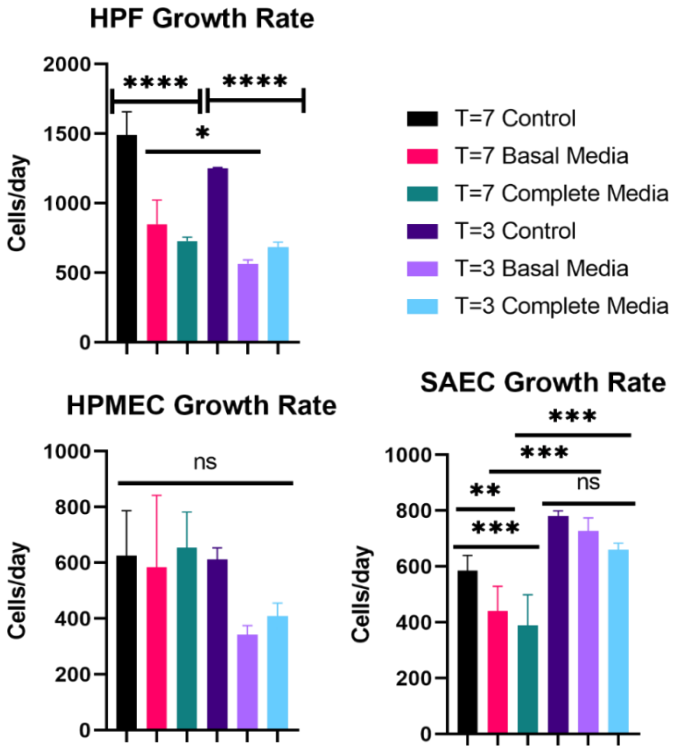

Figure 7. Growth rates of cells in each media type with different media change frequencies. SAECs demonstrated the highest growth rate with media changes every 3 days, with significantly higher growth rates for both basal and complete media when compared to the group with media changes every 7 days. However, HPFs did have significantly higher growth rates in the basal media group when media was changed every 7 days compared to every 3 days. * signifies $p<0.05$; ** signifies $p<0.01$; *** signifies $p<.001$; **** signifies $p<0.001$

2.3.2 Basal media supports increased cell viability when compared to complete media

Viability was measured using CellTiter Blue at the end of the growth period to examine how each media system and media change frequency supported the overall development of the cells. The data reveals that media change frequency does not significantly impact viability of the cells at the end of the growth period. While there are

no significant differences in viability between media changing frequency, there are consistent differences in viability for different media systems. Complete media consistently resulted in lower viability for both SAECs and HPMECs in both media changing frequency groups. Negative controls were measured by adding CellTiter Blue to media without any cells to determine background noise. SAECs that had media changes every 3 days in complete media resulted with viability similar to the negative control, indicating that the majority, if not all, cells were dead by the end of the growth period. It is worth noting that SAECs were grown submerged for the entire 14 day growth period, whereas *in vivo* and in the 3D-HTLM, the SAECs are exposed to an air-liquid interface (ALI) after growing submerged for 7 days. It can be expected that SAECs will demonstrate higher viability grown at ALI compared to submerged culture conditions. Basal media yielded viability similar to, and in most cases higher than, the positive control group. This indicates that all cells are likely to remain viable and functional for longer in the basal media in the 3D-HTLM, regardless of the media change frequency.

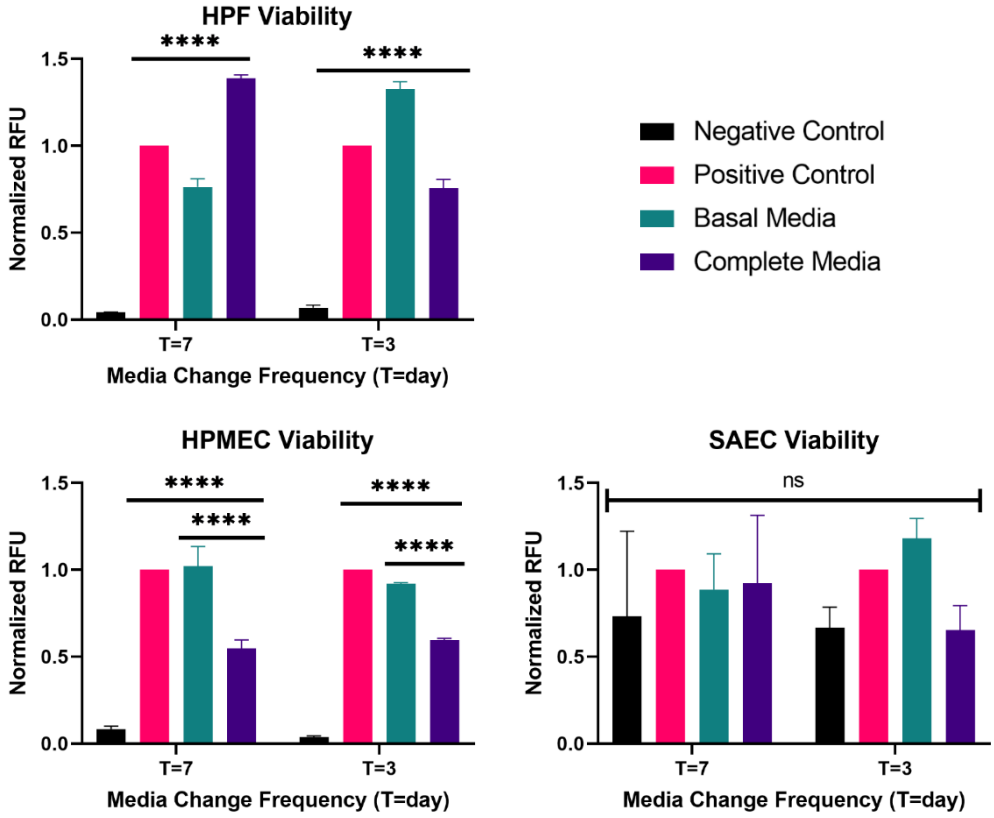

Figure 8. Viability of cells after two-week growth period in different media systems, as well as varied time between media changes. There is no significant difference between the groups when data is normalized to the positive control. However, the cells in complete media resulted in consistently lower viability for both HPMECs and SAECs. SAECs in complete media with a media change frequency of 3 days had similar viability to the negative control group, where no live cells were present. Basal media yielded viability similar to or greater than the PC in each group.

2.4 Discussion

Defining a growth media and culture condition to support triple co-cultures of primary cells is an imperative first step in developing a functional tissue-engineered model. In this experiment, we sought to determine a media system that can support the growth and viability of three primary human cell types critical to developing a 3D-HTLM. The data collected here to characterize each cell type will also help predict expected individual cell behavior within the 3D-HTLM. Cell seeding efficiency was not impacted by the different media systems when compared to the control media. HPFs and SAECs reside in the 3D-HTLM environment for almost three weeks from the time they are seeded into the model to the time they are harvested from the system. The 3D-HTLM is a delicate environment for the cells, so performing frequent media changes may cause additional stress on the cells that hinders their growth and viability. Although cells did experience a slight increase in growth rate after media changes, there was no overall significant increase in growth rate for HPFs and HPMECs when media was changed more frequently. In contrast to SAECs, HPMECs experienced overall higher growth rates with less frequent media changes and similar viability between the media change frequency groups. Another consideration when observing the growth characteristics of the cells is that the cells will be grown in a co-culture when added to the 3D-HTLM. When grown in co-cultures with other cells to mimic a more *in vivo* environment, cells can release growth factors that promote the growth of other cell types [79]. Therefore, by changing the media less frequently, growth factors secreted by cells remain in the system and promote healthy replication and viability among other cells in the 3D-HTLM.

Morphology and viability data both reveal that cells behave the best in the basal media/supplement combination. Cells grown in basal media appear more similar to the standard morphology as seen in the positive control group. Likewise, viability data showed that all cells at both media change frequencies are just as viable in the basal media system as the positive control.

Other studies have also used mixed media systems to promote the growth of cells in 3D lung models. One study examined a Calu-3 epithelial cell line and primary lung microvascular endothelial cells utilized a similar media system, mixing 50% of each cell's specific media for a co-culture media blend [80]. Likewise, in a study examining the effects of inhaled toxicants, a co-culture of primary airway epithelial cells and primary microvascular lung cells grown at ALI were grown on an "organ-on-a-chip" model. The media used to support both of these cell types in a co-culture involved a specialized ALI epithelial cell media combined with 20% of the basal endothelial media, enriched with extra MV2 supplements [81].

From the data presented here, the 3D-HTLM will benefit from using the basal media system and media changes every 7 days to promote growth rates and viability of the cells in the model. HPMECs demonstrate significantly higher viability when the media is changed less frequently, and HPFs and SAECs have no significant difference in viability when media change frequency is varied. Growth rates for HPMECS and HPFs are also higher when the media is changed every 7 days when compared to every 3 days while in the basal media system. While SAECs do have higher growth rates when media is changed more frequently, the addition of the other two cells types in co-culture may promote higher growth rates in the 3D-HTLM. When comparing the two experimental

media types, the basal media consistently promoted higher viability, growth rates, and morphology most similar to cells grown in control media. The complete media may not have been as successful as the basal media due to an oversaturation of growth factors and nutrients, which inhibit the growth of other cell types. Therefore, the basal media, which consists of basal small airway epithelial cell media completed with endothelial cell MV2 supplements, is recommended for the full 3D-HTLM system. However, it is recommended to use the complete small airway epithelial cell media to support growth of SAECs in the first week before adding HPMECs. The 3D-HTLM system used in the following studies was grown in a media system determined by other preliminary data, but future work with the 3D-HTLM will utilize the media system defined by this study.

CHAPTER III

CHARACTERIZATION OF IMMUNE CELLS WITHIN THE 3D-HTLM UNDER INFLAMMATORY CONDITIONS

3.1 Introduction

Lower respiratory infections have been among the top 5 leading causes of death worldwide since 2000 (WHO), and the COVID-19 pandemic has further highlighted the need to understand how respiratory viruses elicit and subvert responses generated by multiple epithelial cell types and resident immune cells of the lung. Tissue-engineered lung models focus on modeling the human lower respiratory system to better understand αthe pulmonary immune response to respiratory pathogens. These models range in complexity based on cell types used and dimensionality, but often use immortalized cell lines, which are limited in how well they mimic a healthy lung environment [82, 83].

A precursor to utilizing these models to study viruses often includes the validation of the model's immunocompetency. Some agents utilized to stimulate acute inflammatory responses include tumor necrosis factor alpha (TNF-α), Poly I:C, and lipopolysaccharide (LPS). TNF-α is a cytokine that causes acute inflammation when overexpressed in the alveolar environment after stimulation from either a pathogenic or other airborne

environmental hazards [84], while LPS and polyinosinic:polycytidylic (poly I:C or PIC) are toll-like receptor (TLR) agonists. TLRs, a member of pathogen-associated pattern molecules (PAMPs), are an integral feature of the innate immune system, expressed on immune cells such as macrophages and dendritic cells (DCs) as well as alveolar epithelial cells [85]. TLRs can be further categorized as extracellular and intracellular. Extracellular TLRs include TLR-1, -2, -4, -5, -6, and -10, while intracellular TLRs consist of TLR-3, -7, -8, -9. LPS is isolated from Gram negative bacterial cell walls and initiates an inflammatory response by specifically adhering to TLR4. PIC is a TLR3 agonist used in the form of a sodium salt and mimics double-stranded RNA to simulate a viral infection. Adhesion to a TLR activated downstream signaling cascades by activating pro-inflammatory transcription factors such as nuclear factor kappa b (NF-κB), leading to production of pro-inflammatory cytokines IL-8, IL-10, and TNF-α [86]. Both TLR3 and TLR4 are stimulated by many respiratory viruses, including RSV [87]. Therefore, TLR agonists are preferential to confirm the immune functionality of the 3D-HTLM for future studies of viral tropism.

The goal of this study was to determine the differentiation of lung tissue resident phenotypes and functional capacity of Mo and DCs from PBMC-derived myeloid cells added to a three-dimensional human tissue-engineered lung model (3D-HTLM). The 3D-HTLM used in this study was constructing using human pulmonary fibroblasts (HPFs) seeded into a collagen hydrogel on a PET membrane in a hanging cell culture insert. A layer of small airway epithelial cells (SAECs) was then added to the top of the collagen hydrogel and grown for one week before exposing to ALI and adding human pulmonary microvascular endothelial cells (HPMECs) to the bottom side of the PET membrane. This

formed a full three-dimensional “sandwich” model to represent the human lung (Fig. 9B). Once constructed, resident cells of the 3D-HTLM (HPFs, HPMECs, and SAECs) were characterized to determine functionality of each cell type within the models.

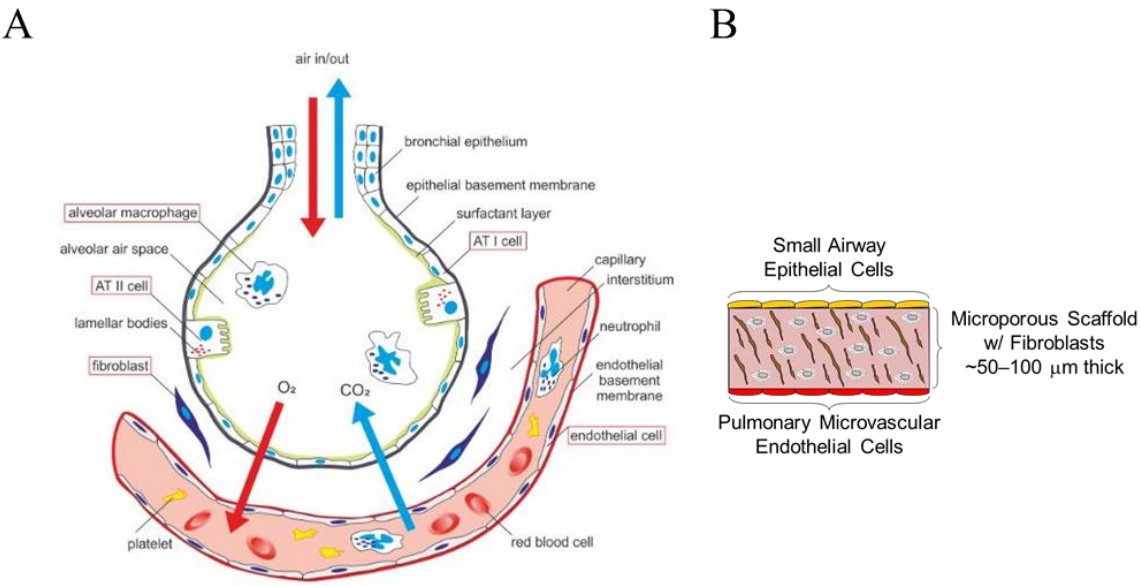

Figure 9. In-depth schematic of alveoli including epithelial cells, macrophages, fibroblasts, and endothelial cells (A) (adapted from Nova et al. [4]), which are included in sandwich model of lung (B).

To validate the immunocompetency of the model, $CD14^{+}$ monocytes enriched with small populations of dendritic cells (DCs) and monocyte-derived dendritic cells (Mo-DCs) were isolated from donor Buffy coats obtained from the Oklahoma Blood Institute (OBI) and added to the endothelial layer of the 3D-HTLM. Once added to the lung environment, it was hypothesized that the myeloid cells would differentiate and adopt characteristics of lung resident immune cells. The lung tissue environment provides a unique network of molecules to instruct the gene expression of differentiating macrophages [88-90]. Two lung tissue resident macrophages include alveolar

macrophages (AMs) and interstitial macrophages. AMs are the most abundant resident myeloid cell within lung in homeostasis, functioning by clearing the airway of surfactant lipoproteins and sampling inhaled antigens. To distinguish the different subpopulations of macrophages, AMs will be classified as CD1c-negtive cells ($CD1c^-$) with low levels of CD14 expression ($CD14^{lo}$), human leukocyte antigen-LR isotype (HLA-DR) positive, $CD169^+$, $CD206^+$, and $CD71^+$. IMs do not express CD71 or CD169 [67, 91], but maintain CD14 expression, so they will be classified as $CD1c^-CD14^+HLA\text{-}DR^+CD169^-CD206^+CD71^-$. Additional lung resident immune cells also express CD206, CD169, and CD163, which are not expressed in circulating monocyte populations [15, 67, 91, 92].

The model presented here demonstrated the ability of circulating monocytes to adopt features of lung resident immune cells when introduced to the lung environment. To further validate the immunocompetence of the 3D-HTLM, LPS was used to stimulate a response from both the resident parenchymal cells as well as the differentiated immune cells. By demonstrating the immunocompetence of the models, future studies will be able to utilize the model to study the human lung's immune response to respiratory pathogens.

3.2 Methods

3.2.1 Cell culture

SAECs, HPMECs, and HPFs were purchased from PromoCell (Catalog #'s 12642, 12281, and 12360, respectively; Heidelburg, Germany). SAECs and HPMECs were grown in 75 cm^2 cell culture flasks coated with fibronectin coating solution (25 μg/mL fibronectin in Dulbecco's phosphate-buffered saline) and incubated at standard conditions (37°C and humidified chamber at 5% CO_2) until 90% confluent. Cells were

then detached using an Accutase (Invitrogen) solution. HPMECs and SAECs were then added directly to respective sections of the 3D-HTLM, while HPFs were expanded and frozen down at $1x10^6$ cells/mL of cryopreservative media.

3.2.2 Development of HPF-enriched collagen hydrogel

The 3D-HTLMs were constructed and cultured on Celltreat 24-well hanging cell culture inserts with a permeable 0.8 μm PET membrane (Celltreat Scientific Products, Pepperell, MA). The collagen hydrogel scaffold consisted of 64.5 vol% 3.1 mg/mL type I bovine collagen (Advanced BioMatrix, Carlsbad, CA), 8.1 vol% 10x M199, 13.3 vol% 0.1 N NaOH, and 14 vol% DPBS. HPFs were thawed from expanded cryopreserved stock and directly seeded into the hydrogel at 75,000 cells/mL, and 0.150 mL of the HPF-enriched hydrogel solution was aliquoted to the top of the PET membranes and placed into the incubator for 45 minutes for polymerization.

3.2.3 Seeding SAECs on collagen hydrogel

Upon polymerization, complete small airway epithelial cell medium (CSAECM) (PromoCell, Catalog #21070) was added to the outer chamber (1 mL/well) as well as to the top of the collagen hydrogel (0.1 mL/gel). After 24 hours incubation, media was removed from the top of the hydrogel and replaced with 0.1 mL/model fibronectin coating solution for one hour. SAECs were detached from the cell culture flask and seeded to the top of the collagen hydrogel with a seeding density of 150,000 cm^2 after removal of the fibronectin coating and grown for 7 days.

3.2.4 Addition of HPMECs and exposure to air-liquid interface (ALI) conditions

Once confluent, media was removed from the surface of the collagen hydrogel and hanging inserts were inverted into 12-well cell culture plates to coat the bottom of the membrane with fibronectin coating solution for one hour. HPMECs were detached from cell culture flask and added to the basal side of the hanging cell culture membrane with a seeding density of 150,000 cells/cm^2. Hanging cell culture inserts remained inverted for 4 hours to allow for the HPMECs to attach to the membrane, after which they were transferred back to the media in the 24-well plate (Fig. 3). During incubation, media was changed to basal small airway epithelial cell media completed with endothelial cell MV2 supplement mix (basal media) (Promocell, Catalog #21270 and 39226, respectively). To maintain models at an air-liquid interface (ALI), 0.4 mL of media was added to the outer chamber of the cell culture plate.

3.2.5 Epithelial barrier integrity

Trans-epithelial electrical resistance (TEER) ($\Omega \cdot cm^2$) was measured using an EVOM3 (World Precision Instruments). To determine the contribution to barrier integrity of each layer of the 3D-HTLM, TEER was measured for collagen hydrogels, HPFs seeded collagen hydrogels, HPFs seeded collagen hydrogels with SAECs, and HPFs seeded collagen hydrogels with SAECs and HPMECs. Measurements were taken at each medium change (every 36 hours) for 13 days. The values were normalized to the resistance of a blank cell culture insert with medium following the equation:

$$TEER = \left(R_{sample} - R_{control}\right) \times A \qquad \text{(Eq. 1)}$$

where R_{sample} is the measured resistance of the experimental sample (Ω), $R_{control}$ is the arithmetic mean of the blank cell culture insert (Ω), and A is the area of the PET membrane in the cell culture insert (0.33 cm^2).

3.2.6 Isolation and addition of myeloid cells

Myeloid cells were isolated from donor Buffy coats obtained from the OBI (male and female; ages 37-62). PBMCs were first separated from plasma and red blood cells using Ficoll-Paque™ PLUS (GM Healthcare) density-gradient centrifugation, and subsequently washed using bovine serum albumin-enriched DPBS buffer. Isolated myeloid cells included classical $CD14^{++}CD16^{-}$, non-classical $CD14^{+}CD16^{++}$, intermediate $CD14^{++}CD16^{+}$ monocytes, and small populations of DCs, which were separated from the PBMC population using a Pan Monocyte Isolation Kit (Miltenyi Biotec, Catalog #130-096-537). Briefly, highly pure monocytes and dendritic cells remained unlabeled, while magnetically conjugated antibodies selectively labeled remaining PBMCs. Cells were separated using magnetic LS columns to isolate monocyte and dendritic cell populations, which were then frozen in $10x10^6$ cell/mL aliquots.

One week after addition of HPMECs, isolated myeloid cells were thawed and added directly to the endothelial layer of the 3D-HTLM (Fig. 10). Cell culture inserts were inverted into 12-well cell culture plates and myeloid cells were added at a density of approximately 758,000 cell/cm^2 (250,000 cells/model) to the endothelial layer of the tissue models and incubated for four hours before being returned to the 24-well plate. Complete models with myeloid cells were incubated four days before analysis in a cytokine-enriched medium containing GM-CSF (10 ng/mL), Flt3 (33 ng/mL), and SCF (20 ng/mL) in basal media.

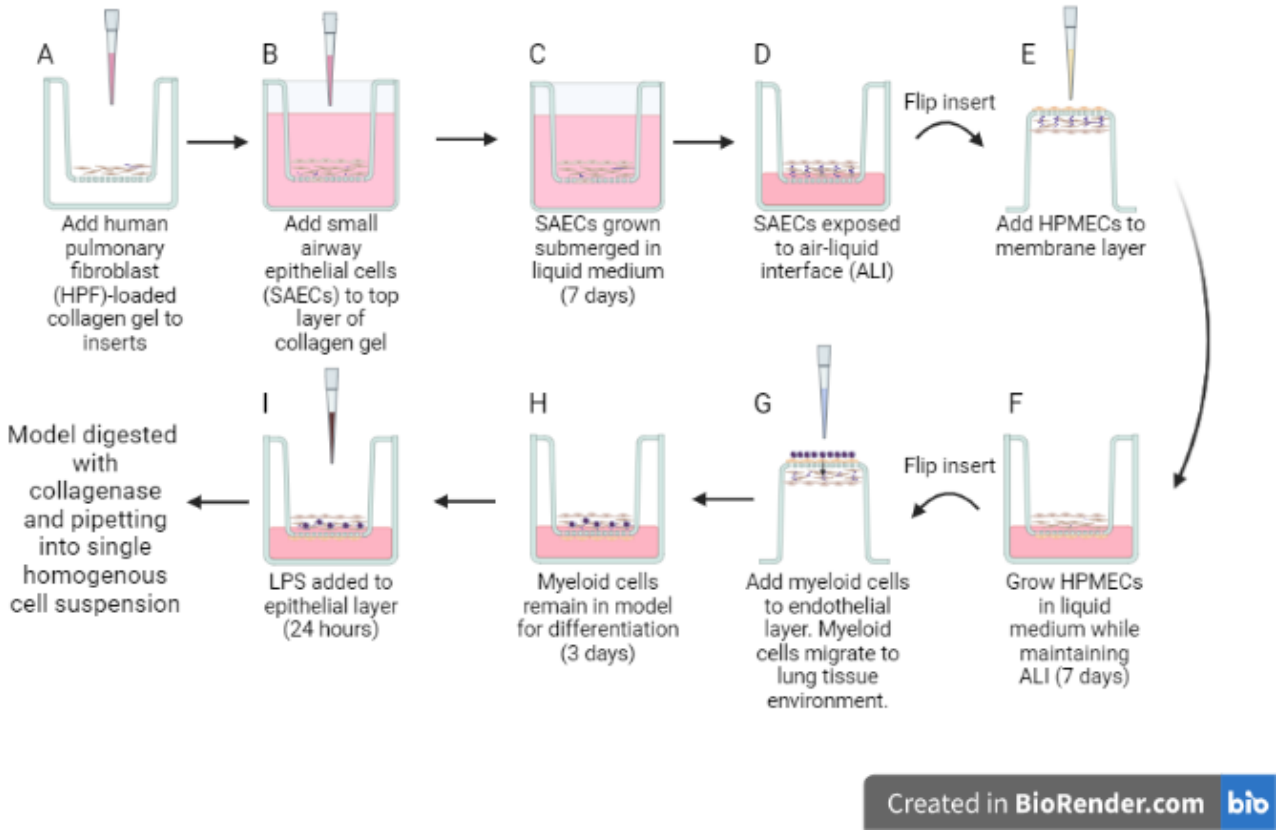

Figure 10. Steps to build complete 3D-HTLM (created using BioRender). HPF-enriched collagen gel matrix was added to hanging cell culture insert with permeable PET membrane (A). SAECs were then seeded on top of collagen gel (B), grown in cell culture medium, and exposed to air-liquid interface (ALI) on day 7. HPMECs were seeded to underside of fibronectin-coated PET membrane (E), given 4 hours for attachment to membrane, then submerged in cell culture medium (F). 7 days after seeding endothelial cells, $CD14^+$ myeloid cells were added to basal layer of model (G). Myeloid cells were given 4 hours for migration into cellular matrix and 4 days for differentiation within the model. After 3 days, LPS was added to the model for the final 24 hours of incubation before digesting and harvesting the cells.

3.2.7 Activation of 3D-HTLM

To test immunocompetency of the 3D-HTLM, the TLR4 agonist lipopolysaccharide (LPS) was added to the fully developed model. Three days after addition of monocytes, LPS (1 μg/mL) was added to the epithelial layer of the model and incubated for 24 hours before digestion. Models without myeloid cells were also activated with LPS to measure the activation of non-immune cells. For some

experiments, 5 μg/mL brefeldin A (BFA) (Millipore Sigma) was added to the medium 6 hours before harvest to analyze cytokine production using flow cytometry.

3.2.8 Phenotypic characterization of cells in the 3D-HTLM

Prior to staining for flow cytometry, models were digested by adding 2.2 mg/mL collagenase-D to the top of the model in the hanging insert and outer chamber, then incubating for 15-20 minutes. To aid in digestion, models were aspirated from the hanging insert and mixed with the collagenase solution, then returned to the incubator until no visible collagen gel remained and cells were suspended in a homogenous suspension. Cell suspensions were collected into respective centrifuge tubes and spun at 1200 rpm for 5 minutes at 4°C and counted using Trypan blue to approximate viability.

Cells collected from models without myeloid cells were rinsed with DPBS and stained with Live/Dead Green Fixable Viability Marker (ThermoFisher) for 15 minutes at room temperature, after which half of the cells were fixed using 4% paraformaldehyde for 15 minutes and permeabilized with a 0.5% Tween20 (FisherScientific) solution in DPBS for 15 minutes. These cells were then intracellularly stained with epithelial cell markers Aquaporin 5 (Aqp5) (Abcam) to approximate alveolar type I epithelial cell population, club cell 10 (CC10) (BioLegend) to approximate club/clara cell population, and pro-surfactant C (pro-SPC) (Abcam) to approximate alveolar type II epithelial cell population. The remaining cells were stained with endothelial marker CD31/PECAM (BioLegend), as well as inflammatory markers CD54/ICAM (BioLegend) and CD106/VCAM (BioLegend) using extracellular staining techniques. Samples were measuring using a BD Accuri C6 flow cytometer and analyzed using FlowJo (v. 10).

Cells collected from models complete with myeloid cells were stained with ZombieAqua viability dye (Biolegend) for 15 minutes at room temperature. Cells were then blocked with FcR block (Invitrogen) for 5 minutes before the addition of antibodies specific for myeloid cells (Table 1). Cells were fixed with 4% paraformaldehyde for 10 minutes on ice. For intracellular staining of cytokines, cells from models incubated with BFA (BD Biosciences) for 6 hours were permeabilized using the Fixation/Permeabilization Kit (BD) as per manufacturer's specifications. Cells were run on an LSRII (BD Biosciences), BD Accuri™ C6, or Cytek Aurora (Cytek).

Table 1. Antibodies used to identify input myeloid cells and populations harvested from lung tissue environment, as well as cytokine levels from experiments utilizing BFA.

Antibody	Clone	Fluorophore	Manufacturer	Cat #
CD14	M5E2	BV605	Biolegend	301834
CD14	Polyclonal	Unconjugated	Abcam	45870
CD16	3G8	PerCP/Cyanine5.5	Biolegend	302027
CD16	3G8	PE	Biolegend	302056
CD163	GHI/61	APC/Fire 750	Biolegend	333633
CD169	REA1176	APC	Milteny Biotec	130-121-116
CD169	HSn 7D2	Unconjugated	Novus Biologicals	NB600-543SS
CD1c	L161	PE-Cy7	Biolegend	331516
CD206	15-2	PerCP-Cy5.5	Biolegend	321122
CD31	WM59	Unconjugated	Biolegend	303102
CD40	5C3	BV421	Biolegend	334331
CD40	5C3	APC/Fire 750	Biolegend	334344
CD45	HI30	BV785	Biolegend	304048
CD45	Polyclonal	Unconjugated	Novus Biologicals	NBP1-88103
CD71	CY1G4	BV421	Biolegend	334121
CD86	IT2.2	PE/Dazzle 594	Biolegend	305434
CK-14	LL001	Unconjugated	Santa Cruz Biotec	53253
Dkα Gt	Polyclonal	AF488	Jackson Immuno-Research Labs	705-546-147
Dkα Ms	Polyclonal	AF594	Jackson Immuno-Research Labs	715-586-151
Dkα Rb	Polyclonal	AF488	Jackson Immuno-Research Labs	711-546-152
FcεR1	AER-37 (CRA-1)	BV711	Biolegend	334637
HLA-DR	L243	BV421	Biolegend	307636
HLA-DR	L243	PE/Dazzle 594	Biolegend	307653
IL-1β	JK1B-1	Alexa Fluor 647	Biolegend	508207
IL-6	MQ2-13A5	PE/Dazzle 594	Biolegend	501121
PDL1	29E.2A3	APC	Biolegend	329707

Immunofluorescence (IF) staining was performed separately on the endothelial and epithelial layers. Complete models were fixed with 4% paraformaldehyde (PFA). Hydrogels containing the epithelial layer and fibroblasts were then removed from PET membrane and probed for CK-14 (1:50) followed by a secondary anti-mouse Ig PE. PET membranes containing HPMECs were probed for CD31/PECAM (1:50) followed by a secondary anti-mouse Ig CFL647. Samples were counterstained using ProLong antifade

mountant with NucBlue (ThermoFisher Catalog #P36983) and were imaged with a Zeiss LSM 980 with Airyscan 2 confocal microscope.

For sectioning, models were fixed overnight in 4% PFA then replaced with PBS. The PFBS was removed from the top portion of the hanging cell culture insert and replaced with warm 4% agarose and allowed to solidify. Next the PBS was removed from the bottom of the and the PET membrane with the agarose plug was removed from the hanging insert. 4% agarose was added to the bottom of the membrane. After solidifying, agarose was trimmed down and embedded in paraffin. Following processing, sectioning, deparaffinizing, and antigen retrieval, longitudinal sections were probed for CD31 (1:50), CD45 (1:100), CD14 (1:100), and Sytox deep red nuclear dye (Invitrogen, cat# S11381). Stained sections were preserved with ProLong Diamond Antifade mountant (Invitrogen, Cat#P36965). Alternatively, some deparaffinized sections were used for H&E staining. H&E sections were imaged with a Zeiss Axiovert 200m inverted fluorescent microscope. Immunofluorescent sections were imaged with a Nikon Eclipse Ni epifluorescence microscope.

3.2.9 Immune cell morphology

To analyze morphology of input and collected immune cells, cells harvested from model were sorted using cytospin techniques. Cells were sorted on an Aria (BD Biosciences). Cell subsets were loaded onto a cytospin^{TM} 4 cytocentrifuge (Thermo Scientific) and spun down at 1000 RPM, medium acceleration for 5 minutes. Slides were fixed with methanol for 5 minutes and Wright-Giemsa stained. Slides were imaged on an Axiovert 200M (Zeiss) at 40x.

3.2.10 Functional response of 3D-HTLM

To measure levels of secreted cytokines, supernatants from complete models was collected during digestion and stored at -80°C. Secretion of IL-1β, IL-10, CCL2, TNFα, and IL-12 were quantified using a Luminex assay (R&D systems cat #LXSAHM) as per the manufacturer's instructions. The Luminex assay was read on a BioPlex 200 (Bio-Rad).

3.2.11 Statistical analysis

Experiments were performed in triplicates with >3 independent replicates. Flow cytometry was analyzed with FlowJo 10. Graphpad Prism 9 was used for statistical analysis. Paired two-tailed t-test or one-way ANOVA with Tukey's multiple comparisons test was used as appropriate. Gene expression was normalized using ΔΔCT to HPRT1 housekeeping gene and the no LPS samples. * signifies $p<0.05$, ** signifies $p<0.01$, *** signifies $p<0.001$, **** signifies $p<0.0001$.

3.3 Results

3.3.1. Presence of functional resident cells in 3D-HTLM

The initial steps of this study, we sought to demonstrate the physiological features of the 3D-HTLM. Morphological and phenotypical characterization of the 3D-HTLM indicates the presence of HSAECs and HPMECs within the model. Hematoxylin and eosin (H&E) staining demonstrates the multilayer formed by the epithelial cells and the presence of the endothelial layer on the PET surface (Fig. 11).

Multilayers of epithelial cells are observed *in vivo*, which creates barrier function of the epithelium (Fig. 11B-C). The model was sandwiched between layers of agarose prior to paraffin-embedding in order to image the cross-section of the complete 3D-HTLM (Fig. 11A).

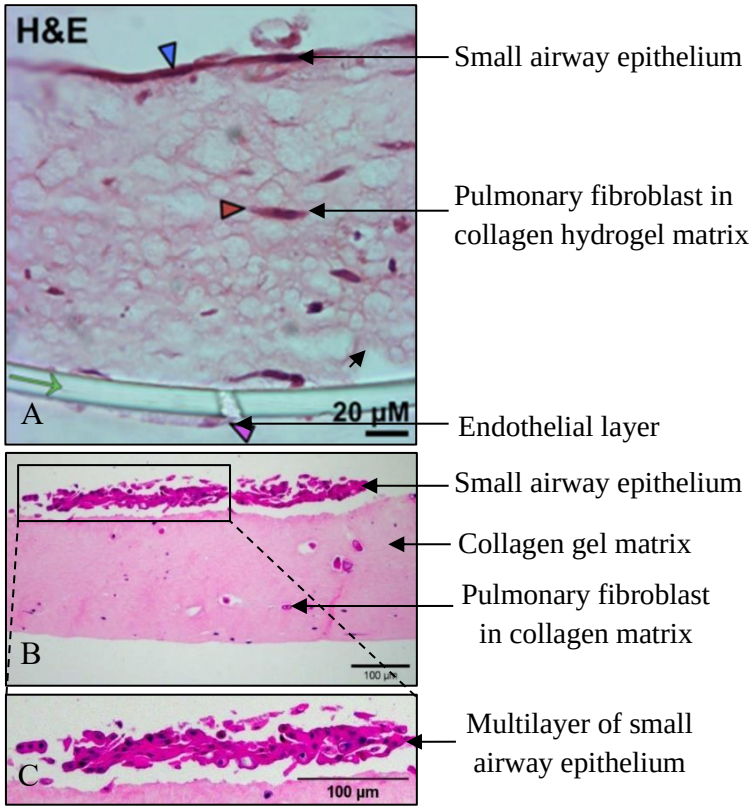

Figure 11. Hematoxylin and eosin (H&E) staining of 3D-HTLM cross-sections. Samples were fixed and sectioned before H&E staining and microscopy analysis. SAECs cultured in 3D and exposed to air-liquid interface (ALI) on a collagen matrix containing HPFs form multilayered epithelium (A-B). Complete model with endothelium attached to PET membrane surface (C).

The model shown here demonstrates a true three-dimensional *in vitro* model where the epithelial cells are exposed to air-liquid interface. Multiple studies have demonstrated the importance of utilizing a three-dimensional system to study viral tropism [64, 93]. Growing epithelial cells at air-liquid interface is also critical in immunological studies by aiding in differentiation and response to pathogenic agonists [94-96].

Immunohistochemical (IHC) staining techniques were then used to further demonstrate morphology of the cells within the 3D-HTLM as well as functionality. HPMECs were probed with CD31 and SAECs were probed with CK-14, conjugated to CFL647 and PE, respectively. Nuclei were counterstained with DAPI. Confluent layers of both HPMECs and SAECs were observed on their respective surface (Fig. 12).

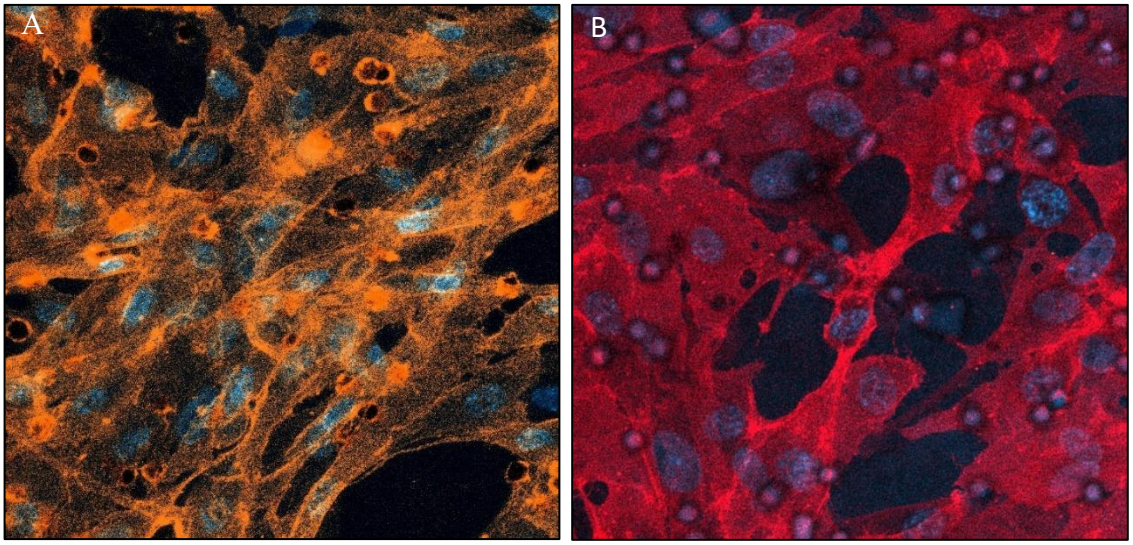

Figure 12. Immunohistochemical (IHC) staining of epithelial and endothelial layers within the 3D-HTLM (400x). Stains include CK-14 (R-PE) (A) and CD31 (CFL 647) (B). Nuclei counterstained with DAPI. CK-14 are expressed on lung epithelial cells, and CD31 are expressed on endothelial cells.

To further determine viability, functionality, and relative subpopulations of resident cells within the 3D-HTLM, the collagen hydrogel was digested with collagenase to bring cells into a homogenous suspension. Cells were then stained with Live/Dead Green Fixable Viability dye. Antibodies against CD31/PECAM, Aquaporin 5 (Aqp5), Prosurfactant protein C (Pro-SPC), and club cell 10 (CC10) were used to probe for endothelial cells, ATI, ATII, and club cells, respectively. Endothelial populations were determined using a probe for CD31. An average of 8.4% of cells collected from the 3D-HTLM were PECAM-positive, 6.1% were CC10 positive, 11% were Aqp5 positive, and 26% were Pro-SPC positive (Fig. 13).

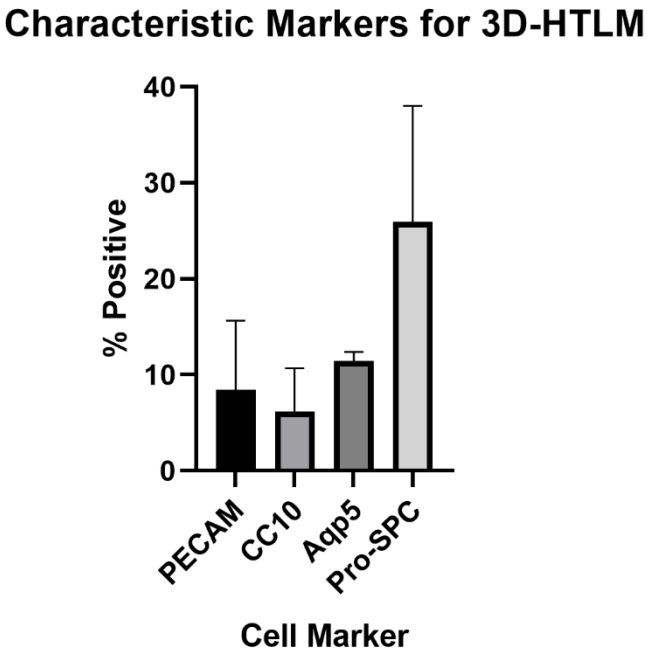

Figure 13. Markers used to determine subpopulations of cells within the 3D-HTLM. PECAM-positive events indicate endothelial cells, club cell 10 (CC10) indicates epithelial club cell populations, Aquaporin 5 (Aqp5) indicates ATI cells, and prosurfactant protein C (Pro-SPC) indicates ATII cells. n = 9 independent experiments performed in triplicate.

Epithelial cell functionality was further proven through trans-epithelial electrical resistance (TEER) tests, which measured the barrier integrity formed by the epithelial layer. Models with an epithelial layer demonstrated a noticeable increase in TEER measurements when compared to collagen hydrogel-only and HPF-loaded collagen hydrogel models. Models containing all three cell types showed a significant increase in resistance when compared to all other models (Fig. 14). This data supports the confluency and functionality of the epithelial layer within the 3D-HTLM.

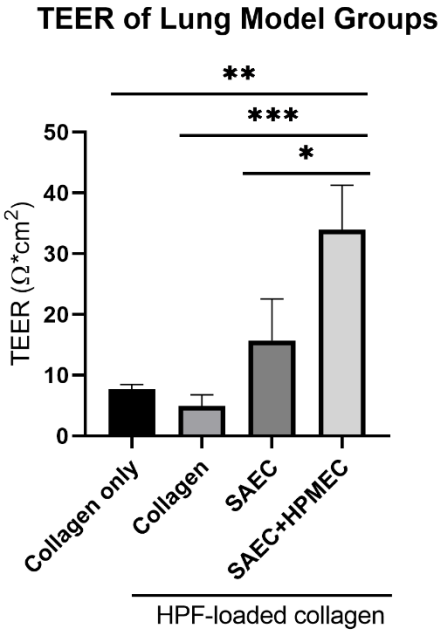

Figure 14. TEER of individual and combined layers of 3D-HTLM on day 13. Data set was normalized to measurements obtained with PET membrane and medium alone. One-way ANOVA with Tukey's multiple comparisons test. * signifies $p<0.05$, ** signifies $p<0.01$, *** signifies $p<.0001$; n=3.

3.3.2 Migration of immune cells into 3D-HTLM environment

Myeloid cells isolated from human donor Buffy coats were added to the endothelial layer of the models to mimic immune cell migration into the lung environment. Four days after introduction to the 3D-HTLM, myeloid cells were characterized by staining paraffin-embedded cross sections. Cell types within the paraffin-embedded sections were identified using antibody probes for CD45, CD31, and CK-14 to visualize myeloid cells, endothelial cells, and epithelial cells, respectively (Fig. 15). Myeloid cells expressing CD45 can be seen distributed throughout the layers of the model, including the epithelial layer (Fig. 15A, blue arrows), the collagen matrix (Fig. 15B, red arrows), and within the endothelial layer (Fig. 15B, pink arrow). CD31 positive endothelial cells maintained a similar morphology to epithelial cells seen in Fig. 15A, denoted by pink arrowheads. Due to difficulty of maintaining the epithelial layer during sample preparation, the epithelial layer was separately characterized by removing the hydrogel from the PET membrane and probing for CK-14 (Fig. 15C). The distribution and confluency of the epithelial layer after addition of the myeloid cells further confirms the similar morphology observed in Fig. 17A. The data presented here further supports the presence of functional resident cells added to the 3D-HTLM, as well as the migration of myeloid cells throughout the model after four days.

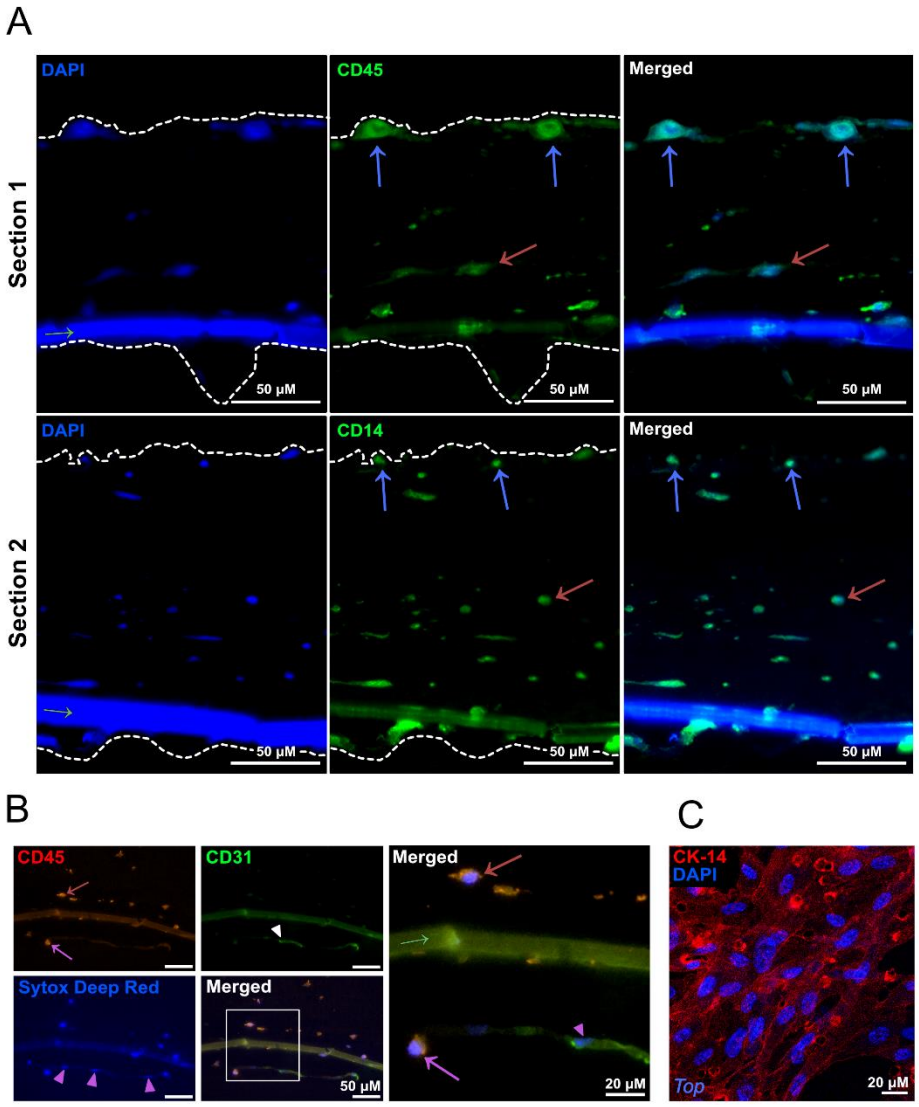

Figure 15. Cross sections of the 3D-HTLM four days after addition of myeloid cells to the endothelial layer (A-B) and characterization of epithelial cells with cytokeratin 14 (CK-14). Myeloid cells are identified using antibody against CD45 and CD14, and nuclei are counterstained with DAPI (A). Blue arrowheads point to the myeloid cell within the epithelial layer, and red arrowheads indicate myeloid cells within the collagen hydrogel matrix. White hashmarks outline the boundary of the model. Myeloid cells can also be seen in the endothelial layer of the model (B), where myeloid cells are probed for with CD45 (pink and red arrows) and endothelial cells are identified with CD31 (arrowheads). Nuclei are counterstained with Sytox Deep Red. Epithelial cells are characterized from a top-down viewpoint using CK-14 and counterstaining nuclei using DAPI (C).

3.3.3 Myeloid cells added to 3D-HTLM adopt tissue-resident immune cell characteristics

Four days following the addition of myeloid cells to the endothelial surface of the 3D-HTLM, cells were harvested into a single suspension by digesting the models with collagenase-D. Myeloid cells were characterized both before and after addition to the 3D-HTLM using antibodies characteristic of resident lung immune cells. Input cells were characterized using flow cytometry and were found to contain populations of classic $CD14^+$ monocytes (Mo), classical dendritic cells 1 and 2 (cDC1s and cDC2s), monocyte-derived dendritic cells (Mo-DCs), and $CD16^+$ Mo. Immune cells harvested from the 3D-HTLM were characterized using flow cytometry staining, cytospin separation techniques with Giesma staining, and quantitative reverse transcription polymerase chain reaction (RT-qPCR).

Flow cytometry was performed on cell suspensions harvested four days after addition to the 3D-HTLM to determine phenotypic response to exposure to the *in vitro* lung environment. Lung tissue resident immune cell markers CD169, CD206, and CD163 were significantly upregulated when compared to all input myeloid cell populations. Introduction to the lung environment also increased activation markers in recovered immune cells when compared to input populations. Furthermore, input cells morphologically differentiated after residing within the 3D-HTLM environment (Fig. 17B). Mo, Mo-DCs, and cDC2s demonstrated increased levels of activation markers CD40, CD86, and programmed-death ligand 1 (PDL1). Additionally, human leukocyte antigen-DR isotype (HLA-DR), a marker indicating T cell activation, was found to be significantly upregulated (Fig. 16). Models containing myeloid cells from both male (M)

and female (F) donors confirmed no distinction in immune cell differentiation between genders.

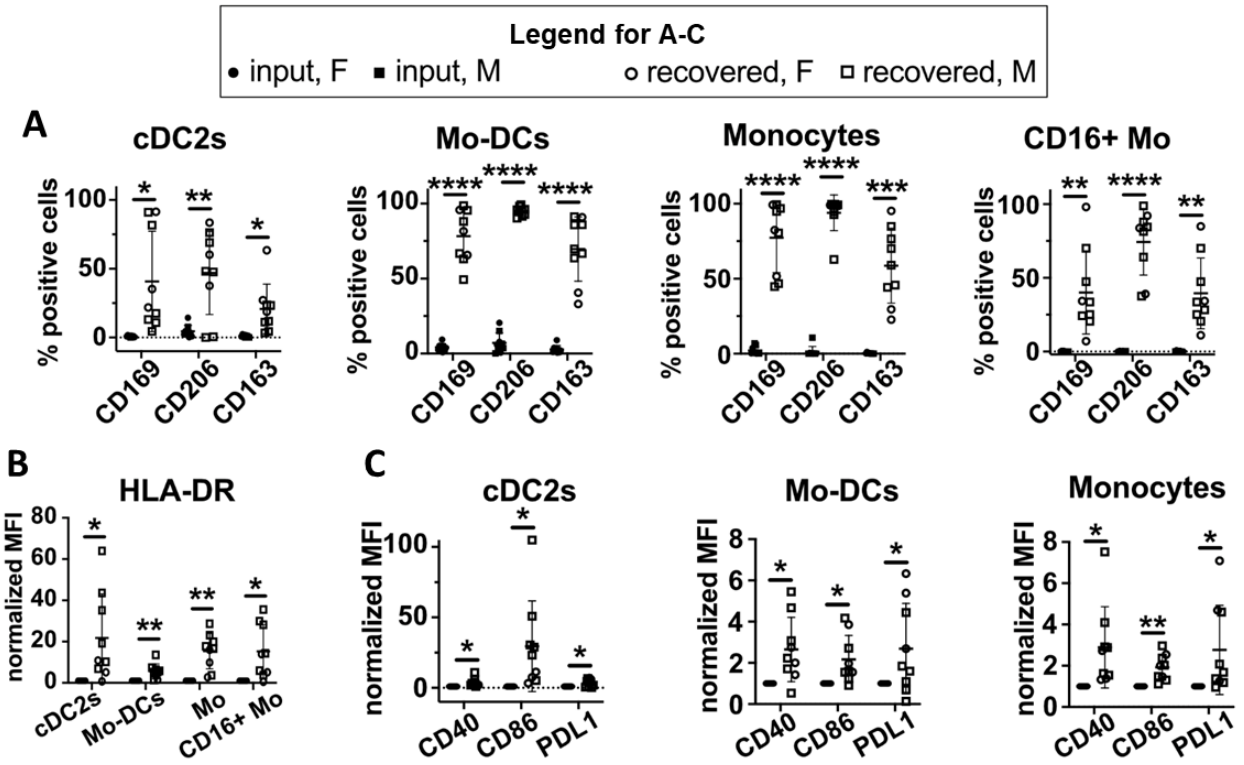

Figure 16. Upregulation of tissue resident markers after exposure to *in vitro* lung environment. All input myeloid subpopulations from both male and female donors significantly increased expression of markers CD169, CD206, and CD163, which indicates differentiation of myeloid cells into lung resident cells (A). Activation marker human leukocyte antigen-DR (HLA-DR) was significantly upregulated by all subpopulations of recovered monocytes and dendritic cells (B), while classical dendritic cell 2 (cDC2s), monocyte-derived dendritic cells (Mo-DCs) and classical $CD14^{+}$ monocytes upregulated CD40, CD86, and programmed-death ligand 1 (PDL1). Harvested myeloid cells demonstrate both differentiation into tissue resident immune cells, as well as activation upon introduction to the 3D-HTLM environment.

Alveolar macrophages (AMs) are a large component of the human lung immune response. Immune cells were isolated onto slides using cytospin centrifugation and stained with Giesma after sorting with flow cytometry. Input cells were compared with

harvested cells to analyze morphological differences after residing in the 3D-HTLM environment for four days. Alveolar macrophages can be identified by a large cytoplasmic space and relatively smaller nucleus when compared to monocytes [91, 97-99]. A subpopulation of cells isolated from the 3D-HTLM shared similar morphological features with AMs isolated from bronchoalveolar lavage (BAL) (Fig. 17A), indicating differentiation of myeloid cells into AMs within the *in vitro* lung model environment.

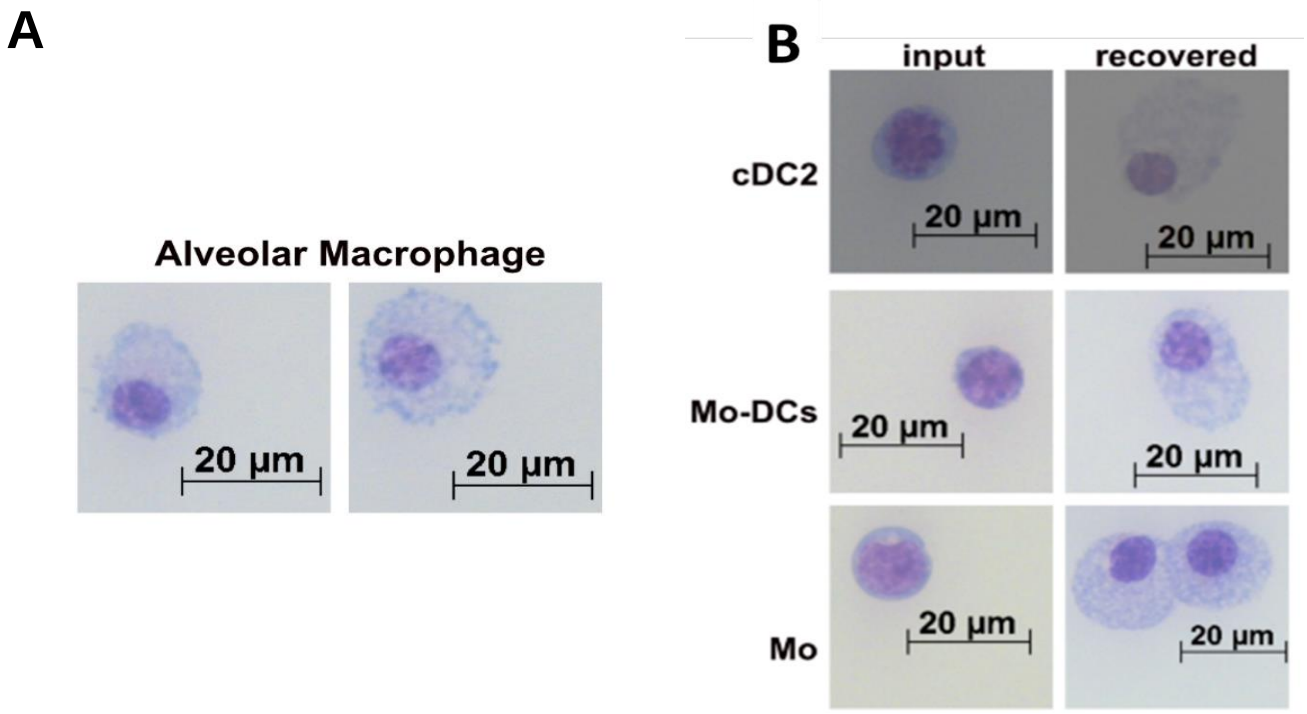

Figure 17. Giemsa staining after isolating cells using flow cytometry and cytospin centrifugation onto microscope slides. A subpopulation of cells harvested from the 3D-HTLM (A; right panel) adopts morphological features of alveolar macrophages (AMs) isolated from bronchoalveolar lavage (BAL) (A; left panel). Input subpopulations of cells also morphologically differentiate after residing within the 3D-HTLM for four days (B).

Within lung resident immune cell populations, AMs can be identified as $CD1c^{-}$ $CD14^{lo}HLA\text{-}DR^{+}CD206^{+}CD169^{+}CD71^{+}$. To confirm the input cells were absent of AMs and that the 3D-HTLM environment instructed the differentiation of circulating monocytes into AMs. As seen in Fig. 16, input myeloid cells were absent of populations expressing CD169, a marker specific for AMs (Fig. 16B). Monocytes incubated in culture enriched with granulocyte macrophage colony stimulating factor (GM-CSF) and fms-like tyrosine kinase 3 (Flt3) were also absent of $CD71^{+}$ cells (Fig. 16C). These results indicate that the intercellular interactions formed within the 3D-HTLM instruct the differentiation of myeloid cells into lung tissue resident immune cells, specifically macrophages and dendritic cells.

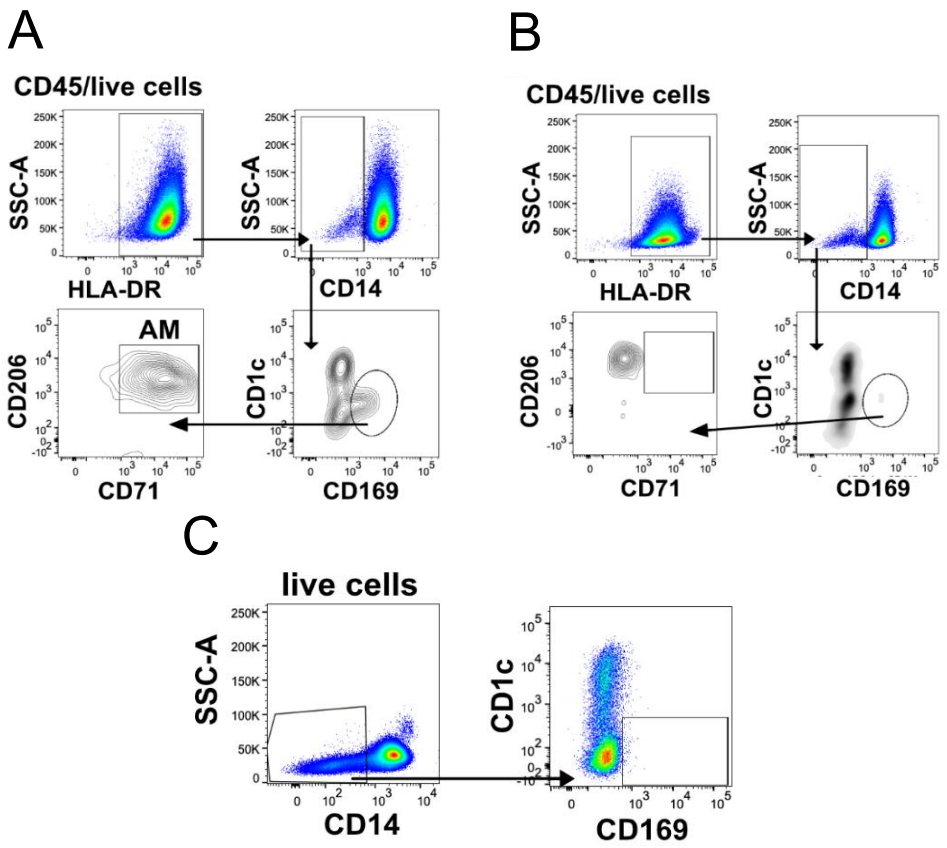

Figure 18. Gating strategies to identify cells expressing alveolar macrophage (AM)-characteristic markers. Cells harvested from the 3D-HTLM after 4 days residence in lung environment were gated into HLA-DRCD14^{lo} cells. CD14^{lo} cells were then selected and further gated into CD1c^{-}CD169^{+} cells. The cells gated as CD71^{+}CD206^{+} were identified as AMs (A). Monocytes cultured in GM-CSF and Flt3 resulted in HLA-DR^{+}CD14^{lo}CD169^{+}CD71^{-} cells, indicating a lack of AM population (B). Input monocytes did not express CD169, confirming input monocytes differentiated into tissue resident immune cells upon exposure to the *in vitro* lung environment (C).

3.3.4 Cells in 3D-HTLM demonstrate response to LPS activation

TLR4-agonist LPS was applied to the 3D-HTLM in order to validate the immunocompetency of the model. LPS was added to the endothelial layer of the model for 24 hours before digesting the models and harvesting the cells. The response to LPS was measured in the endothelial and epithelial cells by analyzing levels of ICAM-1 and

VCAM-1 using flow cytometry. ICAM-1 is expressed on HPMECs and alveolar type I epithelial cells and is upregulated upon exposure to LPS [100, 101]. HPMECs were first identified by gating $CD31^+$ cells from the population. HPMECs did not significantly upregulate VCAM-1 upon exposure to LPS but did significantly upregulate ICAM-1 (Fig. 19B-C). $CD31^-$ cells showed no significant change in expression levels of ICAM-1 or VCAM-1 (Fig. 19D-E), which could be explained by the direct application of LPS to the endothelial side of the model. The data presented here demonstrates a functional response of the endothelial and epithelial cells within the 3D-HTLM.

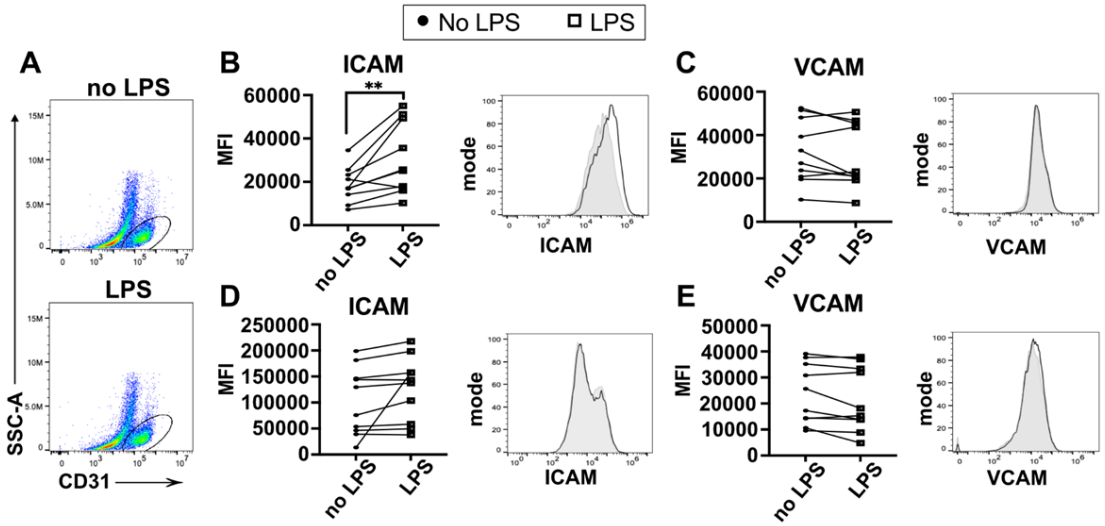

Figure 19. Analysis of ICAM-1 and VCAM-1 in $CD31^+$ and $CD31^-$ cells after 24-hour stimulation with LPS. $CD31^+$ cells were gated out to represent the HPMEC population (A). $CD31^+$ cells demonstrated significant upregulated in ICAM-1 with LPS activation but showed no change in VCAM-1 expression (B-C). $CD31^-$ cells did not show any significant change in ICAM-1 or VCAM-1 expression levels (D-E).

To further investigate functionality of the immune cells in the 3D-HTLM, flow cytometry was used to measure expression levels of costimulatory markers CD40, CD86,

PDL1, and HLA-DR. There was no significant difference in costimulatory marker expression levels between unstimulated cells and cells exposed to LPS (Fig. 20). However, it should be noted that the costimulatory makers were already expressed before LPS activation, so the immune cells may have been activated when added to the 3D-HTLM.

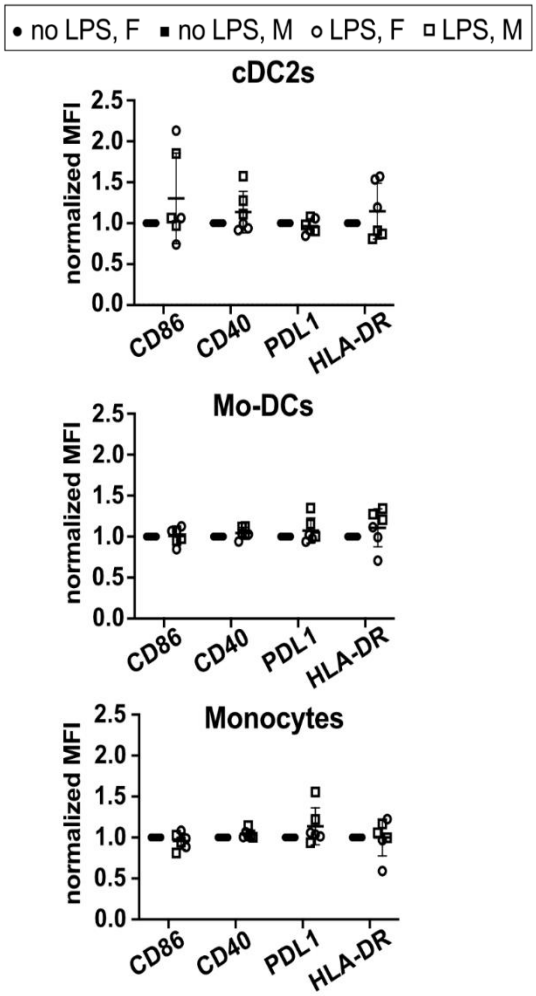

Figure 20. Expression levels of costimulatory molecules in subsets of differentiated immune cells after LPS stimulation. No markers demonstrated significant change after stimulation with LPS.

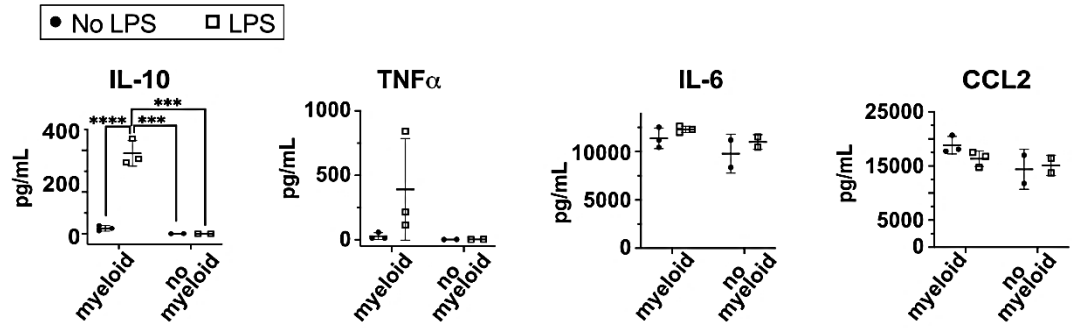

Figure 21. Levels of cytokine expression level from collected supernatant both with and without myeloid cells and/or LPS. IL-10 was significantly increased in the group with myeloid cells stimulated with LPS when compared with both unstimulated models with myeloid cells and models without myeloid cells. TNF-α was increased in individual donors but did not show significant change in expression levels as a whole.

The overall response to LPS stimulation was further investigated by analyzing the cytokine expression from the complete model with and without myeloid cells. Supernatant was collected from models during the digestion process after 24-hour activation with LPS in models both with and without myeloid cells. A multi-plex bead array was used to measure levels of secreted inflammatory cytokines from the supernatant. 3D-HTLMs containing myeloid cells stimulated with LPS demonstrated increased interleukin (IL)-10 levels when compared with models lacking myeloid cells and models not stimulated with LPS. (Fig. 21). Tumor necrosis factor α (TNF-α) was increased with certain individual donors in models with myeloid cells and stimulated with LPS; however, the wide variability in responses from individual donors demonstrated a lack of significant change in the experimental group as a whole (Fig. 21).

Baseline expression levels of IL-6 and IL-1β were further investigated with flow cytometry by halting secretion of cytokines using Brefeldin-A (BFA). BFA was applied to the models 6 hours before digesting and harvesting the cells. IL-6 and IL-1β

expression levels was analyzed using flow cytometry. The data demonstrates that IL-6 and IL-1β expression varies from donor to donor. Some showed increased expression, while others did not change expression levels (Fig. 22A-B). Each myeloid cell subset identified from the 3D-HTLM did exhibit different propensities to produce IL-6 or IL-1β (Fig. 22C-D). The data presented here illustrates the functionality of differentiated myeloid cells in the 3D-HTLM when stimulated with TLR4-agonist LPS, which points to the potential of the 3D-HTLM to study respiratory viruses.

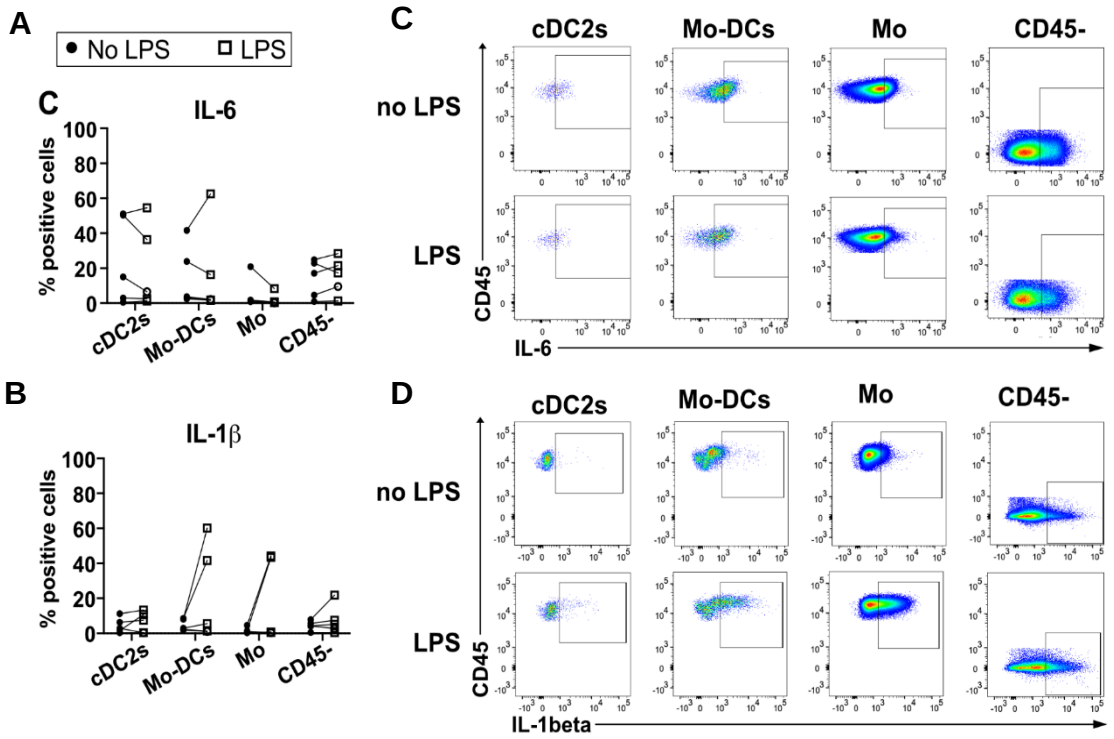

Figure 22. Baseline expression of cytokines IL-6 and IL-1β using flow cytometry analysis. Monocyte-derived dendritic cells are the most responsive to LPS stimulation in expression of IL-1β (B). Each subtype of immune cell demonstrates different ability to express either IL-6 or IL-1β upon stimulation with LPS.

3.4 Discussion

This study presents a functional 3D-HTLM consisting of HPMECs, SAECs, HPFs, and lung resident immune cells differentiated from $CD14^+$ monocytes. The SAECs were grown at ALI to promote differentiation and functionality, as has been demonstrated in previous studies [95, 96, 102]. SAECs grown at ALI continued to develop tight junctions, consequentially increasing the barrier integrity. The 3D positioning of cells within the model also aided in the barrier integrity of the cellular layers, as observed in other similar models [27, 28, 103]. HPMECs within the model demonstrated functionality by expressing markers correlated with intracellular signaling. CD31/PECAM is the "gold standard" for identification of HPMECs, and functions as an inhibitor to reduce cellular activation [104]. HPMECs were identified as $CD31/PECAM^+$ using both flow cytometry and immunofluorescence (IF).

$CD14^+$ myeloid cells isolated from human PBMCs successfully migrated into the 3D lung tissue environment from the endothelial layer. Upon migration into the tissue environment, myeloid cells were able to adapt and differentiate to occupy the resident lung immune cell niche. Input $CD14^+$ myeloid cells upregulated tissue resident markers such as CD169, CD206, and CD163 after residing within the lung environment for four days. AMs were also identified from cells harvested from the 3D-HTLMs in both morphology and functionality. Cells identified as AMs showed increased cytoplasmic space with "lacy" patterns and upregulated CD71 and CD206, which are well-documented characteristics of AM *in vivo* [91, 99, 105]. Other studies have also demonstrated myeloid cell plasticity in adapting to local *in vitro* environments [15, 106]. However, the study presented here is the only known 3D *in vitro* lung model able to

model the migration and differentiation of myeloid cells into an environment consisting of primary human cells.

Cells within the 3D-HTLM were able to demonstrate a response to LPS challenge, indicating the potential for utilizing the models for future viral studies. Twenty-four hours post-activation with LPS, cells were harvested, and the supernatant was collected to measure the response. BFA was added to select models to halt the secretion of cytokines and chemokines for flow cytometry analysis. ICAM is a common activation marker expressed by HPMECs and ATII cells [100, 101]. Activated $CD31^+$ endothelial cells significantly upregulated ICAM, while $CD31^-$ cells showed no change in ICAM expression. This further demonstrates functionality of HPMECs within the 3D-HTLM. Costimulatory markers were not upregulated by immune cells upon LPS activation, which is similar to a study where brochoalveolar lavage (BAL) cells stimulated with heat-killed bacteria showed no change in CD86 expression [107]. These results suggest that input myeloid cells may be activated before or upon introduction to the 3D-HTLM environment. Other functional responses to LPS stimulation includes increased expression of IL-10 and donor-dependent secretion of TNF-α. An *ex vivo* lung tissue study also demonstrated increased TNF-α and IL-10 secretion upon LPS-activation, maintaining macrophages as primary producers of TNF-α [108].

The findings in this study present a unique 3D-HTLM consisting of primary human cells and a collagen hydrogel. Functionality of cells within the model as well as the activation response demonstrate the potential for the model to study immune responses to lung pathogens.

CHAPTER IV

MEASURING IMMUNE RESPONSE TO RSV USING THE 3D-HTLM

4.1 Introduction

Respiratory syncytial virus (RSV) is a leading cause of severe respiratory issues such as bronchiolitis and pneumonia in infants. Severe cases lead to the yearly hospitalization of approximately 58,000 [109] and death of 100-500 children under 5 [110]. In addition to young children, elderly individuals 65 years and older are also susceptible to severe complications from RSV. According to the CDC in 2021, an estimated 177,000 adults over the age of 65 are hospitalized with 14,000 cases resulting in death [111]. With the growing prevalence of RSV complications, researchers have sought to further understand the virus' mechanism and why it adversely affects vulnerable populations.

Many types of models are currently utilized to study RSV tropism and treatment options. For instance, animal models are commonly used to aid in determining vaccinations and treatments for RSV. The most common animal models include non-human primates such as chimpanzees and baboons, sheep, and rodents, such as rats, mice, and ferrets [112].

While animal models are useful in exploring treatment options for RSV, no animal can fully encompass the same pathogenesis as is observed in humans due to different physiological traits. Therefore, *in vitro* models using primary human cells are an ideal candidate for studying the immunological response to RSV infection to create better treatment options in the future. Therefore, the aim of this study was to utilize the three-dimensional human tissue-engineered lung model (3D-HTLM) to examine the response of human primary in different age groups to RSV.

RSV is an enveloped single-stranded RNA virus infects and replicates via lung epithelial cells. Potential cellular receptors to allow for RSV entry includes annexin II [113], CX3 chemokine receptor 1 (CX3CR1) [114, 115], epidermal growth factor (EGF) receptor [116], calcium-dependent lectins [113], toll-like receptor 4 (TLR4) [117, 118], intercellular adhesion molecule 1 (ICAM-1) [119], nucleolin [120, 121], and heparan sulfate proteoglycans (HSPGs) [122]. Once RSV enters epithelial cells, a response cascade is triggered through cytokine and chemokine signaling, which recruits immune cells such as peripheral mononuclear cells (PMNs) and macrophages (Fig. 23). Since these binding and entry sites have been previously defined, this study focused on the downstream innate cellular response post-RSV infection.

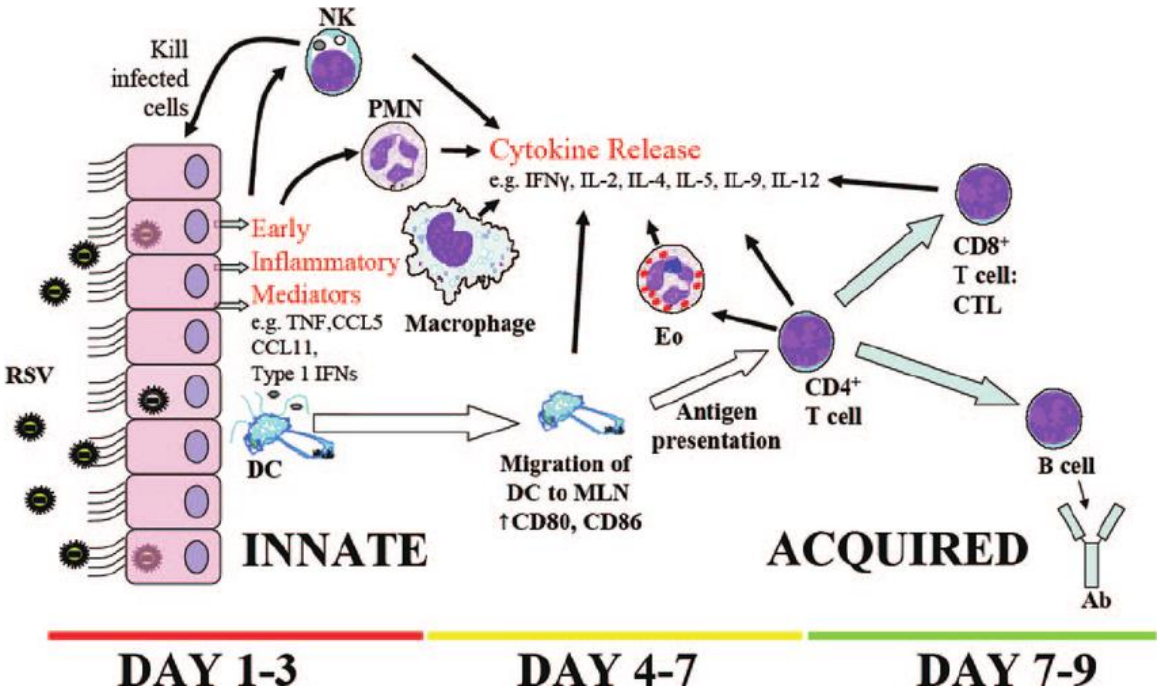

Figure 23. RSV infection and response cascade adapted from Openshaw et. al [2]. Epithelial cells infected with RSV initially trigger recruitment of peripheral mononuclear cells such as monocytes as well as macrophages with early inflammatory mediators. Immune cells recruited to the area then produce both inflammatory and anti-inflammatory cytokines and chemokines. T cells recruited from the cytokine storm aid in acquiring immunity to future RSV infections.

An inflammatory immune response is triggered upon viral entry and replication, with severe cases resulting in airway obstruction [123]. Two immune response mechanisms that are currently understood to aid in mitigating RSV infections are T helper (T_H) cell responses T_H1 and T_H2, each which secrete various cytokines. A T_H1 response releases cytokines that mainly activates T cytotoxic cells and macrophages, where a T_H2 response releases cytokines that activates B cells. Cytokines known to upregulate during a T_H1 response to RSV include interleukins (IL)-2, -1α and 1β, -3, -12, and -18, interferon (IFN)-γ, tumor necrosis factor (TNF)-β, granulocyte macrophage-colony-stimulating factor (GM-CSF), and sCD25. Cytokines upregulated during a T_H2

response to RSV include IL-4, -6, -9, -10, and -13 IL-5, IL-10, and IL-13. Other immune molecules released during an RSV infection include IL-8, -17A, and -33, and chemokine ligands (CCL) -2, -3, -4, -5, and CXCL10 [124]. Specific cells involved in producing these key molecules during the RSV immune response are conventional dendritic cells (cDCs), cDCs produce key cytokines including IL-6, -8, -10, -13, and -2, TNF-α, CCL2 and IFN-γ [125]. Macrophages and monocytes secrete IL-1β, IFNβ, TNF-α, and CCL2 [126, 127]. Other primary lung cells also contribute to the immune response, such as endothelial cells and fibroblasts, which produce IFN-α and -β [128].

Costimulatory molecules, which activates the T-cell response, includes HLA-DR, CD40, CD86, and PDL1, which are secreted by monocytes, dendritic cells, and macrophages [129]. The understood immune response correlated with RSV infection in healthy adults is classified as a T_H1 response, as this is the typical response observed to eliminate viral infections [124, 130, 131]. However, in RSV-infected neonates, an unbalanced T_H2 response is observed with upregulation of proinflammatory cytokines such as IL-4, -5, and -8, resulting in in increased severity of infection [124, 132]. Although these studies have provided initial insight into the immune response of RSV in neonates, most studies utilize mouse models in attempt to understand the human immune response to RSV, which is inherently physiologically and immunologically different from responses observed *in vivo*.

Recent studies have also examined RSV in *in vitro* lung cell culture. One study in particular focused on the infectivity of RSV in primary human bronchial epithelial cells at an air-liquid interface [133]. In this study, RSV successfully infected the primary epithelial cells *in vitro.* Another *in vitro* models have focused strictly on the immune

response, using isolated monocyte-derived dendritic cells (MoDCs) and T cells [134]. While these models give insight into specific cell response to RSV, the 3D-HTLM in this study was able to examine the combined response of multiple primary cell types to an RSV infection.

Immunocompromised populations, including neonates and elderly, are at a higher risk of developing complications caused by an RSV infection. These complications can include bronchiolitis, pneumonia, wheezing, and in neonatal populations, increased risk of developing asthma later in life. While the exact cause of the increased severity is not yet understood, the underlying cause of respiratory complications from a viral infection arises from an unbalanced immune response when uncontrolled levels of proinflammatory cytokines can cause tissue damage [135]. This leads to respiratory issues due to the injury to the epithelial layer, as well as overall inflammation of lung tissues which results in airway obstruction [136]. While neonates seem to primarily suffer from RSV infections due to an imbalance of Th1/Th2 immune response, the elderly population may have increased RSV susceptibility from lower levels of RSV-specific $CD4^+$ and $CD8^+$ T cells when compared to young to middle-aged adults [137, 138].

Although RSV adversely affects other immunocompromised populations such as those over the age of 65, fewer studies have been conducted to analyze the cause of increased severity in these vulnerable groups. One apparent contributing factor to elevated symptoms and complications resulting from RSV infection are preexisting conditions such as cardiovascular or respiratory comorbidities [139]. Additionally, RSV can exacerbate other preexisting diseases in the elderly. One study performed in New York state demonstrated that RSV was the underlying cause of over 10% of lower

respiratory tract infections (LRTIs), 11.4% increase in chronic obstructive pulmonary disease (COPD) complications, 7.2% of asthma exacerbations, and 5.4% of congestive heart failure exacerbations [140]. However, there it has not been distinguished if the actual immune response in elderly adults differs from that of those under the age of 65, and if the disparity in immune response is the cause of increased severity.

The aim of this study was to utilize a novel three-dimensional human tissue-engineered lung model (3D-HTLM) to study the response of immunocompromised populations to RSV infections, particularly neonates and elderly. The 3D-HTLM was constructed using human primary small airway epithelial cells (SAECs), human pulmonary microvascular endothelial cells (HPMECs), and human pulmonary fibroblasts (Fig. 8). After the resident cells grew to confluency, we sought to occupy the immune cell niche using $CD14^{+}$ myeloid cells isolated from three age groups: neonates from donor umbilical cord blood, adults (ages 33-60), and elderly (ages 65+), both of which sourced myeloid cells from donor buffy coats. The myeloid cells resided within the model for four days to allow for migration into the tissue layer, particularly into the epithelium where it has previously been shown that the myeloid cells differentiate into resident alveolar macrophages. Costimulatory markers were measured to determine activation levels within each subpopulation, as well as within the alveolar macrophage (AM) and interstitial macrophage (IM) populations. These results indicated the use of an *in vitro* 3D-HTLM to study immunological response to RSV and response differences between age groups during RSV infection.

4.2 Materials and methods

4.2.1 Cell culture

Primary small airway epithelial cells (SAECs) (PromoCell Cat. #12642, Heidelberg, Germany) and human pulmonary microvascular endothelial cells (HPMECs) (PromoCell Cat. #12281) were cultured as previously described. Briefly, T75 cell culture flasks were coated with a fibronectin solution (25 μg/mL) in DPBS for two hours. The coating solution was then removed and replaced with the manufacturer's recommended media: complete small airway epithelial cell media (PromoCell Cat. #21070) for epithelial cells and complete endothelial cell growth medium MV2 (PromoCell Cat. #22022). Human pulmonary fibroblasts (HPFs) (PromoCell Cat. #12360) were previously expanded from a stock culture and cryopreserved until added directly to the 3D-HTLM.

4.2.2 Isolation of myeloid cells

Peripheral blood mononuclear cells (PBMCs) were isolated from donor Buffy coats as previously described. Briefly, PBMCs were first separated from plasma and red blood cells using Ficoll-Paque™ PLUS (GM Healthcare) density-gradient centrifugation, and subsequently washed using bovine serum albumin-enriched DPBS buffer. Isolated myeloid cells included classical $CD14^{++}CD16^{-}$, non-classical $CD14^{+}CD16^{++}$, intermediate $CD14^{++}CD16^{+}$ monocytes, and small populations of dendritic cells (DCs) such as classic dendritic cell 2 (cDC2s) and monocyte-derived dendritic cells (mo-DCs), which were separated from the PBMC population using a Pan Monocyte Isolation Kit (Miltenyi Biotec, Catalog #130-096-537). Highly pure monocytes and dendritic cells remained unlabeled, while magnetically conjugated antibodies selectively labeled remaining PBMCs. Cells were separated using magnetic LS columns to isolate monocyte and dendritic cell populations, which were then frozen in $10x10^{6}$ cell/mL aliquots.

Neonatal myeloid cells were isolated from donor umbilical cord blood using lymphocyte separate media (LSM; Corning Cat. #25-072-CV) and MojoSort Human Pan Monocyte Isolation Kit (BioLegend Cat. #480060). PBMCs were separated from whole cord blood using centrifugation in 50 mL Leucosep tubes (Greiner Bio-one Cat. #227290). Subsequent PBMCs were then sorted into $CD16^+$ monocytes using MojoSort Human Pan Monocyte Isolation Kit by magnetically labelling non-myeloid cells to negatively select for monocytes and dendritic cells. Myeloid cells were then cryopreserved in $5x10^6$ aliquots until added to complete 3D-HTLM.

4.2.3 Construction of 3D-HTLM

The 3D-HTLM was constructed using the methods described above (Fig. 8). Briefly, HPFs were seeded into a collagen hydrogel in 24 well 0.8 μm PET porous membrane hanging cell culture inserts (CellTreat Cat. #230639, Pepperell, MA) at a concentration of 75,000 cells/mL. SAECs were then seeded on the top of the collagen hydrogels at a concentration of 150,000 cells/cm^2 and grown submerged in CSAEC media for 7 days, or until confluent. Once confluent, media was removed from the top and the cell culture inserts were inverted into a 12 well plate, where HPMECs were added to bottom side of the PET membrane at a concentration of 150,000 cells/cm^2. After the HPMECs attached to the PET membrane (4 hours), the inserts were reverted into the 24 well plates and the SAECs grew at air-liquid interface (ALI), while the HPMECs remained submerged. The media was changed to BASAL media upon the addition of the HPMECs. The models complete with the resident cells grew for an additional week, or until the HPMECs were confluent.

Once the HPMECs were confluent, myeloid cells were added to the endothelial layer of the model. For one age comparison study, neonate cord blood myeloid cells were added to 12 models, middle-aged donor (ages 37-62) myeloid cells were added to 12 models, and elder (ages 65+) myeloid cells were added to 12 models. Myeloid cells resided in the complete model for 4 days to allow for migration and differentiation into resident immune cells. Cells were infected with RSV titer on the third day, 24 hours before digesting and harvesting cells from models.

4.2.4 RSV infection

RSV was acquired from Dr. Oomen's lab at Oklahoma State University College of Veterinary Medicine. Wildtype RSV used in these experiments are from A2 strain, and red fluorescence protein (RFP)-RSV have SH open reading frame (ORF) replaced with turboRFP (Evrogen). Models were infected with a multiplicity of infection of 10 (MOI 10) 24 hours prior to harvesting the cells. MOI was based on approximated SAEC number per model, calculated based on seeding density and doubling time. RSV titer was thawed and diluted in BASAL media to required concentration. MOI 10 RSV was then added to the epithelial layer of each model in 30 μL aliquots. 30 μL of media was removed from the bottom well to maintain ALI during the 24-hour incubation.

4.2.5 Phenotypic characterization of cells in 3D-HTLM

Prior to staining for flow cytometry, models were digested by adding 2.2 mg/mL collagenase-D to the top of the model in the hanging insert and outer chamber, then incubating for 15-20 minutes. To aid in digestion, models were aspirated from the hanging insert and mixed with the collagenase solution, then returned to the incubator

until no visible collagen gel remained and cells were suspended in a homogenous suspension. Cell suspensions were collected into respective centrifuge tubes and spun at 1200 rpm for 5 minutes at 4°C and counted using Trypan blue to approximate viability.

Cells collected from models were stained with ZombieAqua viability dye (Biolegend) for 15 minutes at room temperature. Cells were then blocked with FcR block (Invitrogen) for 5 minutes before the addition of antibodies specific for myeloid cells (Table 1). Cells were fixed with 4% paraformaldehyde for 10 minutes on ice. Cells were run on an LSRII (BD Biosciences), BD Accuri™ C6, or Cytek Aurora (Cytek).

To determine infectivity of epithelial cells in the model, SAECs were grown on collagen hydrogels. Collagen hydrogels were first added to hanging cell culture inserts as previously described. After polymerization, the hydrogels were then coated with fibronectin coating solution for 2 hours. The coating solution was then removed and SAECs were seeded on top of the hydrogels. SAECs were grown submerged in complete small airway epithelial cell media (PromoCell, Heidelberg, Germany) for one week, and were then exposed to air-liquid interface for an additional week. On day 14, the SAECs were infected with red-fluorescence protein (RFP)-labeled RSV with multiplicities of infection (MOI) 10 and 15. Samples were fixed 24, 48, and 72 hours after infection using 4% paraformaldehyde. Fixed samples were then removed from the cell culture insert and stained with cytokeratin 14 (CK-14) (1:50) followed by a secondary anti-mouse Ig PE. Samples were then counterstained and mounted onto microscope slides using ProLong antifade mountant with NucBlue (ThermoFisher Catalog #P36983) and were analyzed using a Zeiss LSM 980 with Airyscan 2 confocal microscope.

4.2.6 Functional response of 3D-HTLM to RSV infection

To measure levels of secreted cytokines, supernatants from complete models was collected during digestion and stored at -80°C. Supernatant was collected from models both with and without myeloid cells (middle-aged donors only). Secretion of CXCL10, CCL2, IL-1β, IFNβ, IL-10, and IL-6 were quantified using a Luminex assay (R&D systems cat #LXSAHM) as per the manufacturer's instructions. The Luminex assay was read on a BioPlex 200 (Bio-Rad).

4.2.7 Epithelial barrier integrity

Trans-epithelial electrical resistance (TEER; $\Omega \cdot cm^2$) was measured using an EVOM3 (World Precision Instruments) to analyze the effect of RSV on the epithelial barrier integrity of the model. To determine the contribution to barrier integrity of each layer of the 3D-HTLM, TEER was measured for collagen hydrogels, HPFs seeded collagen hydrogels, HPFs seeded collagen hydrogels with SAECs, and HPFs seeded collagen hydrogels with SAECs and HPMECs. TEER was measured on models without myeloid cells. Measurements were taken at each medium change (every 36 hours) for 13 days, and then 24, 48, and 72 hours after infection with RSV (MOI 10). The values were normalized to the resistance of a blank cell culture insert with medium following the equation:

$$TEER = \left(R_{sample} - R_{control}\right) \times A \qquad \text{(Eq. 1)}$$

where R_{sample} is the measured resistance of the experimental sample (Ω), $R_{control}$ is the arithmetic mean of the blank cell culture insert (Ω), and A is the area of the PET membrane in the cell culture insert (0.33 cm^2).

4.2.8 Statistical analysis

Experiments were performed in triplicates and models containing middle-aged myeloid cell donors were performed with >3 independent replicates. Flow cytometry was analyzed with FlowJo 10. Graphpad Prism 9 was used for statistical analysis. Paired two-tailed t-test or one-way ANOVA with Tukey's multiple comparisons test or Sidak's multiple comparisons test was used as appropriate. Flow cytometry in experiment comparing age difference was normalized to uninfected 40-year-old donor. * signifies $p<0.05$, ** signifies $p<0.01$, *** signifies $p<0.001$, **** signifies $p<0.0001$.

4.3 Results

4.3.1 Functional response to RSV determines concentration and infection time

The first step of utilizing the 3D-HTLM to study the response of human primary lung cells to an RSV infection was determining the appropriate concentration and infection time to measure a response to RSV. A preliminary experiment was performed to examine infectivity of epithelial cells at varying RSV concentrations and infection times, which helped determine the RSV concentration for the following experiments (Fig.25). These results indicate an increased infection rates over time at MOI 10, with peak infectivity at 72 hours. However, at MOI 15, infectivity decreased between 48 and 72 hours, which could be caused by viral death in the culture or epithelial cell death. Infectivity presented by these images help provide insight into RSV infection rate with models containing only epithelial cells. Furthermore, the myeloid cells reside in the model for 3 days when RSV is introduced to the culture, which could present different infectivity data than epithelial cells alone. One study demonstrated that primary human

monocyte-derived macrophages show significant decrease in macrophage survival at MOI 10 48 hours post-infection, proving the delicate state of macrophages and myeloid cells in activated culture conditions [141]. Future experiments can investigate the optimal infection conditions for resident cells within the 3D-HTLM.

As previously mentioned, myeloid cells do not remain viable in cell culture for extended periods of time, so to maintain myeloid cell populations, the 3D-HTLMs were infected for 24 hours. To determine the RSV concentration for models containing myeloid cells in order to observe an immune response from cells in the 3D-HTLM, full models were infected with RSV at multiplicities of infection (MOI) of 0.1, 1, 2 and 10. Response of the cells was measured by performing a Luminex assay to measure secretion of CCL2, IL-1β, IL-10, IL-6, IFNβ, and CXCL10. This panel of cytokines and chemokines gives a profile of both upstream and downstream responses to RSV infection (Fig. 24). For instance, CCL2, also known as monocyte chemoattractant protein-1 (MCP-1) recruits monocytes to respond to initial infection, and is primarily expressed by myeloid cells. Additionally, CXCL10 is another early inflammatory mediator that recruits immune cells that secrete IFNγ in response to respiratory infections. Increased CXCL10 levels have been shown to reduce viral load and pathogenesis and are primarily associate with a type 1 immune response [142] IL-6 and IL-10 are expressed further downstream as inflammatory and anti-inflammatory cytokines, respectively. IL-6 promotes recruitment and differentiation of macrophages in viral infections. Another pro-inflammatory cytokine is IL-1β, which is commonly upregulated in viral infections. IL-10 is a potent anti-inflammatory cytokine and works to maintain balance in the immune response by preventing prolonged inflammatory conditions, which can ultimately damage tissue.

IFNβ is a precursor to IL-10, and has shown to increase IL-10 production in dendritic cells [143]. IFN-β is produced by macrophages, dendritic cells, fibroblasts, and epithelial cells.

Early mediator CCL2 demonstrated a significant increase in expression in both uninfected and infected models containing myeloid cells when compared to models without myeloid cells (Fig. 24). CCL2 is produced by monocytes, fibroblasts, endothelial, and epithelial cells, which could explain the increased expression levels in models with myeloid cells. Given the diverse population involved in CCL2 production, CCL2 signaling is a complex mechanism. However, it can be postulated that the MOI 2 group experienced lower levels of CCL2 when compared to the uninfected (UI) and MOI 10 group due to lower levels of CCL2-producing monocytes and a decreased production of CCL2 from other cells within the models. Monocytes may have increased production of CCL2 at MOI 10 in response to the higher viral load. Both CXCL10 and IFNβ noticeably increased in models with and without myeloid cells infected with MOI 10 RSV, while IL-10 was significantly upregulated in uninfected and RSV MOI 10-infected models with myeloid cells. Similar to CCL2, the concentration of IL-10 in models infected with RSV MOI 2 could be caused by lower levels of monocytes within the system. Increased levels of IFNβ may have induced increased levels of IL-10 production among myeloid cells within the model. IL-10 is also produced by myeloid cells, which could also explain the higher levels in models with myeloid cells. While there was no significant difference between any groups in production of IL-6 and IL-1β, there was a noticeable decrease in IL-1β in models with myeloid cells. The upregulation of IL-10 in models with myeloid cells could suppress levels of pro-inflammatory cytokines such as IL-1β.

Models infected with MOIs 0.1-2 did not demonstrate a significant response to RSV infection, while MOI 10 induced a response significantly different compared to the control and MOI 2 group by noticeably upregulating CXCL10, and significantly upregulating CCL2 (Fig. 24). Models infected with RSV at MOI 2 responded in a similar manner to uninfected models. Increased levels of CXCL10 in infected models indicates signaling to recruit additional immune cells upon RSV infection. The data also support that the presence of myeloid cells increases signaling for recruitment of monocytes with CCL2, which ultimately aids in immune response to RSV. Myeloid cells within the model also increases levels of anti-inflammatory cytokine IL-10, which may suppress IL-1β secretion.

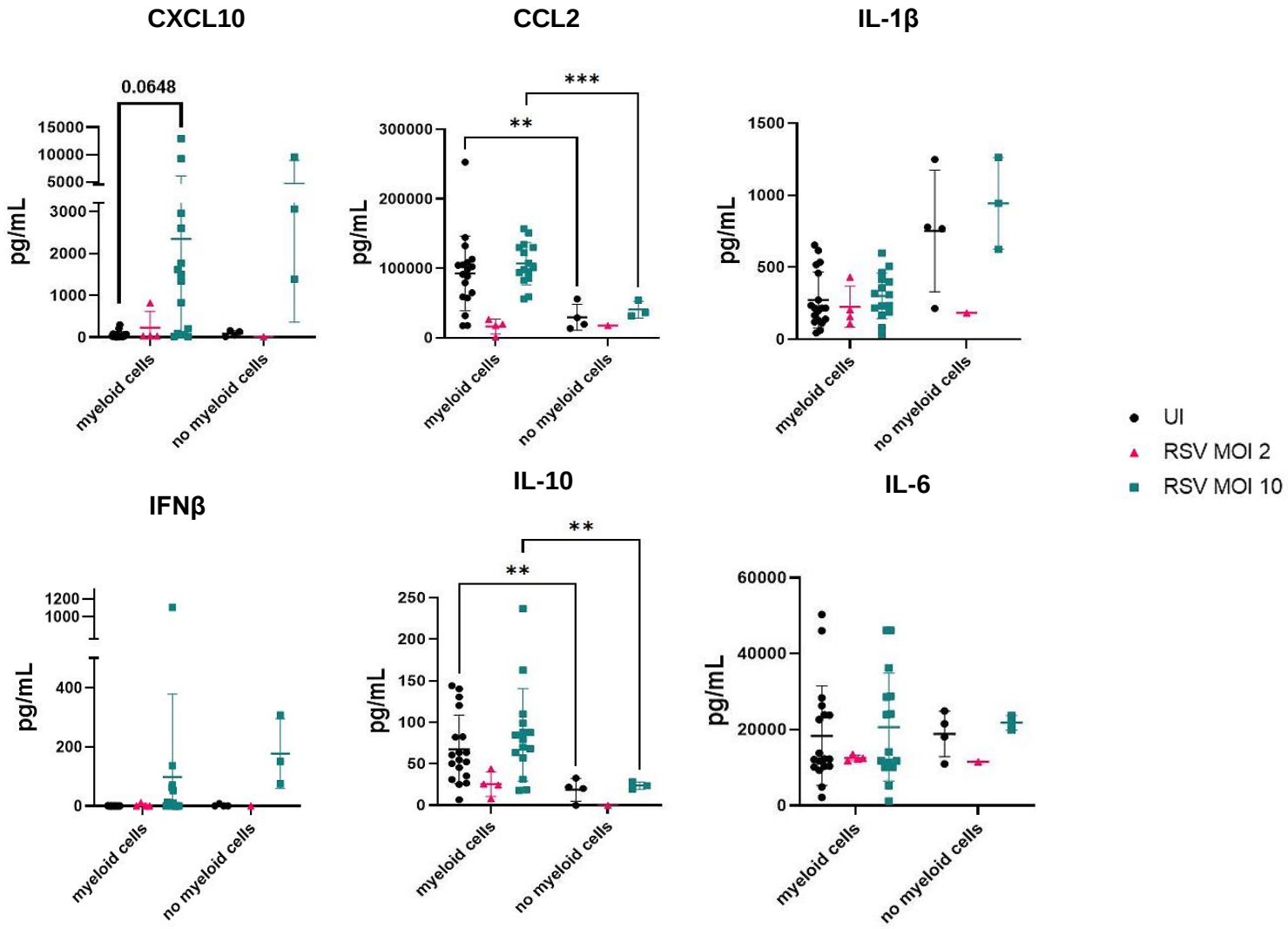

Figure 24. Chemokine and cytokine response to indicate response of 3D-HTLM to RSV infection. There was a noticeable increase in CXCL10, interferon β (IFNβ), and interleukin (IL)-10 between the uninfected (UI) and infected groups with myeloid cells, indicating a response to RSV. There was also a significant difference in expression of CCL2 and IL-10 between the groups with and without myeloid cells, which supports the main immune response observed in the 3D-HTLM originates from the myeloid cells. * signifies $p<0.05$, ** signifies $p<0.01$, *** signifies $p<0.001$. Myeloid cells N=18; no myeloid cells N=3.

In addition to characterizing the immune response to an RSV infection in the 3D-HTLM, we also sought to measure physiological response of endothelial and epithelial layers. The first objective was to analyze infectivity of varying concentrations of RSV

over a period of 72 hours in epithelial cells. SAECs were seeded onto collagen hydrogels and grown to confluence at air-liquid interface (ALI). Once confluence, the SAECs were then infected with either MOI 10 or MOI 15 red-fluorescence protein RSV. Samples were then fixed at 24, 48, and 72 hours, after which they were stained using PE-conjugated CK-14 to visualize epithelial cells. Samples were counterstained with DAPI and mounted onto slides to analyze using confocal microscopy (Fig. 25). The results show that RSV infectivity increased in epithelial cells over time at MOI 10, with the peak infectivity at 72 hours, while infectivity with MOI 15 peaked between 24 and 48 hours. Decreased infectivity at MOI 15 can possibly be explained by either death of the virus in the sample, or epithelial cell death from the high RSV concentration.

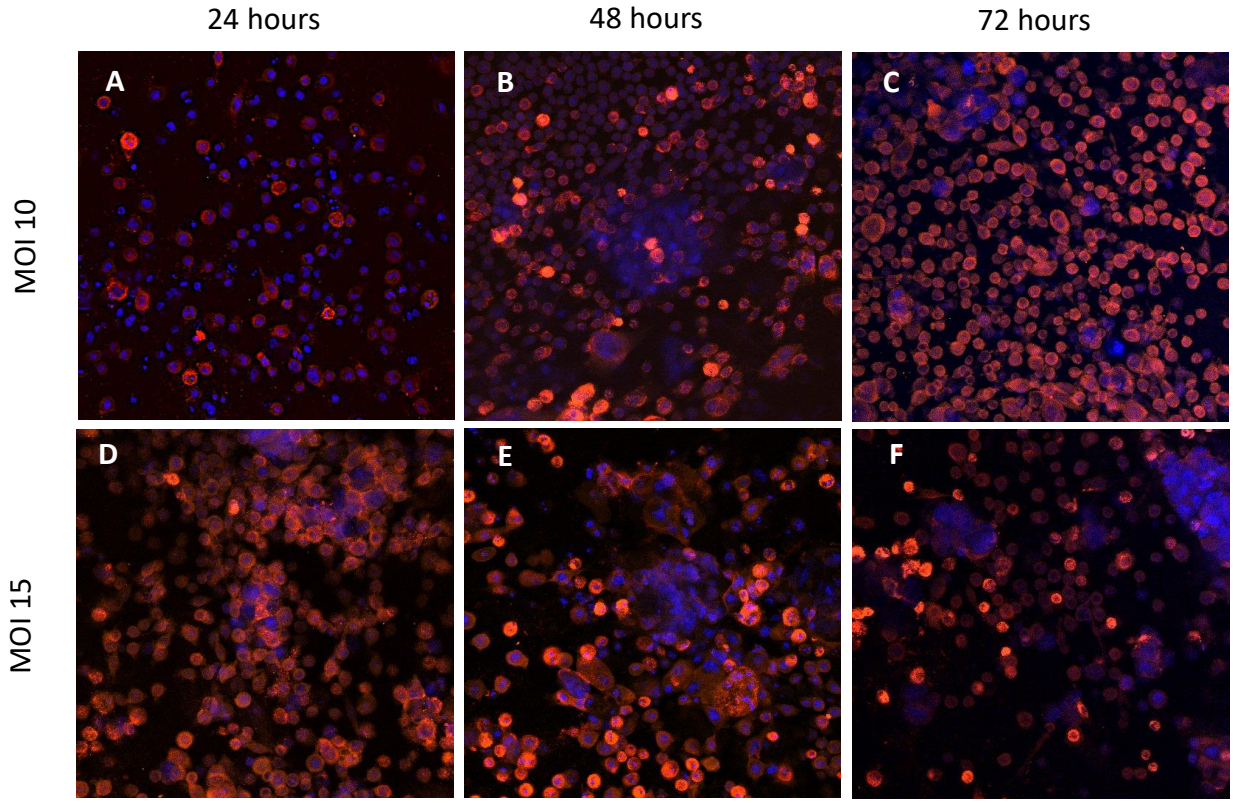

Figure 25. Confocal imaging (400x) of SAECs infected RSV MOI 10 for 24, 48, and 72 hours (A-C, respectively) and MOI 15 for 24, 48, and 72 hours (D-F, respectively). The nuclei of the cells are labeled with DAPI (blue) and SAECs are identified with CK-14 (R-PE) (orange). The RSV expresses a red fluorescence protein (RFP) once the epithelial cells are infected.

To further understand the physiological effects of RSV on the human lung over time, TEER tests were performed to measure the barrier integrity of the epithelial layer after infection of MOI 10 RSV. Measurements were taken during the growth period of the epithelial cells and 24, 48, and 72 hours after RSV infection. Data was normalized to uninfected SAEC-only models.

Before RSV infection at t=0 hr, models containing both HPMECs and SAECs had a significantly higher TEER reading when compared to models with only SAECs (Fig. 26). This indicates significantly higher barrier integrity when the cells are grown in co-culture, which reinstates the importance of both cells in co-culture to develop increased barrier integrity as well as mimic more *in vivo*-like conditions. Within 24 hours after infection with RSV, all infected models experienced barrier damage. However, 48 hours after infection, models with both HPMECs and SAECs recovered barrier integrity relatively greater than uninfected SAEC models as well as infected SAEC models. It is possible that the presence of the endothelial cells aids in the repair of the epithelial barrier upon physiological damage induced by RSV infection. The SAEC-only infected models were also able to begin recovery of barrier integrity 48 hours after infection, but the rate of recovery was lower than the models with HPMECs and SAECs. 72 hours after RSV infection, there was no significant difference in the barrier integrity relative to the uninfected SAEC models.

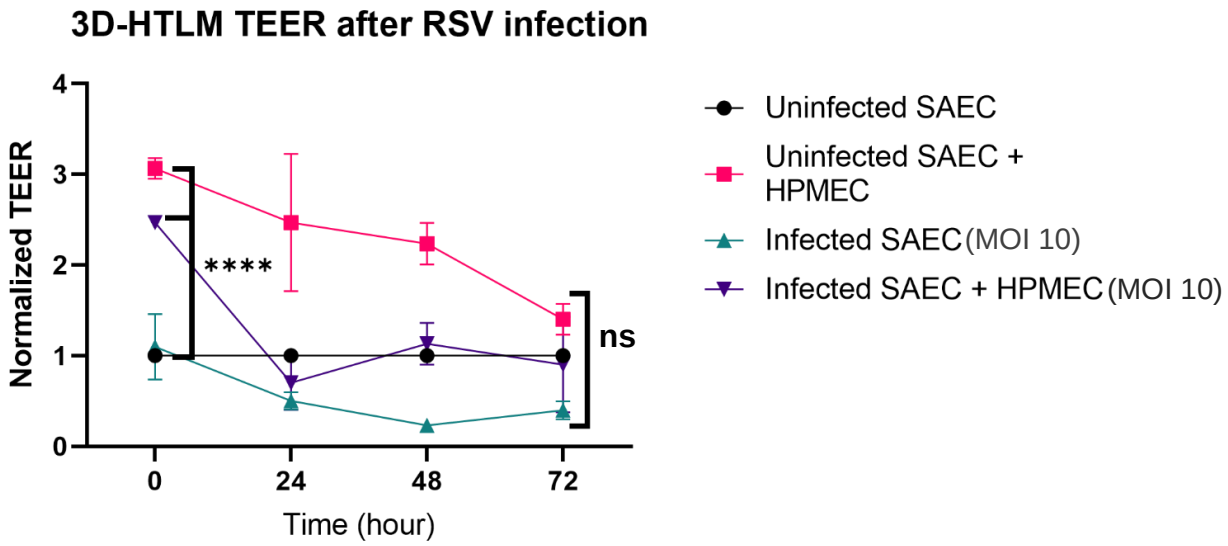

Figure 26. Trans-epithelial electrical resistance (TEER) measurements of different cell layers of 3D-HTLM after infection with RSV (MOI 10). Data normalized to uninfected SAEC group. Initial TEER measurements reveal that the models with both SAEC and HPMEC cell layers have significantly higher TEER than SAEC only models. After 72 hours of RSV infection, models do not have significantly different TEER readings when compared to uninfected SAEC models.

4.3.2 Adult myeloid cells in the 3D-HTLM demonstrate response to RSV infection

In order to establish the capability of cells to demonstrate a response to RSV infection within the 3D-HTLM, we first sought to characterize the response of normal adult cells to RSV in the 3D-HTLM environment. Known tissue resident markers for lung immune cells include CD169, CD206, and CD163. Models were infected with RSV by adding the virus to the epithelial layer and incubating for 24 hours before digesting and harvesting the cells. Once harvested from the models, cells were stained for flow cytometry to confirm populations of each myeloid cell subgroup, conventional dendritic cell 2s (cDC2s), monocyte-derived dendritic cells (mo-DCs), classic monocytes (monocytes), and non-classical $CD16^{+}$ monocytes ($CD16^{+}$ monocytes). The

differentiation of each subpopulation into resident immune cells was then determined using tissue resident markers CD169, CD206, and CD163 (Fig. 27). Although both infected and uninfected subpopulations of each group demonstrated high donor variability in differentiation into resident tissue immune cells, tissue residency markers were expressed in all subsets of myeloid cells. Additionally, the proportion of myeloid cells was not affected after a 24-hour RSV infection. Since both uninfected and infected populations showed no significant difference in resident cell marker expression, the presence of RSV did not alter the proportion of differentiated immune cells present before infection.

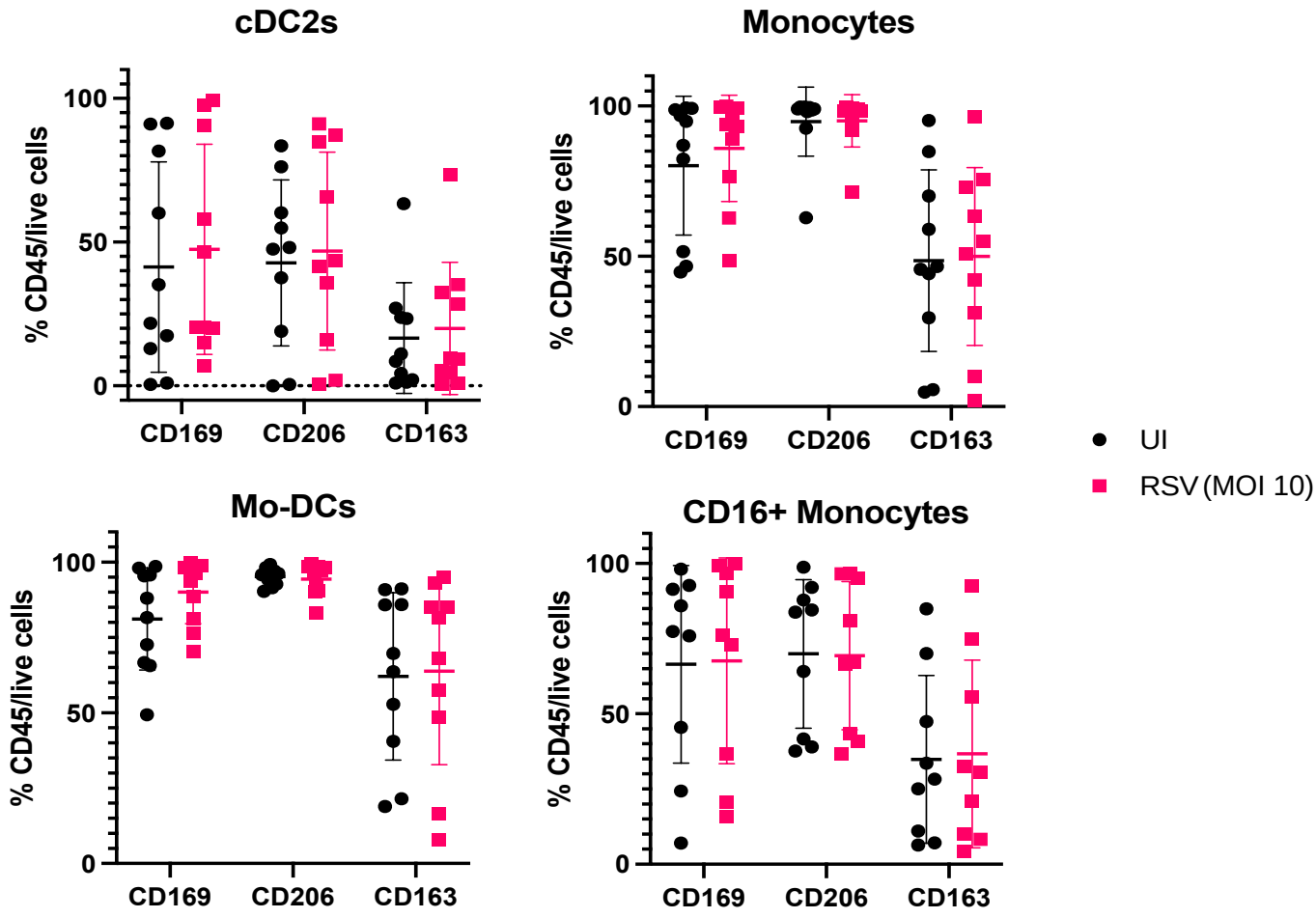

Figure 27. Characterization of subpopulations of myeloid cells to identify tissue resident immune cells. Classic monocytes (Mo), non-classic CD16^{+} monocytes (CD16^{+} Mo) and monocyte-derived dendritic cells (Mo-DCs) show skewed populations high in levels of CD169 and CD206, indicative of alveolar macrophages (AMs) in both uninfected and RSV-infected (MOI 10) models. n=10, ages 30-60

Flow cytometry was also used to measure activation levels of myeloid cell subpopulations using characteristic costimulatory T cell activation markers CD40, CD86, HLA-DR, and PDL1 (Fig. 28). While there was no significant increase in activation markers, certain individuals demonstrated upregulation of CD86 and PDL1 in the mo-DC and classic monocyte populations. It can be observed that HLA-DR decreased expression

in certain individuals in all myeloid cell populations. It was shown in the previous study that the cells are activated upon introduction to the 3D-HTLM environment, which could upregulate levels of costimulatory markers before activation with RSV.

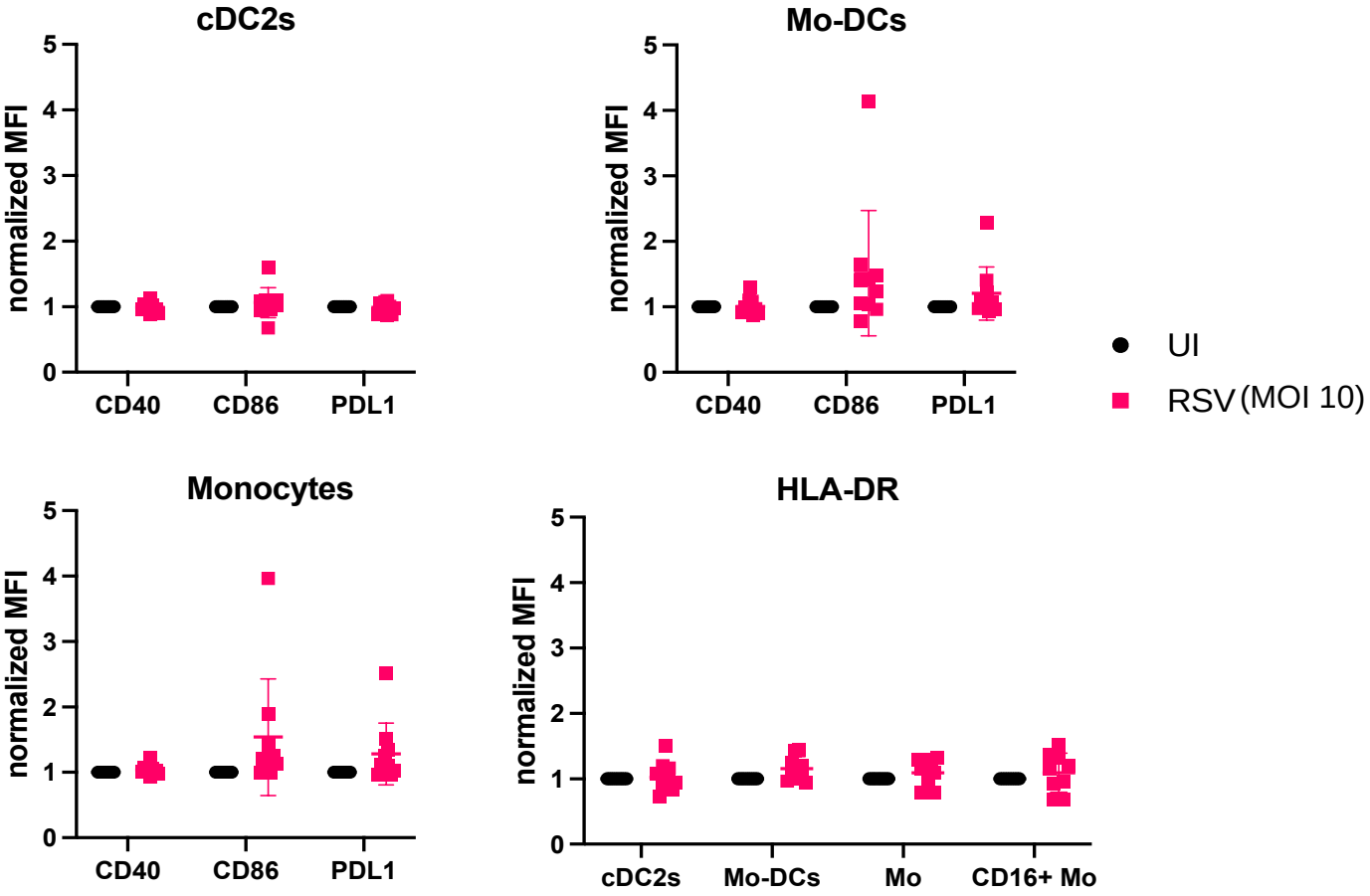

Figure 28. Activation levels of different myeloid cell subpopulations in individuals after 24-hour RSV infection (MOI 10). There was no significant change in costimulatory activation markers of any subpopulation, and there was decreased expression of HLA-DR in some individuals of each subpopulation. Likewise, one individual demonstrated a dramatic increase in expression of CD86 and PDL1 in classic monocytes (Mo) and monocyte-derived dendritic cells (Mo-DCs), and a few individuals also showed slight increase in CD86 and PDL1 in classic monocytes and Mo-DCs. This indicates that the 3D-HTLM environment induced activation. Data normalized to uninfected group. N=10 ages 30-60

4.3.3 Costimulatory expression levels remain consistent between normal and immunocompromised individuals after RSV infection

Immunocompromised individuals at a higher risk of developing severe complications due to RSV infection include children under the age of 2 and adults over the age of 65. We sought to identify potential contributing factors to the cause of severe RSV infections in these immunocompromised groups by first investigating the levels of characteristic costimulatory markers CD40, CD86, PDL1, and HLA-DR with flow cytometry. Costimulatory markers regulate T cell activation, proliferation, and migration, and are an indicator of early immune cells triggering an immune response cascade.

Four distinct subpopulations of myeloid cells from all three age groups expressed varying levels of each marker (Fig. 29). Input cells are myeloid cells characterized directly after isolation from donor blood samples, while uninfected and RSV-infected cells reside within the 3D-HTLM for a total of four days. Neonatal Mo-DCs and Mo increased levels of HLA-DR after RSV infection, while the other groups decreased expression level after infection. Another consistent difference was a noticeable decrease in CD86 expression in neonatal myeloid cell populations after RSV infection while all but $CD16^{+}$ Mo increased expression. CD40 also demonstrated a slight change in expression level in the neonatal myeloid cells when compared to the two adult groups. However, these levels do not significantly vary between vulnerability level and cell type. The difference in normalized expression levels between both infected and uninfected cells recovered from the model can be accounted for in donor variability (Fig. 28). Previous work has shown that myeloid cells become activated upon introduction to the

3D-HTLM, which can explain increased levels of costimulatory markers in both uninfected and RSV-infected models.

Tissue resident cells also expressed distinct levels of costimulatory markers. Cells were first sorted into AMs and IMs using tissue resident markers CD206, CD169, CD71, and CD163. IMs were distinguished from AMs by selecting for $CD14^{+}$ expression. Measurements of costimulatory marker expression was then quantified in both macrophage populations (Fig. 30). Although there are slight differences in marker expression among age groups, the change in normalized mean fluorescence intensity (MFI) is comparable to the differences observed between donors in previous work (Fig. 28). It can also be noted that the cells appear to be activated upon introduction to the 3D-HTLM environment due to a baseline expression of costimulatory markers in uninfected input cells.

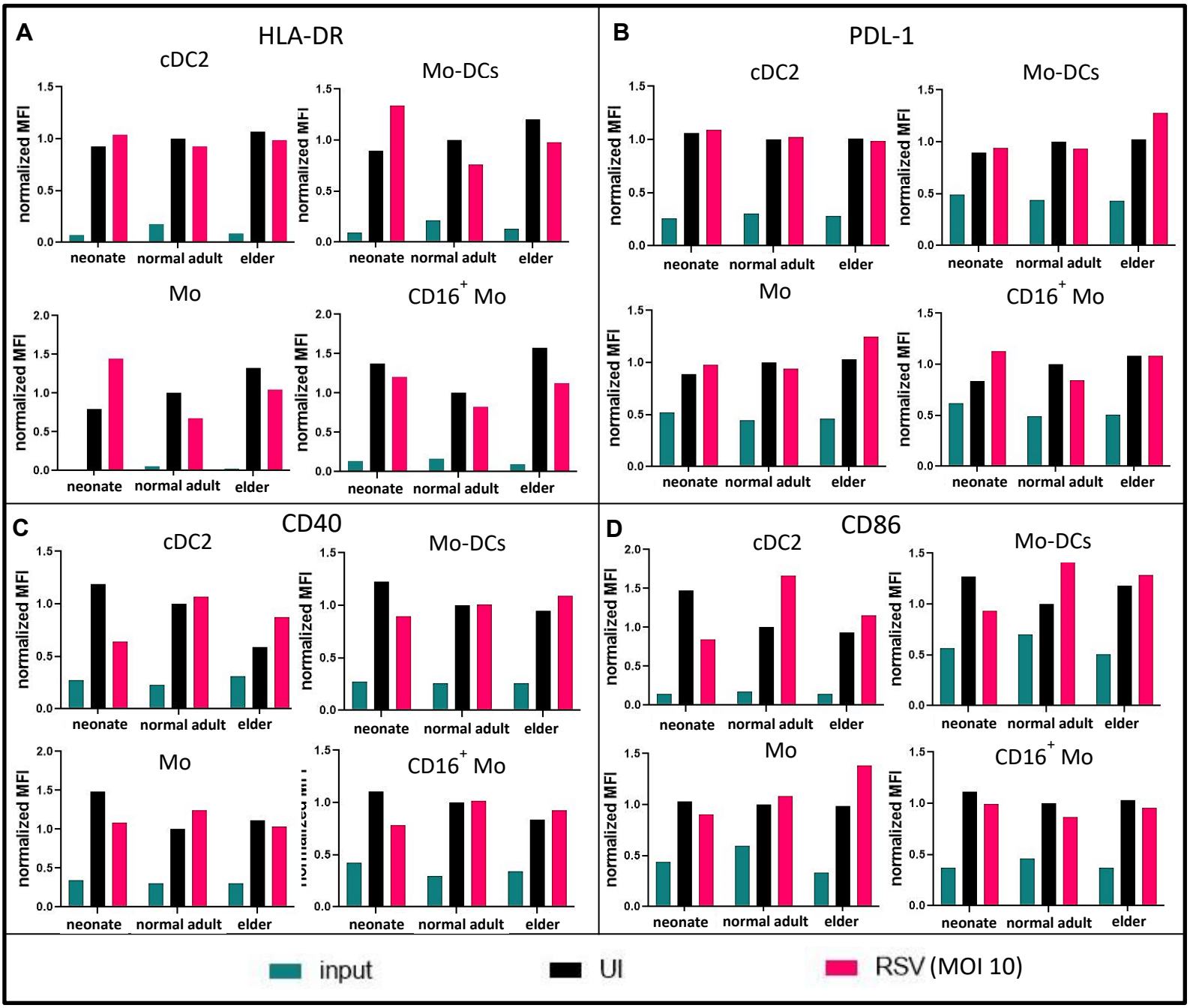

Figure 29. Costimulatory marker levels in subpopulations of cells in three different donor age groups. Input cells are myeloid cells not introduced to the 3D-HTLM environment and not infected with RSV. While some cells show a noticeable change in costimulatory markers after a 24-hour RSV infection (MOI 10), these differences are similar to variation in expression levels between normal adult donors. MFI normalized to 40-year-old uninfected female.

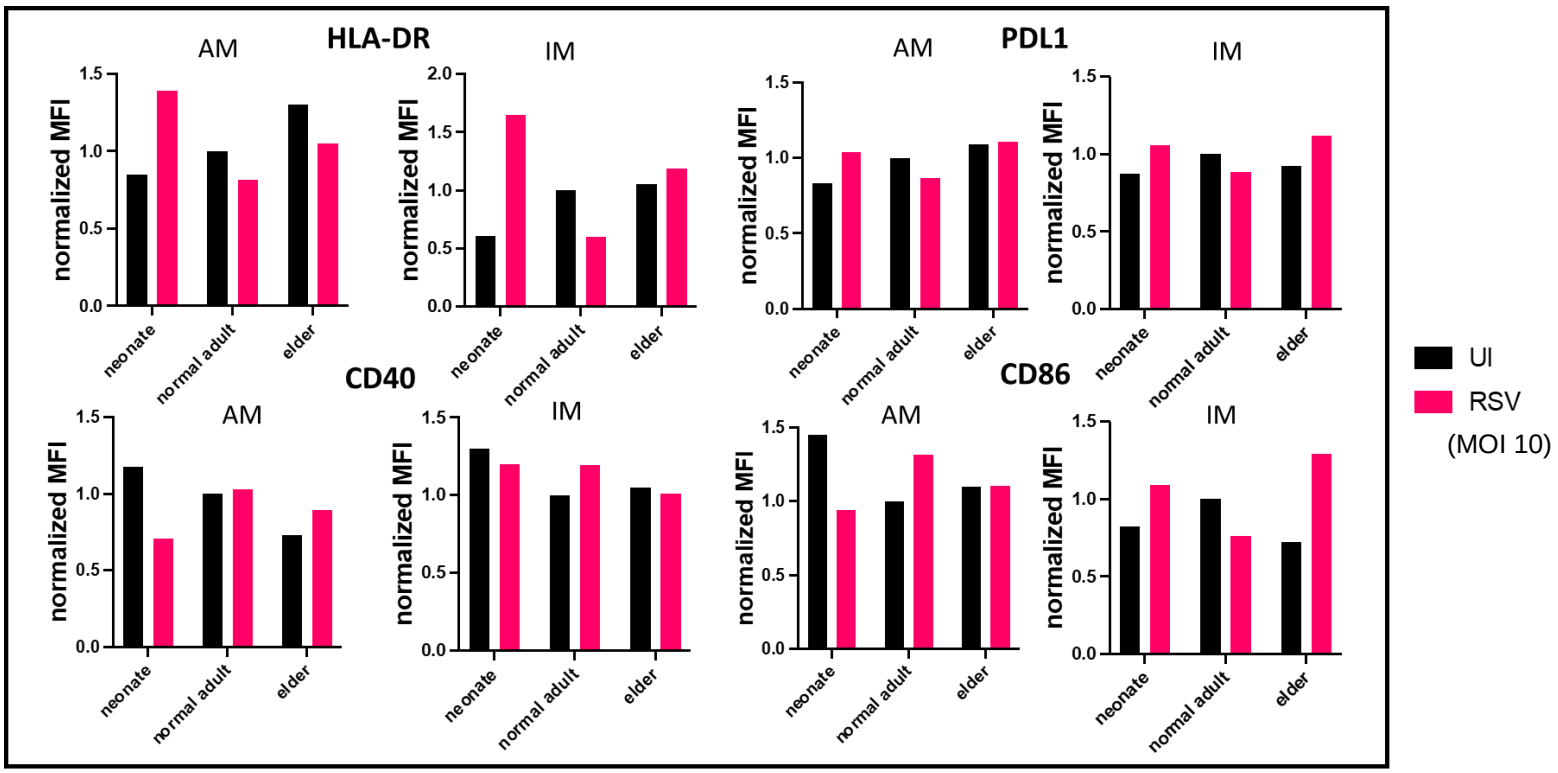

Figure 30. Expression levels of costimulatory markers in tissue resident immune cells. While there are noticeable differences in some costimulatory marker expression, such as HLA-DR after RSV (MOI 10) infection in neonatal interstitial macrophages (IM) and alveolar macrophages (AM), as well as increased expression in CD 86 in elder interstitial macrophages (IMs), these distributions are similar to variability between individuals. This indicates insignificant overall expression levels and impact of costimulatory markers in macrophages in response to RSV infection across all age groups. MFI normalized to uninfected 40-year-old-female.

4.4 Discussion

In this study, we demonstrate the ability of the 3D-HTLM to be utilized to study the response of immunocompromised groups to RSV. Cells isolated from neonatal and elderly individuals were able to differentiate into resident immune cells within the 3D-HTLM and demonstrated similar costimulatory marker levels when compared to normal adult populations. The presence of RSV did not significantly affect the proportion of cells expressing tissue resident markers in adult myeloid cells (Fig. 27). However, there was great variability between donors in the expression levels of tissue resident markers

CD169, CD206, and CD163. High donor variability was also observed in the previous study that compared input myeloid cells to cells harvested from 3D-HTLM.

The physiological properties of models with HPMECs and SAECs were characterized with infectivity and TEER. Infectivity of SAECs at different concentrations and time points was tracked using IHC staining and confocal microscopy. SAECs demonstrated highest infectivity at 72 hours when infected with MOI 10 of RSV. However, SAECs infected with MOI 15 had peak infectivity at 48 hours. This could be caused by death of virus particles in the models or SAEC death. Future studies can look to optimize RSV concentration and time when infecting the 3D-HTLM, which is limited by myeloid cell viability in the model.

Models containing HPMECs and SAECs as well as only SAECs demonstrated a decreased barrier integrity to RSV infection in the 3D-HTLM. Models containing only SAECs had lower TEER values overall when compared to models with both HPMECs and SAECs. This indicates lower barrier integrity, which shows that cell-cell interactions do impact cellular barrier functionality. As was expected from the results of other studies, all models experienced decreased barrier integrity after infection with RSV [144, 145]. However, models with both HPMECs and SAECs were able to recover barrier integrity 24 hours after infection, whereas models with only SAECs only slightly recovered barrier integrity between 48 and 72 hours. This is consistent with a similar study that compared the barrier integrity of a monoculture of an alveolar epithelial cell line with a co-culture of the same cell line with microvascular endothelial cells after a lipopolysaccharide (LPS) challenge [103].

Costimulatory markers, such as CD40, CD86, PDL1, and HLA-DR regulate T cell recruitment and migration. Adult myeloid cells (ages 37-62) did not demonstrate significant upregulation in costimulatory markers upon infection with RSV. While these models did not noticeably increase or decrease levels of the costimulatory markers, it may be worthwhile to create future models with T cells to examine if the presence of T cells affects costimulatory marker expression. However, the micro-bead array revealed a noticeable upregulation in CXCL10, which has been observed in a clinical RSV with adults [146]. Other upregulated cytokines included IFNβ and a significant upregulation in IL-10, both of which are anti-inflammatory and were also highly upregulated in other published work studying RSV infection [147, 148]. Models without myeloid cells had significantly lower levels of CCL2 and IL-10. Along with the fibroblasts, epithelial cells, and endothelial cells, myeloid cells produce CCL2. CCL2 also regulates monocyte recruitment and migration, so the presence of myeloid cells in the model could explain higher levels of CCL2 when compared to the models lacking myeloid cells. Interestingly, one study demonstrated supplemented levels of IL-10 in neonatal mouse models decreased the severity of RSV response [148]. Complications from RSV infections arise from an overabundance of inflammation, and IL-10 is a powerful anti-inflammatory cytokine. It is a possible that 3D-HTLMs developed with myeloid cells from neonatal and elderly populations infected with RSV will demonstrate reduced levels of IL-10 production when compared to cells from healthy adults. Some of these studies also resulted in significant upregulation of IL-6 upon RSV infection, but as previously noted, IL-6 appears to express in high levels before RSV infection in models both with and without myeloid cells. Cytokines such as IL-6 and CCL2 can be expressed in

homeostasis, which can explain similar expression levels between uninfected and infected groups [149-151].

Myeloid cells from immunocompromised populations were also able to differentiate into resident immune cells within the 3D-HTLM (Fig. 30). When comparing costimulatory markers between the age groups, there was an increase in CD86 in all groups except for the neonatal cells. However, the differences in the normalized levels of costimulatory markers between age groups is similar to variability between individuals in our previous study. Furthermore, from the data presented here, it can be concluded that cells from all age groups are able to differentiate into tissue resident immune cells as well as respond to an RSV challenge with costimulatory marker expression within the 3D-HTLM.

This study validated the use of a novel 3D-HTLM to study the response of RSV in immunocompromised populations using primary myeloid cells. The model presented here can be a useful tool to better understand the disparity between the immune response of a healthy adult and immunocompromised populations to an RSV infection, which could be the next step in finding better treatment options to reduce and hopefully prevent virus-related complications.

CHAPTER V

CONCLUSIONS AND FUTURE WORK

In this study, a novel three-dimensional human tissue-engineered lung model (3D-HTLM) was characterized and validated to study the difference in immunological responses to respiratory syncytial virus (RSV) between varying age groups. In doing so, this 3D-HTLM can be used in the future to understand the difference in immune response to RSV in immunocompromised groups such as children under the age of 2 and elderly adults over the age of 65. These groups are at an increased risk of suffering severe complications from an RSV infection, such as bronchiolitis and pneumonia [152]. These complications are caused by an unbalanced immune response, which leads to inflammation in the lungs and airway obstruction [124]. By understanding the immune response in these immunocompromised groups, steps can be taken to reduce or eliminate complications caused by RSV infection.

The main objective of this study was to develop and characterize a 3D-HTLM to study the immune response of vulnerable populations to RSV. We used the characterized 3D-HTLM to test the hypothesis that myeloid cells would successfully differentiate into resident immune cells when introduced to the 3D lung environment and demonstrate a

response to LPS. Furthermore, we also tested the hypothesis that myeloid cells introduced to the 3D-HTLM from immunocompromised individuals would demonstrate a different response to RSV infection when compared to a normal healthy adult.

To meet this objective, we performed three separate studies. The first part focused on determining culture conditions that could support the growth and development of all three resident cell types within the 3D-HTLM. The second study included characterizing and validating the immunocompetence of the 3D-HTLM. To achieve this, myeloid cells isolated from normal adult donor PBMCs were introduced to the 3D-HTLM to migrate into and differentiate within the model. The models were then challenged with LPS to measure the immune response. The third study involved determining the response of immune cells from neonatal and elderly donors to RSV infection within the 3D-HTLM to compare the response of immunocompromised populations with healthy adults to RSV. We demonstrated the differentiation of myeloid cells into resident immune cells within the 3D-HTLM and immunocompetence by challenging the cells with lipopolysaccharide (LPS). The 3D-HTLM was then utilized to observe the immune response of vulnerable individuals to RSV.

From our first study, we can conclude:

i. All three resident cell types (HPFs, HPMECs, and SAECs) within the 3D-HTLM were able to grow in a basal small airway epithelial cell media completed with endothelial cell MV2 supplements (defined as “basal media” for these studies). The growth and viability of cells in this media system was comparable to the control media, which was defined as the manufacturer’s recommended media for

all respective cell types. As a result, the 3D-HTLM was grown in the basal media once HPMECs were added to the model.

ii. The majority of resident cells used in the 3D-HTLM experienced increased growth rates and viability when media was changed every 7 days when compared to every 3 days.

iii. SAECs demonstrated low viability when grown submerged for the growth period of the 3D-HTLM. SAECs were expected to remain more viable at an air-liquid interface (ALI), which resembles *in vivo* conditions.

From our second study, we can conclude:

i. SAECs grown at air-liquid interface (ALI) on the collagen hydrogel develop tight junctions, which increases the barrier integrity to form a more *in vivo*-like environment.

ii. SAECs and HPMECs were identified in the 3D-HTLM using characteristic markers cytokeratin 14 and CD31, respectively. This demonstrates normal phenotype of the resident cells within the 3D-HTLM.

iii. $CD14^+$ cells isolated from peripheral blood mononuclear cells (PBMCs) were able to migrate into the matrix of the 3D-HTLM after entering through the endothelial layer. Myeloid cells were identified in images of immunohistochemical (IHC)-stained samples between the endothelial and epithelial layers.

iv. Myeloid cells differentiated and adopted characteristic resident tissue markers CD169, CD206, and CD163 after residing four days within the 3D-HTLM environment. Alveolar macrophages were identified from the model both morphologically and functionally by upregulating CD71 and CD206. Alveolar

macrophages are key in studying immune responses, particularly to lower respiratory viruses such as RSV.

v. Cells demonstrated a response to LPS challenge. HPMECs upregulated key inflammatory marker ICAM. Additionally, costimulatory markers were not upregulated after LPS challenge, which could indicate activation prior to or upon entry into the 3D-HTLM environment. However, LPS stimulation upregulated IL-10 and TNF-α, which demonstrated a response to LPS and established the immunocompetency of the 3D-HTLM.

From our third study, we can conclude:

i. 24 hours of RSV infection did not affect the viability of myeloid cells or the proportion of cells expressing tissue resident markers, CD206, CD169, and CD163.

ii. Costimulatory markers are not significantly upregulated for any age group when infected with RSV. This further supports that the 3D-HTLM environment alone may activate the cells.

iii. Adult immune cell response to RSV included a significant upregulation in CXCL10, IFNβ, and IL-10, which demonstrates the ability for immune cells to respond to RSV while in the 3D-HTLM, and that the immune cells are the primary source of the response to an RSV infection.

iv. Costimulatory markers were expressed in each population group, demonstrating how the 3D-HTLM can be utilized to study the response to RSV in immunocompromised populations.

v. Immunocompromised age groups were able to differentiate into distinct populations of myeloid cells and macrophages, validating the use of the 3D-HTLM to continue to study the immune response of these vulnerable populations to RSV.

vi. RSV damages barrier integrity of epithelial cell layer within the model, but the presence of endothelial cells supports faster recovery of the barrier integrity after physiological damage when compared to models with only epithelial cells.

In conclusion, the 3D-HTLM used in these studies was able to support cellular responses to challenges from LPS as well as RSV infection. Myeloid cells from vulnerable populations were also able to differentiate into resident tissue immune cells after residing within the 3D-HTLM for four days. From this study, it can be concluded that costimulatory marker expression does not drive progression of RSV infection in vulnerable populations such as elders and neonates. However, future studies can focus on more functional responses to RSV using the 3D-HTLM, such as cytokine and chemokine expression levels. This 3D-HTLM also provides an alternative to other models, such as monoculture or animal models, to study immune responses from respiratory viruses. In addition to studying the immune response to RSV, the 3D-HTLM can be utilized to study the immune response of other respiratory viruses in vulnerable populations.

Consequently, future work will be directed to addressing the following points:

1) **Examine effect on functionality of immune cells after RSV reinfection in the 3D-HTLM**

The studies presented here focused on a singular RSV infection in human lung cells *in vitro* for 24 hours. However, adults are often reinfected with RSV multiple times throughout their lives. Other studies have shown that immune cells respond differently after RSV reinfection, particularly focusing on the pathogenic recall response. For instance, one study examined reinfecting adult mice with RSV after recovering from neonatal RSV infection [153]. Reinfected adults demonstrated increased proinflammatory cytokine release when compared to mice only infected as adults. Additionally, an increase in innate effector cell recruitment was observed after a secondary exposure to RSV. These functional disparities can now be studied in the 3D-HTLM to observe any change in immune functionality after a secondary RSV infection.

2) **Analyze functional response of myeloid cells from vulnerable groups to RSV within 3D-HTLM**

While costimulatory markers often indicate immune response levels of cells, additional functional response to an RSV infection also includes cytokine and chemokine expression. Cytokines are an integral part of immune functionality, and unbalanced cytokine levels are often the cause of increased disease severity. Therefore, studying functional cytokine response to an RSV infection in vulnerable populations is imperative to understanding the full immune response and understanding the difference between RSV infection in healthy adults and vulnerable individuals. Proinflammatory cytokines such as IL-1, TNF-α, IFN-γ, and IL-6 have been shown to upregulate during RSV infection and are linked to tissue damage [154-156]. Anti-inflammatory

cytokines including IL-10 and IL-12 help maintain homeostasis of inflammation during infection [157, 158]. Therefore, it can be hypothesized that severe RSV infection in vulnerable populations can be linked to imbalanced cytokine expression when compared to healthy adults.

3) **Investigate response of $CD4^+$ and $CD8^+$ T cells to RSV infection in 3D-HTLM**

In addition to studying monocyte, dendritic cell, and macrophage response to RSV infection, another immune cell that could pose valuable insight into different response mechanisms includes T cells, including $CD4^+$ and $CD8^+$ T cells. Other studies have utilized T cells in conjunction with myeloid cells isolated from PBMCs to examine immune responses in different age groups. For instance, one study used $CD4^+$ T cells and isolated monocytes to test an RSV vaccine in *in vitro* models [134]. However, this study only utilized immune cells, whereas the 3D-HTLM will be able to provide a full lung tissue environment to study additional cell-cell interactions, which will show the response cascade from infection to T cell response. Another study linked a lack of RSV-specific memory $CD8^+$ T cells to increased RSV severity in the elderly and immunocompromised individuals with chronic obstructive pulmonary disease (COPD) [159]. Furthermore, by including additional immune cells in the 3D-HTLM, the model will be closer to mimicking an *in vivo* environment to not only study RSV infections, but also infection from other lung viruses in vulnerable populations.

REFERENCES

1. Promega, *CellTiter-Blue Cell Viability Assay*, Promega, Editor. 2016. p. 2.
2. Openshaw, P. and J. Tregoning, *Immune Responses and Disease Enhancement during Respiratory Syncytial Virus Infection.* Clinical microbiology reviews, 2005. **18**: p. 541-55.
3. Bhowmick, R. and H. Gappa-Fahlenkamp, *Cells and Culture Systems Used to Model the Small Airway Epithelium.* Lung, 2016. **194**(3): p. 419-428.
4. Nova, Z., H. Skovierova, and A. Calkovska, *Alveolar-Capillary Membrane-Related Pulmonary Cells as a Target in Endotoxin-Induced Acute Lung Injury.* International Journal of Molecular Sciences, 2019. **20**(4): p. 831.
5. Spacova, I., et al., *Topical Microbial Therapeutics against Respiratory Viral Infections.* Trends in Molecular Medicine, 2021. **27**(6): p. 538-553.
6. Medicine, J.H.U.o. *COVID-19 Dashboard by the Center for Systems Science and Engineering at John Hopkins University*. 2020 10/21/2020; Available from: https://coronavirus.jhu.edu/map.html.
7. Jeffery, P.K., *Morphologic features of airway surface epithelial cells and glands.* American Review of Respiratory Disease, 1983. **128**(2P2): p. S14-S20.
8. Pack, R., L. Al-Ugaily, and G. Morris, *The cells of the tracheobronchial epithelium of the mouse: a quantitative light and electron microscope study.* Journal of anatomy, 1981. **132**(Pt 1): p. 71.
9. Plopper, C.G., *Comparative morphologic features of bronchiolar epithelial cells: the Clara cell.* American Review of Respiratory Disease, 1983. **128**(2P2): p. S37-S41.
10. Bal, H. and N. Ghoshal, *Morphology of the terminal bronchiolar region of common laboratory mammals.* Laboratory animals, 1988. **22**(1): p. 76-82.
11. Reznik, G.K., *Comparative Anatomy, Physiology, and Function of the Upper Respiratory Tract.* Environmental health perspectives, 1990. **85**: p. 171.
12. Rehli, M., *Of mice and men: species variations of Toll-like receptor expression.* Trends in Immunology, 2002. **23**(8): p. 375-378.
13. Shultz, L.D., et al., *Humanized mice for immune system investigation: progress, promise and challenges.* Nature Reviews Immunology, 2012. **12**(11): p. 786-798.
14. Rongvaux, A., et al., *Human Hemato-Lymphoid System Mice: Current Use and Future Potential for Medicine.* Annual review of immunology, 2013. **31**(1): p. 635-674.

15. Evren, E., et al., *Distinct developmental pathways from blood monocytes generate human lung macrophage diversity.* Immunity, 2021. **54**(2): p. 259-275.e7.
16. Allen, T.M., et al., Humanized immune system mouse models: progress, challenges and opportunities. Nature Immunology, 2019. 20(7): p. 770-774.
17. Miller, L.A., et al., Nonhuman Primate Models of Respiratory Disease: Past, Present, and Future. ILAR Journal, 2017. 58(2): p. 269-280.
18. Groenen, M.A.M., et al., Analyses of pig genomes provide insight into porcine demography and evolution. Nature, 2012. 491(7424): p. 393-398.
19. Judge, E.P., et al., Anatomy and Bronchoscopy of the Porcine Lung. A Model for Translational Respiratory Medicine. American Journal of Respiratory Cell and Molecular Biology, 2014. 51(3): p. 334-343.
20. Stittelaar, K., et al., Ferrets as a Novel Animal Model for Studying Human Respiratory Syncytial Virus Infections in Immunocompetent and Immunocompromised Hosts. Viruses, 2016. 8(6): p. 168.
21. Thompson, C.I., et al., Infection of Human Airway Epithelium by Human and Avian Strains of Influenza A Virus. Journal of Virology, 2006. 80(16): p. 8060-8068.
22. Chen, A.-J., et al., Anti-H7N9 avian influenza A virus activity of interferon in pseudostratified human airway epithelium cell cultures. Virology Journal, 2019. 16(1).
23. Zhang, L., et al., Respiratory Syncytial Virus Infection of Human Airway Epithelial Cells Is Polarized, Specific to Ciliated Cells, and without Obvious Cytopathology. Journal of Virology, 2002. 76(11): p. 5654-5666.
24. Zhang, L., et al., Infection of Ciliated Cells by Human Parainfluenza Virus Type 3 in an In Vitro Model of Human Airway Epithelium. Journal of Virology, 2005. 79(2): p. 1113-1124.
25. Sims, A.C., et al., Severe Acute Respiratory Syndrome Coronavirus Infection of Human Ciliated Airway Epithelia: Role of Ciliated Cells in Viral Spread in the Conducting Airways of the Lungs. Journal of Virology, 2005. 79(24): p. 15511-15524.
26. Gorin, A.B. and P.A. Stewart, Differential permeability of endothelial and epithelial barriers to albumin flux. Journal of Applied Physiology, 1979. 47(6): p. 1315-1324.

27. Bian, Y., et al., Protective Effect of Kaempferol on LPS-Induced Inflammation and Barrier Dysfunction in a Coculture Model of Intestinal Epithelial Cells and Intestinal Microvascular Endothelial Cells. Journal of agricultural and food chemistry, 2020. 68(1): p. 160-167.

28. Kaeokhamloed, N., et al., New In Vitro Coculture Model for Evaluating Intestinal Absorption of Different Lipid Nanocapsules. Pharmaceutics, 2021. 13(5): p. 595.

29. Wang, J.H., et al., Effect of co-culturing human primary basic fibroblasts with respiratory syncytial virus-infected 16-HBE cells. Genetics and Molecular Research, 2016. 15(1).

30. Deng, Y., et al., An in vitro transepithelial migration assay to evaluate the role of neutrophils in Respiratory Syncytial Virus (RSV) induced epithelial damage. Scientific Reports, 2018. 8(1).

31. Ugonna, K., et al., Macrophages Are Required for Dendritic Cell Uptake of Respiratory Syncytial Virus from an Infected Epithelium. 2014. 9(3): p. e91855.

32. Foster, K.A., et al., Characterization of the A549 Cell Line as a Type II Pulmonary Epithelial Cell Model for Drug Metabolism. Experimental Cell Research, 1998. 243(2): p. 359-366.

33. Benam, K.H., et al., Small airway-on-a-chip enables analysis of human lung inflammation and drug responses in vitro. Nature Methods, 2016. 13(2): p. 151-157.

34. Johnson, M.D., et al., Alveolar Epithelial Type I Cells Contain Transport Proteins and Transport Sodium, Supporting an Active Role for Type I Cells in Regulation of Lung Liquid Homeostasis. Proceedings of the National Academy of Sciences - PNAS, 2002. 99(4): p. 1966-1971.

35. Dobbs, L., et al., The Great Big Alveolar TI Cell: Evolving Concepts and Paradigms. Cellular physiology and biochemistry, 2009. 25(1): p. 55-62.

36. Strengert, M. and U.G. Knaus, Analysis of epithelial barrier integrity in polarized lung epithelial cells, in Permeability Barrier. 2011, Springer. p. 195-206.

37. Chuquimia, O.D., et al., The role of alveolar epithelial cells in initiating and shaping pulmonary immune responses: communication between innate and adaptive immune systems. PLOS ONE, 2012. 7(2): p. e32125-e32125.

38. Mayer, A.K., et al., Airway epithelial cells modify immune responses by inducing an anti-inflammatory microenvironment. European Journal of Immunology, 2008. 38(6): p. 1689-1699.

39. Bonnans, C., et al., Synthesis and anti-inflammatory effect of lipoxins in human airway epithelial cells. Biomedicine & pharmacotherapy, 2007. 61(5): p. 261-267.

40. Chan, M.C.W., et al., Proinflammatory cytokine responses induced by influenza A (H5N1) viruses in primary human alveolar and bronchial epithelial cells. Respiratory research, 2005. 6(1): p. 135-135.

41. Matsukura, S., et al., Synthetic double-stranded RNA induces multiple genes related to inflammation through Toll-like receptor 3 depending on NF-kappaB and/or IRF-3 in airway epithelial cells. Clinical and experimental allergy, 2006. 36(8): p. 1049-1062.

42. Stegemann-Koniszewski, S., et al., Alveolar Type II Epithelial Cells Contribute to the Anti-Influenza A Virus Response in the Lung by Integrating Pathogen- and Microenvironment-Derived Signals. mBio, 2016. 7(3).

43. Gereke, M., et al., Alveolar Type II Epithelial Cells Present Antigen to CD4+ T Cells and Induce Foxp3+ Regulatory T Cells. American journal of respiratory and critical care medicine, 2009. 179(5): p. 344-355.

44. Debbabi, H., et al., Primary type II alveolar epithelial cells present microbial antigens to antigen-specific CD4+ T cells. American journal of physiology. Lung cellular and molecular physiology, 2005. 289(2): p. L274-L279.

45. Gomi, K., et al., Activation of NOTCH1 or NOTCH3 signaling skews human airway basal cell differentiation toward a secretory pathway. PloS one, 2015. 10(2): p. e0116507-e0116507.

46. Zuo, W.-L., et al., Ontogeny and Biology of Human Small Airway Epithelial Club Cells. American Journal of Respiratory and Critical Care Medicine, 2018.

47. Short, K.R., et al., Pathogenesis of influenza-induced acute respiratory distress syndrome. The Lancet Infectious Diseases, 2014. 14(1): p. 57-69.

48. Cheung, C.Y., et al., Induction of proinflammatory cytokines in human macrophages by influenza A (H5N1) viruses: a mechanism for the unusual severity of human disease? The Lancet (British edition), 2002. 360(9348): p. 1831-1837.

49. Coyne, C.B., et al., Regulation of airway tight junctions by proinflammatory cytokines. Molecular biology of the cell, 2002. 13(9): p. 3218-3234.

50. Herold, S., et al., Influenza virus-induced lung injury: pathogenesis and implications for treatment. European Respiratory Journal, 2015. 45(5): p. 1463-1478.

51. Zeng, H., et al., Human Pulmonary Microvascular Endothelial Cells Support Productive Replication of Highly Pathogenic Avian Influenza Viruses: Possible Involvement in the Pathogenesis of Human H5N1 Virus Infection. Journal of Virology, 2012. 86(2): p. 667-678.

52. Armstrong, S.M., et al., Influenza infects lung microvascular endothelium leading to microvascular leak: role of apoptosis and claudin-5. PloS one, 2012. 7(10): p. e47323-e47323.

53. Chan, M.C.W., et al., Influenza H5N1 virus infection of polarized human alveolar epithelial cells and lung microvascular endothelial cells. Respiratory research, 2009. 10(1): p. 102-102.

54. Ocana-Macchi, M., et al., Hemagglutinin-Dependent Tropism of H5N1 Avian Influenza Virus for Human Endothelial Cells. Journal of Virology, 2009. 83(24): p. 12947-12955.

55. Kwok, H.-H., et al., Anti-inflammatory effects of indirubin derivatives on influenza A virus-infected human pulmonary microvascular endothelial cells. Scientific Reports, 2016. 6(1): p. 18941.

56. Arnold, R. and W. König, Respiratory Syncytial Virus Infection of Human Lung Endothelial Cells Enhances Selectively Intercellular Adhesion Molecule-1 Expression. The Journal of Immunology, 2005. 174(11): p. 7359-7367.

57. Chang, C.-H., Y. Huang, and R. Anderson, Activation of vascular endothelial cells by IL-1α released by epithelial cells infected with respiratory syncytial virus. Cellular Immunology, 2003. 221(1): p. 37-41.

58. Pageau, S.C., et al., The effect of stromal components on the modulation of the phenotype of human bronchial epithelial cells in 3D culture. Biomaterials, 2011. 32(29): p. 7169-7180.

59. Sundström, K.B., et al., Andes Hantavirus-Infection of a 3D Human Lung Tissue Model Reveals a Late Peak in Progeny Virus Production Followed by Increased Levels of Proinflammatory Cytokines and VEGF-A. PLoS One, 2016. 11(2).

60. Wilkinson, D.C., et al., Development of a Three-Dimensional Bioengineering Technology to Generate Lung Tissue for Personalized Disease Modeling. STEM CELLS Translational Medicine, 2017. 6(2): p. 622-633.

61. Chen, Y.-W., et al., A three-dimensional model of human lung development and disease from pluripotent stem cells. Nature Cell Biology, 2017. 19(5): p. 542-549.

62. Derakhshani, S., et al., Measles Virus Infection Fosters Dendritic Cell Motility in a 3D Environment to Enhance Transmission to Target Cells in the Respiratory Epithelium. Frontiers in Immunology, 2019. 10.

63. Parenteau-Bareil, R., R. Gauvin, and F. Berthod, Collagen-Based Biomaterials for Tissue Engineering Applications. Materials, 2010. 3(3): p. 1863-1887.

64. Bhowmick, R., et al., A Three-Dimensional Human Tissue-Engineered Lung Model to Study Influenza A Infection. Tissue Engineering Part A, 2018. 24(19-20): p. 1468-1480.

65. Suzuki, T., C.-W. Chow, and G.P. Downey, Role of innate immune cells and their products in lung immunopathology. The International Journal of Biochemistry & Cell Biology, 2008. 40(6): p. 1348-1361.

66. Patel, V.I., et al., Transcriptional Classification and Functional Characterization of Human Airway Macrophage and Dendritic Cell Subsets. J Immunol, 2017. 198(3): p. 1183-1201.

67. Yu, Y.R., et al., Flow Cytometric Analysis of Myeloid Cells in Human Blood, Bronchoalveolar Lavage, and Lung Tissues. Am J Respir Cell Mol Biol, 2016. 54(1): p. 13-24.

68. Evren, E., et al., Distinct developmental pathways from blood monocytes generate human lung macrophage diversity. Immunity, 2021. 54(2): p. 259-275 e7.

69. Hu, G. and J.W. Christman, Editorial: Alveolar Macrophages in Lung Inflammation and Resolution. Front Immunol, 2019. 10: p. 2275.

70. van de Laar, L., et al., Yolk Sac Macrophages, Fetal Liver, and Adult Monocytes Can Colonize an Empty Niche and Develop into Functional Tissue-Resident Macrophages. Immunity, 2016. 44(4): p. 755-68.

71. Arango Duque, G. and A. Descoteaux, Macrophage Cytokines: Involvement in Immunity and Infectious Diseases. Frontiers in Immunology, 2014. 5(491).

72. Eichinger, K.M., et al., Alveolar macrophages support interferon gamma-mediated viral clearance in RSV-infected neonatal mice. Respir Res, 2015. 16: p. 122.

73. Short, K.R., et al., Influenza virus damages the alveolar barrier by disrupting epithelial cell tight junctions. European Respiratory Journal, 2016. 47(3): p. 954-966.

74. Pollara, G., et al., Dendritic cells in viral pathogenesis: protective or defective? Int J Exp Pathol, 2005. 86(4): p. 187-204.

75. Blom, B., et al., Developmental origin of pre-DC2. Hum Immunol, 2002. 63(12): p. 1072-

76. de Melo, B.A.G., et al., 3D culture models to study SARS-CoV-2 infectivity and antiviral candidates: From spheroids to bioprinting. Biomed J, 2021. 44(1): p. 31-42.

77. Rajan, D., et al., Response to Rhinovirus Infection by Human Airway Epithelial Cells and Peripheral Blood Mononuclear Cells in an In Vitro Two-Chamber Tissue Culture System. PLoS ONE, 2013. 8(6): p. e66600.

78. Franks, T.J., et al., Resident Cellular Components of the Human Lung: Current Knowledge and Goals for Research on Cell Phenotyping and Function. Proceedings of the American Thoracic Society, 2008. 5(7): p. 763-766.

79. Brody, A.R., et al., Analyzing the Genes and Peptide Growth Factors Expressed in Lung Cells in Vivo Consequent to Asbestos Exposure and in Vitro. Environmental health perspectives, 1997. 105(suppl 5): p. 1165-1171.

80. Pasman, T., et al., Development of an In Vitro Airway Epithelial–Endothelial Cell Culture Model on a Flexible Porous Poly(Trimethylene Carbonate) Membrane Based on Calu-3 Airway Epithelial Cells and Lung Microvascular Endothelial Cells. Membranes, 2021. 11(3): p. 197.

81. Sakolish, C., et al., A Model of Human Small Airway on a Chip for Studies of Subacute Effects of Inhalation Toxicants. Toxicological Sciences, 2022. 187(2): p. 267-278.

82. He, R.W., et al., Optimization of an air-liquid interface in vitro cell co-culture model to estimate the hazard of aerosol exposures. J Aerosol Sci, 2021. 153: p. 105703.

83. Joris, F., et al., Assessing nanoparticle toxicity in cell-based assays: influence of cell culture parameters and optimized models for bridging the in vitro-in vivo gap. Chem Soc Rev, 2013. 42(21): p. 8339-59.

84. Yao, Y., et al., Association between tumor necrosis factor-α and chronic obstructive pulmonary disease: a systematic review and meta-analysis. Therapeutic Advances in Respiratory Disease, 2019. 13: p. 175346661986609.

85. Armstrong, L., et al., Expression of Functional Toll-Like Receptor-2 and -4 on Alveolar Epithelial Cells. American Journal of Respiratory Cell and Molecular Biology, 2004. 31(2): p. 241-245.

86. Mubarak, R.A., et al., Comparison of pro- and anti-inflammatory responses in paired human primary airway epithelial cells and alveolar macrophages. Respiratory Research, 2018. 19(1).

87. Lambert, L., et al., Immunity to RSV in Early-Life. Frontiers in Immunology, 2014. 5.

88. Kopf, M., C. Schneider, and S.P. Nobs, The development and function of lung-resident macrophages and dendritic cells. Nature immunology, 2015. 16(1): p. 36.

89. Lavin, Y., et al., Regulation of macrophage development and function in peripheral tissues. Nature Reviews Immunology, 2015. 15(12): p. 731-744.

90. Lavin, Y., et al., Tissue-resident macrophage enhancer landscapes are shaped by the local microenvironment. Cell, 2014. 159(6): p. 1312-1326.

91. Patel, V.I., et al., Transcriptional Classification and Functional Characterization of Human Airway Macrophage and Dendritic Cell Subsets. 2016: p. 1600777.

92. Patel, V.I. and J.P. Metcalf, Airway macrophage and dendritic cell subsets in the resting human lung. Critical Reviews™ in Immunology, 2018. 38(4).

93. Chen, Y.X., et al., Three-dimensional Culture of Human Airway Epithelium in Matrigel for Evaluation of Human Rhinovirus C and Bocavirus Infections. Biomedical and Environmental Sciences, 2018. 31(2): p. 136-145.

94. Ghio, A.J., et al., Growth of human bronchial epithelial cells at an air-liquid interface alters the response to particle exposure. Particle and fibre toxicology, 2013. 10(1): p. 1-8.

95. Hackett, T.-L., et al., Intrinsic phenotypic differences of asthmatic epithelium and its inflammatory responses to respiratory syncytial virus and air pollution. American journal of respiratory cell and molecular biology, 2011. 45(5): p. 1090-1100.

96. Schneider, D., et al., Increased cytokine response of rhinovirus-infected airway epithelial cells in chronic obstructive pulmonary disease. American journal of respiratory and critical care medicine, 2010. 182(3): p. 332-340.

97. Bronchoalveolar lavage constituents in healthy individuals, idiopathic pulmonary fibrosis, and selected comparison groups. The BAL Cooperative Group Steering Committee. Am Rev Respir Dis, 1990. 141(5 Pt 2): p. S169-202.

98. Lewis, S., D. Singh, and C.E. Evans, Cyclic hydrostatic pressure and cotton particles stimulate synthesis by human lung macrophages of cytokines in vitro. Respiratory Research, 2009. 10(1): p. 44.

99. Yu, Y.-R.A., et al., Flow Cytometric Analysis of Myeloid Cells in Human Blood, Bronchoalveolar Lavage, and Lung Tissues. American Journal of Respiratory Cell and Molecular Biology, 2016. 54(1): p. 13-24.

100. Sawa, Y., et al., LPS-induced IL-6, IL-8, VCAM-1, and ICAM-1 Expression in Human Lymphatic Endothelium. Journal of Histochemistry & Cytochemistry, 2008. 56(2): p. 97-109.

101. Cho, R.-L., et al., Lipopolysaccharide induces ICAM-1 expression via a c-Src/NADPH oxidase/ROS-dependent NF-κB pathway in human pulmonary alveolar epithelial cells. American Journal of Physiology-Lung Cellular and Molecular Physiology, 2016. 310(7): p. L639-L657.

102. Kletting, S., Co-culture of human alveolar epithelial (hAELVi) and macrophage (THP-1) cell lines. ALTEX, 2018: p. 211-222.

103. Janga, H., et al., Site-specific and endothelial-mediated dysfunction of the alveolar-capillary barrier in response to lipopolysaccharides. J Cell Mol Med, 2018. 22(2): p. 982-998.

104. Privratsky, J.R. and P.J. Newman, PECAM-1: regulator of endothelial junctional integrity. Cell and Tissue Research, 2014. 355(3): p. 607-619.

105. Misharin, A.V., et al., Flow Cytometric Analysis of Macrophages and Dendritic Cell Subsets in the Mouse Lung. American Journal of Respiratory Cell and Molecular Biology, 2013. 49(4): p. 503-510.

106. Rebelo, S.P., et al., 3D-3-culture: A tool to unveil macrophage plasticity in the tumour microenvironment. Biomaterials, 2018. 163: p. 185-197.

107. Patel, V.I., et al., Transcriptional classification and functional characterization of human airway macrophage and dendritic cell subsets. The Journal of Immunology, 2017. 198(3): p. 1183-1201.

108. Hackett, T.-L., et al., Dynamics of pro-inflammatory and anti-inflammatory cytokine release during acute inflammation in chronic obstructive pulmonary disease: an ex vivo study. Respiratory Research, 2008. 9(1): p. 47.

109. Rha, B., et al., Respiratory Syncytial Virus-Associated Hospitalizations Among Young Children: 2015-2016. Pediatrics, 2020. 146(1).

110. Thompson, W.W., et al., Mortality associated with influenza and respiratory syncytial virus in the United States. Jama, 2003. 289(2): p. 179-86.

111. Control, C.f.D. Increased Interseasonal Respiratory Syncytial Virus (RSV) Activity in Parts of the Southern United States. Health Alert Network 2021; Available from: https://emergency.cdc.gov/han/2021/han00443.asp#:~:text=Each%20year%20in%20the%20United,aged%2065%20years%20or%20older.

112. Taylor, G., Animal models of respiratory syncytial virus infection. Vaccine, 2017. 35(3): p. 469-480.

113. Malhotra, R., et al., Isolation and characterisation of potential respiratory syncytial virus receptor(s) on epithelial cells. Microbes and infection, 2003. 5(2): p. 123-133.

114. Johnson, S.M., et al., Respiratory Syncytial Virus Uses CX3CR1 as a Receptor on Primary Human Airway Epithelial Cultures. PLOS Pathogens, 2015. 11(12): p. e1005318.

115. Tripp, R.A., et al., CX3C chemokine mimicry by respiratory syncytial virus G glycoprotein. Nature Immunology, 2001. 2(8): p. 732-738.

116. Currier, M.G., et al., EGFR Interacts with the Fusion Protein of Respiratory Syncytial Virus Strain 2-20 and Mediates Infection and Mucin Expression. PLOS Pathogens, 2016. 12(5): p. e1005622.

117. Kurt-Jones, E.A., et al., Pattern recognition receptors TLR4 and CD14 mediate response to respiratory syncytial virus. Nature Immunology, 2000. 1(5): p. 398-401.

118. Marchant, D., et al., Toll-Like Receptor 4-Mediated Activation of p38 Mitogen-Activated Protein Kinase Is a Determinant of Respiratory Virus Entry and Tropism. Journal of Virology, 2010. 84(21): p. 11359-11373.

119. Behera, A.K., et al., Blocking Intercellular Adhesion Molecule-1 on Human Epithelial Cells Decreases Respiratory Syncytial Virus Infection. Biochemical and Biophysical Research Communications, 2001. 280(1): p. 188-195.

120. Tayyari, F., et al., Identification of nucleolin as a cellular receptor for human respiratory syncytial virus. Nature Medicine, 2011. 17(9): p. 1132-1135.

121. Holguera, J., E. Villar, and I. Muñoz-Barroso, Identification of cellular proteins that interact with Newcastle Disease Virus and human Respiratory Syncytial Virus by a two-dimensional virus overlay protein binding assay (VOPBA). Virus Research, 2014. 191: p. 138-142.

122. Krusat, T. and H.J. Streckert, Heparin-dependent attachment ofrespiratory syncytial virus (RSV) to host cells. Archives of Virology, 1997. 142(6): p. 1247-1254.

123. Johnson, J.E., et al., The histopathology of fatal untreated human respiratory syncytial virus infection. Modern Pathology, 2007. 20(1): p. 108-119.

124. Russell, C.D., et al., The Human Immune Response to Respiratory Syncytial Virus Infection. Clinical Microbiology Reviews, 2017. 30(2): p. 481-502.

125. Kerrin, A., et al., Differential lower airway dendritic cell patterns may reveal distinct endotypes of RSV bronchiolitis. Thorax, 2017. 72(7): p. 620-627.

126. Midulla, F., et al., Respiratory Syncytial Virus Lung Infection in Infants: Immunoregulatory Role of Infected Alveolar Macrophages. The Journal of infectious diseases, 1993. 168(6): p. 1515-1519.

127. Panuska, J.R., et al., Respiratory Syncytial Virus Infection of Alveolar Macrophages in Adult Transplant Patients. American Review of Respiratory Disease, 1992. 145(4_pt_1): p. 934-939.

128. Zhou, Q., et al., Aryl Hydrocarbon Receptor Interacting Protein Targets IRF7 to Suppress Antiviral Signaling and the Induction of Type I Interferon. Journal of Biological Chemistry, 2015. 290(23): p. 14729-14739.

129. Muntjewerff, E.M., L.D. Meesters, and G.v.d. Bogaart, Antigen Cross-Presentation by Macrophages. Frontiers in immunology, 2020. 11: p. 1276-1276.

130. Johnson, T.R., et al., NK T Cells Contribute to Expansion of CD8⁺ T Cells and Amplification of Antiviral Immune Responses to Respiratory Syncytial Virus. Journal of Virology, 2002. 76(9): p. 4294-4303.

131. Kaiko, G.E., et al., NK Cell Deficiency Predisposes to Viral-Induced Th2-Type Allergic Inflammation via Epithelial-Derived IL-25. The Journal of Immunology, 2010. 185(8): p. 4681-4690.

132. Chen, Z., et al., Association of cytokine responses with disease severity in infants with respiratory syncytial virus infection. Acta Paediatrica, 2002. 91(9): p. 914-922.

133. Mirabelli, C., et al., Differential antiviral activities of respiratory syncytial virus (RSV) inhibitors in human airway epithelium. Journal of Antimicrobial Chemotherapy, 2018. 73(7): p. 1823-1829.

134. Chirkova, T., et al., In vitro model for the assessment of human immune responses to subunit RSV vaccines. PLOS ONE, 2020. 15(3): p. e0229660.

135. Bohmwald, K., et al., Contribution of Cytokines to Tissue Damage During Human Respiratory Syncytial Virus Infection. Frontiers in immunology, 2019. 10: p. 452-452.

136. Bohmwald, K., et al., Inflammatory damage on respiratory and nervous systems due to hRSV infection. Current Opinion in Immunology, 2015. 36: p. 14-21.

137. Cherukuri, A., et al., Adults 65 Years Old and Older Have Reduced Numbers of Functional Memory T Cells to Respiratory Syncytial Virus Fusion Protein. Clinical and Vaccine Immunology, 2013. 20(2): p. 239-247.

138. de Bree, G.J., et al., Respiratory Syncytial Virus—Specific CD8+ Memory T Cell Responses in Elderly Persons. The Journal of Infectious Diseases, 2005. 191(10): p. 1710-1718.

139. Nam, H.H. and M.G. Ison, Respiratory syncytial virus infection in adults. BMJ (Online), 2019. 366: p. l5021-l5021.

140. Falsey, A.R., et al., Respiratory Syncytial Virus Infection in Elderly and High-Risk Adults. The New England journal of medicine, 2005. 352(17): p. 1749-1759.

141. Machado, D., et al., RSV infection in human macrophages promotes CXCL10/IP-10 expression during bacterial co-infection. International Journal of Molecular Sciences, 2017. 18(12): p. 2654.

142. Lindell, D.M., T.E. Lane, and N.W. Lukacs, CXCL10/CXCR3-mediated responses promote immunity to respiratory syncytial virus infection by augmenting dendritic cell and CD8+ T cell efficacy. European journal of immunology, 2008. 38(8): p. 2168-2179.

143. Yen, J.-H., et al., Differential effects of IFN-β on IL-12, IL-23, and IL-10 expression in TLR-stimulated dendritic cells. Journal of Leucocyte Biology, 2015. 98(5): p. 689-702.

144. Singh, D., K.L. McCann, and F. Imani, MAPK and heat shock protein 27 activation are associated with respiratory syncytial virus induction of human bronchial epithelial monolayer disruption. American Journal of Physiology-Lung Cellular and Molecular Physiology, 2007. 293(2): p. L436-L445.

145. Linfield, D.T., et al., Airway tight junctions as targets of viral infections. Tissue Barriers, 2021. 9(2): p. 1883965.

146. Guvenel, A., et al., Epitope-specific airway-resident CD4+ T cell dynamics during experimental human RSV infection. Journal of Clinical Investigation, 2019. 130(1): p. 523-538.

147. Ptaschinski, C., et al., RSV-Induced H3K4 Demethylase KDM5B Leads to Regulation of Dendritic Cell-Derived Innate Cytokines and Exacerbates Pathogenesis In Vivo. PLOS Pathogens, 2015. 11(6): p. e1004978.

148. Laubreton, D., et al., Regulatory B Lymphocytes Colonize the Respiratory Tract of Neonatal Mice and Modulate Immune Responses of Alveolar Macrophages to RSV Infection in IL-10-Dependant Manner. Viruses, 2020. 12(8): p. 822.

149. Spencer, S., et al., Loss of the interleukin-6 receptor causes immunodeficiency, atopy, and abnormal inflammatory responses. J Exp Med, 2019. 216(9): p. 1986-1998.

150. Gou, X., et al., IL-6 During Influenza-Streptococcus pneumoniae Co-Infected Pneumonia-A Protector. Front Immunol, 2019. 10: p. 3102.

151. Plosa, E.J., et al., β1 Integrin regulates adult lung alveolar epithelial cell inflammation. JCI Insight, 2020. 5(2).

152. Coultas, J.A., R. Smyth, and P.J. Openshaw, Respiratory syncytial virus (RSV): a scourge from infancy to old age. Thorax, 2019. 74(10): p. 986-993.

153. Harker, J.A., et al., Delayed sequelae of neonatal respiratory syncytial virus infection are dependent on cells of the innate immune system. J Virol, 2014. 88(1): p. 604-11.

154. Shachar, I. and N. Karin, The dual roles of inflammatory cytokines and chemokines in the regulation of autoimmune diseases and their clinical implications. Journal of Leukocyte Biology, 2013. 93(1): p. 51-61.

155. Holdsworth, S.R. and P.-Y. Gan, Cytokines: Names and Numbers You Should Care About. Clinical Journal of the American Society of Nephrology, 2015. 10(12): p. 2243-2254.

156. Cavaillon, J.-M., Pro-versus anti-inflammatory cytokines: myth or reality. CELLULAR AND MOLECULAR BIOLOGY-PARIS-WEGMANN-, 2001. 47(4): p. 695-702.

157. Turner, M.D., et al., Cytokines and chemokines: At the crossroads of cell signalling and inflammatory disease. Biochimica et Biophysica Acta (BBA) - Molecular Cell Research, 2014. 1843(11): p. 2563-2582.

158. CHANG, H.-D. and A. RADBRUCH, The Pro- and Anti-Inflammatory Potential of Interleukin-12. Annals of the New York Academy of Sciences, 2007. 1109(1): p. 40-46.

159. de Bree, G.J., et al., Respiratory syncytial virus—specific CD8+ memory T cell responses in elderly persons. Journal of Infectious Diseases, 2005. 191(10): p. 1710-1718

VITA

Taylor Do

Candidate for the Degree of

Doctor of Philosophy

Dissertation: DEVELOPMENT AND CHARACTERIZATION OF A NOVEL THREE-DIMENSIONAL HUMAN TISSUE-ENGINEERED LUNG MODEL TO STUDY IMMUNE RESPONSE TO RESPIRATORY SYNCYTIAL VIRUS IN VULNERABLE POPULATIONS

Major Field: Chemical Engineering

Biographical:

Education:

Completed the requirements for the Doctor of Philosophy in Chemical Engineering at Oklahoma State University, Stillwater, Oklahoma in May, 2023.

Completed the requirements for the Master of Science in Biosystems Engineering at Oklahoma State University, Stillwater, Oklahoma in 2018.

Completed the requirements for the Bachelor of Science in Biosystems Engineering at Oklahoma State University, Stillwater, Oklahoma in 2016.

Experience:

Graduate Research Assistant – 2019-2022

Professional Memberships:

Biomedical Engineering Society – 2021-2022